2012-02-02

The Influence of Nozzle Spacing and Diameter on the Acoustic Emissions of Closely Spaced Supersonic Jet Arrays

Ian S. Coltrin
Brigham Young University - Provo

The Influence of Nozzle Spacing and Diameter on the Acoustic Emissions of Closely Spaced Supersonic Jet Arrays

Ian S. Coltrin

A thesis submitted to the faculty of
Brigham Young University
in partial fulfillment of the requirements for the degree of

Master of Science

Jonathan D. Blotter, Chair
R. Daniel Maynes
Kent L. Gee

Department of Mechanical Engineering

Brigham Young University

April 2012

ABSTRACT

The Influence of Nozzle Spacing and Diameter on the Acoustic Emissions of Closely Spaced Supersonic Jet Arrays

Ian S. Coltrin
Department of Mechanical Engineering, BYU
Master of Science

The acoustic emissions from supersonic jets represent an area of significant research needs; not only in the field of aero-acoustics, but in industry as well where high pressure let down processes have been known to cause acoustically induced vibrations. A common method to reduce the acoustic emissions of such processes involves dividing the single larger supersonic flow into several smaller ones. Though this is common practice, there is not yet a current model which describes the reduction of acoustic emissions from an array of smaller supersonic jets. Current research which studies supersonic jet arrays are mainly focused on the effects of screech. Though screech is important, due to its high amplitude acoustic pressure, this research focuses on the overall acoustic emissions radiated from supersonic jet arrays which can cause severe acoustic loadings.

This research investigated the acoustic emissions and shock formations from several eight by eight arrays of axisymmetric jet experimentally. The array nozzle diameters investigated ranged from 1/8 inch to 1/4 inch and the spacing over diameter ratio ranged from 1.44 to 3. The net pressure ratios investigated ranged from 2 to 24.

Results revealed a strong correlation between the acoustic emissions and the shock formations of the flow. Up until a critical net pressure ratio, the overall sound pressure levels were comparable to that of a single jet within an array. At net pressure ratios beyond the critical the overall sound pressure levels transitioned to higher decibel levels; equivalent to a single jet with an equivalent exit area of an entire array. Also, the characteristic acoustic frequency emitted from a nozzle array remained ultrasonic (above 20 kHz) at lower net pressure ratios and then shifted to audible levels (between 20 Hz to 20 kHz) at net pressure ratios beyond the critical. Also, before the critical net pressure ratio the shock cells from the jets within the array remained unmerged, but at net pressure ratios beyond the critical the shock cells merged and formed lattices of weak oblique shocks at first and then strong oblique shocks as the net pressure ratio continued to increase.

The critical net pressure ratio was investigated by non-dimensional analysis. The non-dimensional analysis revealed that the critical net pressure ratio was a strong linear function of the spacing over diameter ratio. A linear model was derived which is able to predict the critical net pressure ratio, and in turn, predict a critical shift in the acoustic emissions of a nozzle array.

Keywords: acoustic emissions, supersonic, net pressure ratio, diameter, spacing over diameter ratio, overall sound pressure levels, frequency, characteristic, Strouhal number, acoustic pressure over the dynamic pressure ratio

ACKNOWLEDGEMENTS

I would like to thank all the people who helped and supported me; not only through my graduate career, but throughout all of college. The support of all the people I had the opportunity of interacting with, whether great or small, contributed to this success. Specifically I would like to thank Dr. Blotter and Dr. Maynes for their instruction, advice, and overall interest in what I do. I would also like to thank those I've had the great opportunity to work with; Curtis Weiderhold, Brad Solomon, and Rich Berry.

I would also like to thank Control Components Inc. (CCI) for their financial support in this research as well as contributing their overall interest. I would specifically like to thank Farhan Ahmed from CCI for working with me on this project.

Most of all I would like to thank my family who have supported and encouraged me all of my life; my parents especially for always giving me their unconditional love.

I also would like to recognize the help I've received from my Father in Heaven who has guided me though my life's trials and who I will continue to look to, always.

I would lastly like to recognize Capt. McCardle, USMC, who, before my college career, once advised me, "… you should study engineering, that's the way to go."

TABLE OF CONTENTS

LIST OF TABLES vii

LIST OF FIGURES ix

NOMENCLATURE xi

Chapter 1. Introduction 1
1.1 Research Objectives 2
1.2 Project Scope 2
1.3 Overview 3

Chapter 2. Background 5
2.1 Turbulent Mixing Noise 6
2.2 Broadband Shock Associated Noise 6
2.3 Narrowband Shock Associated Noise 7
2.4 Multi-Jets 9
2.5 Research Contribution 12

Chapter 3. Overall Sound Levels Radiated From Closely Spaced Supersonic Jet Arrays 13
3.1 Contributing Authors and Affiliations 13
3.2 Abstract 13
3.3 Introduction 14
3.4 Experiment 17
3.5 Shock Formations 22
3.6 Overall Sound Pressure Levels 26
3.7 Shock Formations and Overall Sound Pressure Levels 33
3.8 Conclusion 34
3.9 Acknowledgements 35

Chapter 4. Influence of Nozzle Spacing and Diameter on the Acoustic Emissions of Closely Spaced Supersonic Jets 37
4.1 Contributing Authors and Affiliations 37
4.2 Abstract 37
4.3 Introduction 38
4.4 Experiment 40
4.5 Results 44
4.5.1 Single Jets 44
4.5.2 Jet Arrays 46
4.6 Analysis 48
4.6.1 Non-Dimensional Spectra 55
4.6.2 Characteristic Values 58
4.6.3 Critical Net Pressure Ratio 65
4.7 Conclusion 68

4.8 Acknowledgments 69

Chapter 5. Conclusion 71
5.1 Summary 71
5.2 Recommendations for Future Work 75

References 77

Appendix A: Experimental Setup 79

Appendix B: Numerical Results 87

Appendix C: Shadowgraph Imagery 97

Appendix D: Frequency Domain Spectra 113

Appendix E: Strouhal Domain Spectra 123

Appendix F: Matlab Code for the Method of Characteristics 133

LIST OF TABLES

Table 3.1: Nominal Net Pressure Ratios Investigated for 8x8 Jet Arrays 18
Table 3.2: Nominal Net Pressure Ratios Investigated for Single Jets 18
Table 3.3: Net Pressure Ratios, Fully Expanded Mach Numbers,..... 19

Table 4.1: Nominal Net Pressure Ratios Investigated for 8x8 Jet Arrays 42
Table 4.2: Nominal Net Pressure Ratio Investigated for Single Jets..... 42

LIST OF FIGURES

Figure 2.1: Strouhal Number Domain for Supersonic Jet Noise.[5] 5
Figure 2.2: Supersonic Jet Flow with Mach Waves Radiating off the Shear Layer.[8] 6
Figure 2.3: Shock Cells Produced From Supersonic Jet Flow.[9] 7
Figure 2.4: Vortical Shock Waves Which Produce Screech in Supersonic Jet Flow.[13] 8
Figure 2.5: Shadowgraph Images of Parallel Rectangular Supersonic Jets Which Have Eliminated Each Other's Vortical Shock Formations. Images (a) and (b) are seen from the side.[13] 10
Figure 2.6: Shadowgraph Images of Multi-Jet Arrays Featuring The Vortical Shock Formations.[17] 10
Figure 2.7: Overall Sound Pressure Levels for a Single Jet, Two Jet Array, and Four Jet Array.[17] 11

Figure 3.1: Schematic View of a Typical Jet Array 17
Figure 3.2: Microphone Experimental Setup 21
Figure 3.3: Shadowgraph Images for a 4.0 mm Diameter Jet Array and S/d ratio of 1.44 and at NPR values ranging from 3.0 to 24.2 22
Figure 3.4: Shadowgraph Images for a 4.0 mm Diameter Jet Array and S/d ratio of 2.5 and at NPR values ranging from 5.5 to 23.5. 23
Figure 3.5: Shadowgraph Images for a 4.0 mm Diameter Jet Array and S/d ratio of 3 and at NPR values ranging from 6.3 to 23.2. 23
Figure 3.6: Frequency Spectra for a 4.0 mm Diameter Jet Array and S/d ratio of 1.44. 25
Figure 3.7: Overall Sound Pressure Levels as a function of the NPR for Single Jets of Diameters 3.2 mm, 6.4 mm, 25.4 mm, and 50.8 mm. 27
Figure 3.8: Overall Sound Pressure Levels as a function of the NPR for Jet Arrays with S/d ratios of 1.44. 28
Figure 3.9: Overall Sound Pressure Levels as a function of the NPR for Jet Arrays with S/d ratios of 2. 28
Figure 3.10: Overall Sound Pressure Levels as a function of the NPR for Jet Arrays with S/d ratios of 2.5. 29
Figure 3.11: Overall Sound Pressure Levels as a function of the NPR for Jet Arrays with S/d ratios of 3. 29
Figure 3.12: Overall Sound Pressure Levels as a function of the NPR for 3.2 mm Diameter Jet Arrays, a 3.2 mm Diameter Single Jet, and a 25.4 mm Diameter Single Jet. 31
Figure 3.13: Overall Sound Pressure Levels as a function of the NPR for 6.4 mm Diameter Jet Arrays, a 6.4 mm Diameter Single Jet, and a 50.8 mm Diameter Single Jet. 32

Figure 4.1: Schematic View of a Typical Nozzle Array 41
Figure 4.2: Microphone Experimental Setup 44
Figure 4.3: Frequency Spectra for a Single 3.2 mm Diameter Nozzle Jet and NPR Ranging From 2.2 to 23.7. 45
Figure 4.4: Frequency Spectra for a Single 25.4 mm Diameter Nozzle Jet and NPR Ranging From 2.2 to 24.3. 45
Figure 4.5: Frequency Spectra for a 4.0 mm Diameter Jet Array of S/d = 1.44 and NPR ranging from 2.1 to 24.2 46

Figure 4.6: Frequency Spectra for a 4.0 mm Diameter Jet Array of S/d = 2.5 and NPR Ranging From 2.2 to 23.5 47
Figure 4.7: Frequency Spectra for a 4.0 mm Diameter Jet Array of S/d = 3 and NPR Ranging From 2.3 to 23.2. 47
Figure 4.8: Diagram of Characteristic Lines Forming an Underexpanded Supersonic Jet Shock Cell with Labeled Regions 1 - 7. 51
Figure 4.9: Diagram of Characteristic Lines Forming an Underexpanded Supersonic Jet Shock Cell with Labeled Points 1 - 4. 54
Figure 4.10: Non-Dimensional Spectra for a 3.2 mm Diameter Single Nozzle Jet and NPR Ranging From 2.2 to 23.7. 56
Figure 4.11: Non-Dimensional Spectra for a 25.4 mm Diameter Single Nozzle Jet and NPR Ranging From 2.2 to 23.7. 56
Figure 4.12: Non-Dimensional Spectra for a 4.0 mm Diameter Jet Array of S/d = 1.44 and NPR Ranging From 2.1 to 24.2. 57
Figure 4.13: Non-Dimensional Spectra for a 4.0 mm Diameter Jet Array of S/d = 2.5 and NPR Ranging From 2.2 to 23.5. 58
Figure 4.14: Non-Dimensional Spectra for a 4.0 mm Diameter Jet Array of S/d = 3 and NPR Ranging From 2.3 to 23.2. 58
Figure 4.15: Characteristic Strouhal Numbers for Jet Arrays of S/d = 1.44. 59
Figure 4.16: Characteristic Strouhal Numbers for Jet Arrays of S/d = 2. 59
Figure 4.17: Characteristic Strouhal Numbers for Jet Arrays of S/d = 2.5. 60
Figure 4.18: Characteristic Strouhal Numbers for Jet Arrays of S/d = 3. 60
Figure 4.19: Characteristic ADP for Jet Arrays of S/d = 1.44. 61
Figure 4.20: Characteristic ADP for Jet Arrays of S/d = 2. 62
Figure 4.21: Characteristic ADP for Jet Arrays of S/d = 2.5. 62
Figure 4.22: Characteristic ADP for Jet Arrays of S/d = 3. 63
Figure 4.23: Characteristic ADP for 3.2 mm Diameter Jet Arrays and 3.2 mm and 25.4 mm Diameter Single Nozzle Jets. 64
Figure 4.24: Characteristic ADP for 6.4 mm Diameter Jet Arrays and 6.4 mm and 50.8 mm Diameter Single Nozzle Jets. 65
Figure 4.25: Critical Net Pressure Ratios. 66
Figure 4.26: Averaged Critical Net Pressure Ratios. 67

NOMENCLATURE

ADP	Acoustic Pressure over the Dynamic Pressure Ratio
d	Nozzle Diameter
d_j	Fully Expanded Jet Diameter
f	Acoustic Frequency
NPR	Net Pressure Ratio
$OASPL$	Overall Sound Pressure Level
$P_{acoustic}$	Acoustic Pressure
S	Nozzle Array Center to Center Spacing
SPL	Sound Pressure Level
St	Strouhal Number
u_j	Fully Expanded Jet Velocity
ρ_j	Fully Expanded Jet Density

Chapter 1. Introduction

Acoustic emissions from supersonic jet arrays are an area of significant research need. Practical applications not only exist in the area of aero-acoustics, where high pressure sound waves from engine exhausts can induce structural fatigue as well as significant human discomfort, they also exist in the energy industry, among others which involve high pressure let down processes. In these types of industries high pressure acoustical loadings have caused severe fatigue within piping networks, and other mechanical systems, sometimes causing them to fail within hours[1].

From the point of view of industry, high acoustical loadings were first examined from the aspect of sound transmission and noise generation in the surroundings of piping systems. Work that combined structural fatigue and the acoustic loading within a pipe was done by Carucci and Mueller[1]; and which was later refined by Eisinger[2]. As a method to reduce the acoustic emissions, Carucci and Mueller suggested dividing a single jet into multiple smaller jets. Their suggestion was to implement Venturi slots into valves which would create several smaller parallel plane jets out of a single, larger jet.

This research works off of the similar principle discovered by Carucci and Mueller by investigating the characteristics of dividing a single larger supersonic flow into several smaller flows using an axisymmetric nozzle array. Seiner, McLaughlin, and Lui[3], discovered that for a single supersonic axisymmetric jet the characteristic Strouhal number is approxiamtely 0.2. The Strouhal number is a non-dimensional parameter defined as the frequency times a characteristic

length scale over the velocity($St = f \cdot l/u$). In the case of jet noise, the frequency comes from the acoustic pressure wave, the characteristic length scale is the fully expanded jet diameter, and the velocity is the fully expanded jet velocity. Thus, if a single larger flow were divided into several smaller flows the larger fully expanded jet diameter would be reduced which would in turn alter the acoustic emissions of the jet flow.

The acoustic emissions of several 8x8 arrays of axisymmetric supersonic jets were characterized experimentally in this research. The purpose of the arrays is to replace a single supersonic flow of equivalent exit area to a jet array. The focus of this research was to create predictive measures to use when implementing a jet array in order to reduce the acoustic emissions of supersonic flow.

1.1 Research Objectives

The three main research objectives are outlined as follows:

1. Perform experiments that characterize the acoustic emissions of 8x8 jet arrays in terms of controlled variables; i.e. pressure drop, nozzle spacing, and nozzle diameter of a nozzle array.
2. Perform flow visualization to observe shock structure formations.
3. Perform experiments that correlate the flow regime to the acoustic emissions of a jet array.
4. Derive a model(s) that produce optimal operating conditions for implementing a jet array.

1.2 Project Scope

The scope of this research was to investigate experimentally the influence of nozzle spacing and diameter on the acoustic emissions of supersonic nozzle arrays. The primary

parameters of interest that were investigated include: nozzle diameter, nozzle spacing, and the net pressure drop.

This research was limited to supersonic air flow. The nozzle diameters investigated ranged from 1/8 inch to 1/4 inch. The nozzle spacing over diameter (S/d) ratios investigated ranged from 1.44 to 3. And the net pressure ratios (NPR) investigated ranged from 2 to 24.

1.3 Overview

Chapter 2 provides a background into the noise mechanics of supersonic jet flow. Chapter 2 concludes with an overview of the most current research into multi-nozzle supersonic flow. Chapters 3 and 4 present manuscripts which will be submitted to the Journal of the Acoustical Society of America. Chapter 3 presents an investigation into the flow regime and the overall noise emitted from 8x8 jet arrays; more specifically the shock formations and overall sound pressure levels. The flow regime and the overall noise were also correlated. Chapter 4 presents an investigation into the frequency content of jet arrays. Chapter 4 also presents analysis of the acoustic emissions and produces a model which can predict critical characteristics of jet arrays. Contained in Chapters 3 and 4 are example data sets used to explain the characteristics of interest for supersonic jet arrays. The full compilation of data can be observed in Appendices B – E. Chapter 5 provides a summary and conclusion of this research as well as giving recommendations for future work into this field.

The appendices provide the overall compilation of the experimental setup, results, and analysis done for this research. Appendix A includes the images of the experimental setup including the blowdown facility, jet arrays, shadowgraph imagery experimental setup, and microphone experimental setup. Appendix B includes all of the numerical results including the

net pressure ratio (NPR), temperature (T), mass flow rate ($\dot{m}$), fully expanded Mach number, diameter, velocity, and density (M_j, d_j, u_j, ρ_j), characteristic Strouhal number (St), and characteristic acoustic pressure over the dynamic pressure ratio (AP/DP). These parameters with be more fully discussed later on i n the thesis. Appendix C includes all of the shadowgraph imagery acquired. Appendix D includes all of the spectra displaying the acoustic pressure in the frequency domain. Appendix E includes all of the spectra displaying all the AP/DP in the Strouhal domain. Appendix E includes the Matlab code which applies the Method of Characteristics to determine the fully expanded diameter of an underexpanded supersonic jet.

Chapter 2. Background

Three characteristic frequencies, or the frequencies where the largest sound pressure reside, were observed from an axisymmetric supersonic jet through an investigation done by Norum and Seiner[4]. These three characteristic frequencies correlate to the three main mechanisms of jet noise. In a review on jet noise, Tam[5] described the three mechanisms as turbulent mixing noise, broadband shock associated noise, and narrowband shock associated noise, or screech. The supersonic jet noise spectrum can be seen in Fig. 2.1. Though these mechanisms all contribute to acoustic loadings, they are generated differently. This section reviews the three jet noise mechanisms and concludes with a review on the most current research into multi-nozzle supersonic jet flow.

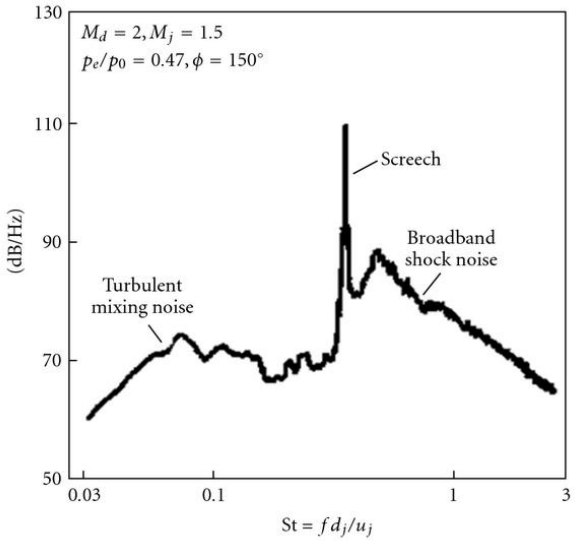

Figure 2.1: Strouhal Number Domain for Supersonic Jet Noise.[5]

2.1 Turbulent Mixing Noise

Turbulent mixing of supersonic jet flow is generated from the shear layer which exists between the jet and the quiescent medium. The turbulent flow of the jet acts much like a wavy wall against the quiescent medium. This can be true even if the fluids are the same due to large density differences caused by compressibility effects. The unstable shear layer causes Mach waves to build up a nd radiate outward and downstream. The pressure decrease across the continually radiating Mach waves form acoustic pressure waves. The acoustic waves which radiate from turbulent mixing have broad characteristic frequency content when observing the acoustic pressure in the frequency domain. Several researchers have investigated the acoustic emissions of turbulent mixing noise including Yu[6], Tanna[7], Norum and Seiner[4], and Seiner *et al.*[3] Figure 2.2 displays a shadowgraph image of a supersonic jet emitting Mach waves.

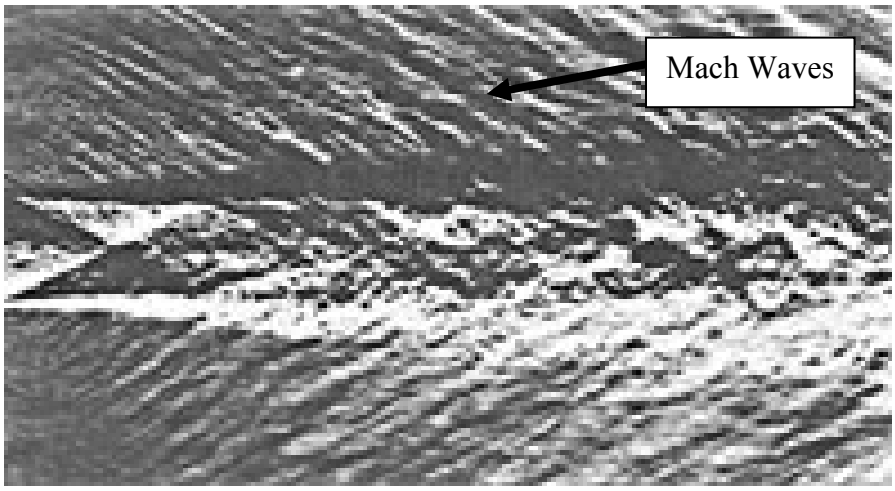

Figure 2.2: Supersonic Jet Flow with Mach Waves Radiating off the Shear Layer.[8]

2.2 Broadband Shock Associated Noise

Broadband shock associated noise is generated through the interaction between the shock cells of a supersonic jet and the turbulent flow of the jet. The shock cells are formed by the

expanding supersonic fluid of the jet which then creates an oblique shockwave against the quiescent medium. Due to the high pressure increase across the shock, the flow of the supersonic jet is reflected back towards the centerline axis of the jet stream where it expands again. This process can repeat itself several times within a jet stream. Figure 2.3 displays a formation of shock cells.

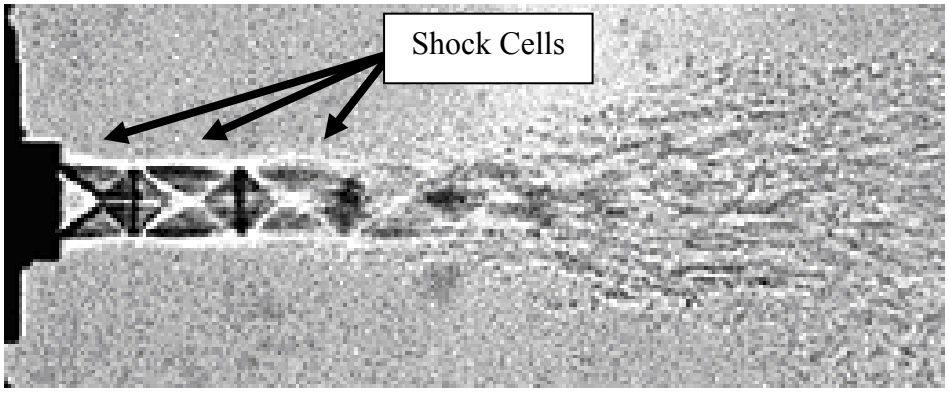

Figure 2.3: Shock Cells Produced From Supersonic Jet Flow.[9]

As seen from the fluid flow's perspective, the shock cells are treated as a disturbance which creates turbulent kinetic energy. This turbulent energy is then translated into acoustic energy. The frequency content for broadband shock associated noise is broad, similar to that of turbulent mixing noise, though broadband shock associated noise's characteristic frequency is nominally higher. The first to investigate this noise mechanism was Yu[6] and Harper-Bourne and Fisher[10], as well as Norum and Seiner[4], Tam[5], and Tanna[11].

2.3 Narrowband Shock Associated Noise

The last noise mechanism is narrowband shock associated noise, or screech. Screech was first observed by Powell[12] when he noticed a discrete tone which existed within underexpanded supersonic jets. In Raman's[13] review on screech he described screech generation from a feedback

loop created from a distinct formation of shocks. These distinct shocks have a vortical structure, either toroidal or helical, which are convected downstream in the near field. Figure 2.4 displays the vortical shock structures which form around supersonic jet flow.

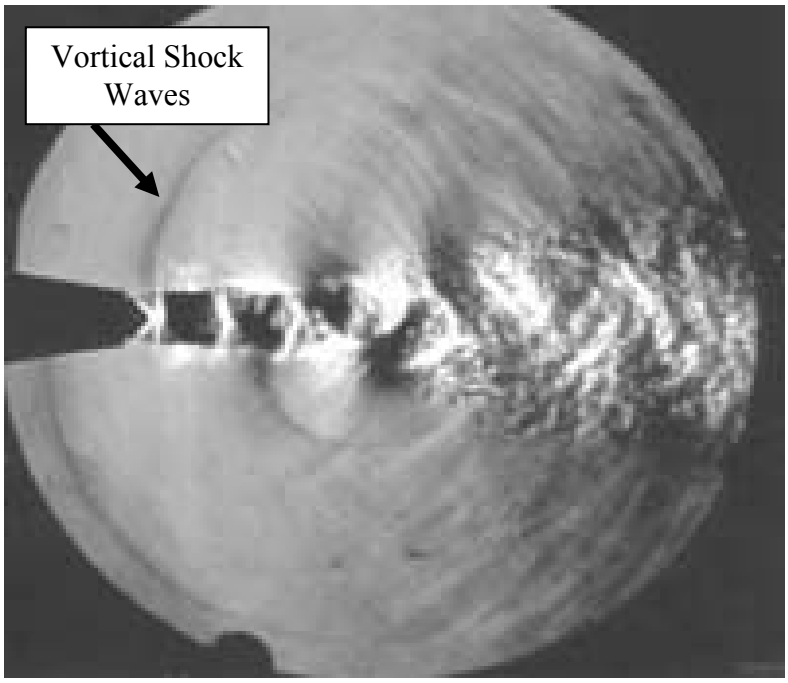

Figure 2.4: Vortical Shock Waves Which Produce Screech in Supersonic Jet Flow.[13]

The vortical nature of the shocks causes the jet flow to become unstable and wavy. The unstable flow would in turn cause the shock cells of the jet to interact with the vortical shock waves which then would generate a discrete acoustic tone. The frequency content for screech is very narrow, much like a single tone; sometimes screech tones are even accompanied by harmonics. Also, the pressure amplitude of screech is most always much higher than the broadband noise emitted from a jet. Since Powell, a few that have continued to study screech include Sherman, Glass, and Duleep[14], Norum[15], and Massey, Ahuja, and Jones[16].

2.4 Multi-Jets

Methods to predict the acoustic loads from supersonic jets are of great interest. Models derived by Carucci and Mueller[1], and Eisinger[2] were derived in order to predict acoustic loads caused by high pressure gases in piping networks based upon parameters upstream of the flow. Though these models are used as a standard in most cases, they are not able to reduce acoustic emissions. In Carucci and Mueller's paper on flow induced noise they suggest a form of reducing acoustic emissions which can be implemented within valves. They suggested using Venturi slots to divide a single larger flow into several smaller parallel plane jets.

Multiple jet streams have been commonly used for their abilities to restrict and reduce the noise mechanisms of supersonic jets, particularly screech[5, 13 - 19]. As mentioned before the key component to the feedback loop, which is essential to generate screech, is the vortical shockwave structure. Raman[13] reported that in the case of two parallel rectangular jets the votical shock waves cancel the effects of each other due to a phase mismatch in their vortical structures. Figure 2.5 presents shadowgraph images of parallel rectangular supersonic jets which have eliminated each other's vortical shock structure.

Current research on axisymmetric multi-jet arrays has been conducted by Umeda and Ishii[17, 18]. Umeda and Ishii characterized the shockwave structures and the narrowband shock associated noise response from arrays of two and four nozzles as well as comparative research on single jets. Since the phase mismatch effect which occurs with rectangular jets doesn't work the same way with axisymmetric jets, the main goal of their research was to characterize the effects from multiple closely spaced nozzles had on the oscillation modes which generate screech. Figure 2.6 presents shadowgraph images of how multiple jets effect the vortical shock waves of each other.

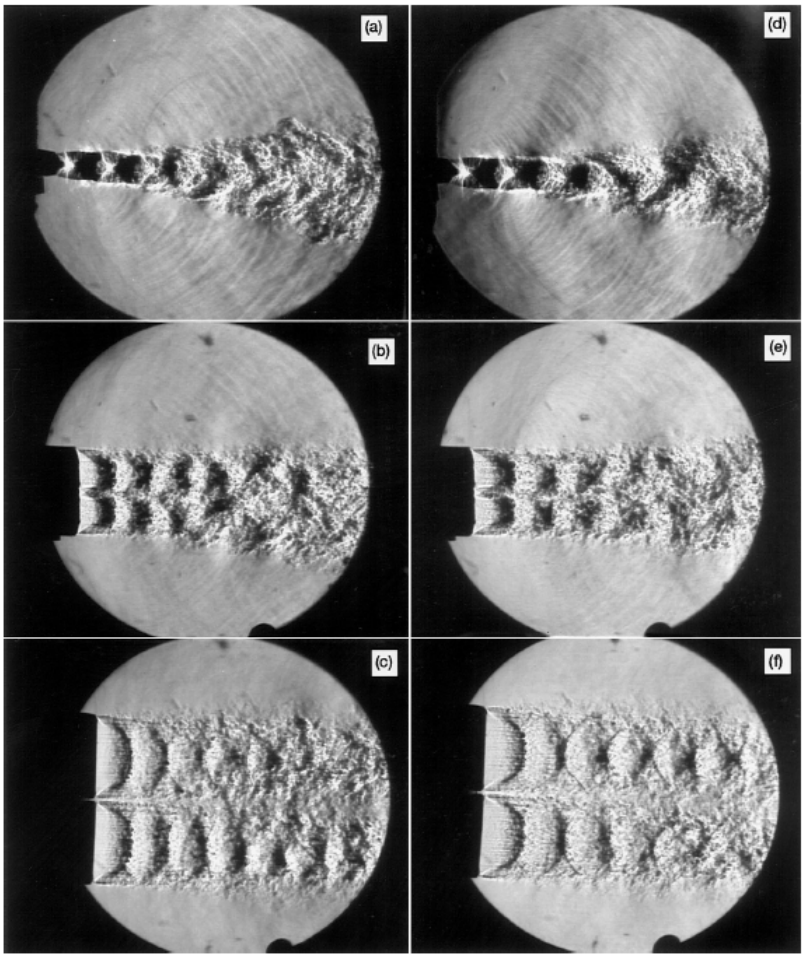

Figure 2.5: Shadowgraph Images of Parallel Rectangular Supersonic Jets Which Have Eliminated Each Other's Vortical Shock Formations. Images (a) and (b) are seen from the side.[13]

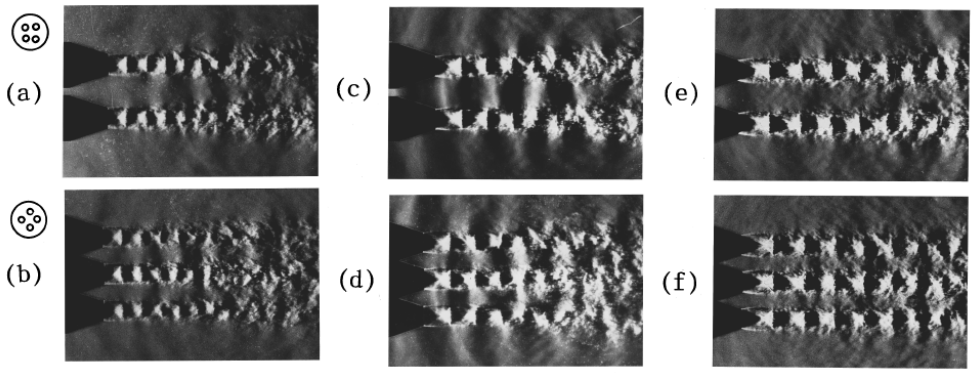

Figure 2.6: Shadowgraph Images of Multi-Jet Arrays Featuring The Vortical Shock Formations.[17]

Umeda and Ishii also confirmed a trend in the overall sound pressure levels which was also investigated by Powell, Umeda, and Ishii[19]. Figure 2.7 displays the overall sound pressure levels for different nozzle arrays investigated by Umeda and Ishii.

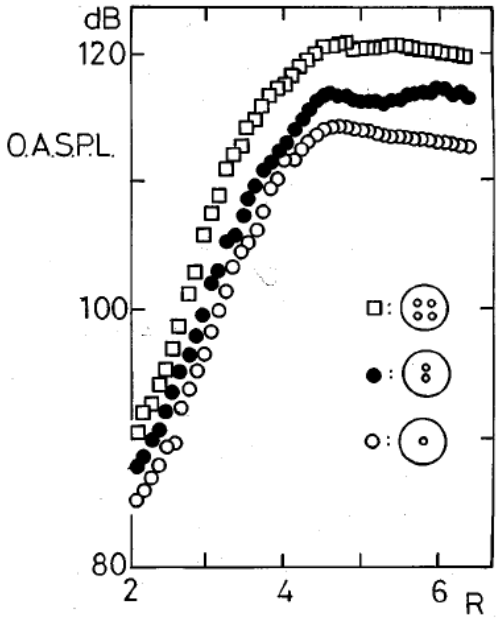

Figure 2.7: Overall Sound Pressure Levels for a Single Jet, Two Jet Array, and Four Jet Array.[17]

The data shown in Fig. 2.7 displays the overall sound pressure levels (OASPL) with respect to the pressure ratio (R), defined as the static pressure of the fluid taken upstream of the jet arrays over the ambient pressure outside of the jet arrays. The data shown in Fig. 2.7 display similar trends in the data between the jet arrays and the single nozzle. Up to a pressure ratio of approximately 5 there is a steep increase in the decibel levels. As the pressure continues to increase the slope in the acoustic pressure reduces and only exhibits modest increase or decrease.

2.5 Research Contribution

Since screech produces significantly higher sound pressure levels, current research into multi-jet arrays is mainly focused on that aspect of jet noise. The work presented in this thesis does not limit itself to a single mechanism but investigates the overall noise emitted from turbulent energy and narrowband shock associated noise for a nozzle array by correlating the overall acoustic pressures and frequency content to the flow regime. Current state of the art investigates pressure ratios up to approximately 6. This research investigates pressure ratios up to approximately 24. At higher pressure ratios the shock cells of the individual jets in an array are able to interact with each other; a process unobtainable at the pressure ratios typically explored. Also, current state of the art investigates nozzle arrays with a maximum of four jets. This research investigates nozzle arrays consisting of 64 parallel.

Chapter 3. Overall Sound Levels Radiated From Closely Spaced Supersonic Jet Arrays

This chapter is a manuscript to be submitted to the Journal of the Acoustical Society of America. The Formatting of the paper has been modified to meet the stylistic requirements of this thesis.

3.1 Contributing Authors and Affiliations

Ian S. Coltrin, R. Daniel Maynes, Jonathan D. Blotter
Department of Mechanical Engineering, Brigham Young University, Provo, UT 84602

Kent L. Gee
Department of Physics and Astronomy, Brigham Young University, Provo, UT 84602

3.2 Abstract

Overall sound pressure levels from fourteen different 8x8 arrays of small, axisymmetric supersonic jets were characterized experimentally. The results have also been compared to behavior for single jets of similar dimensions. The jet diameters ranged from 3.2 to 6.4 mm and the jet-spacing-to-diameter ratio ranged from 1.44 to 3. The arrays were tested at net pressure ratios ranging from approximately 2 to 24. Through shadowgraph imagery, it was found that above a certain net pressure ratio the array of jets coalesced into an interacting lattice of oblique shock interactions. As the net pressure ratio increased, these fluid shocks evolve from unsteady, oscillatory shock structures to stable shock structures. The formation of the interacting shock

lattices is strongly correlated with the changes in the measured overall sound pressure levels. Initially the arrays emitted low sound pressure levels, similar to that of a single jet within the array. However, as the jets coalesce and the interacting shock structures transitioned from oscillatory to stable the sound pressure levels transitioned to a decibel level similar to that of a single nozzle with an exit area equivalent of the entire array.

3.3 Introduction

Acoustic emissions from supersonic jet arrays represent an area of significant research need. Practical applications of closely spaced jet arrays not only exist in the area of aero-acoustics, where high amplitude noise radiated engine exhausts can induce structural fatigue as well as significant human discomfort, but also facilities requiring high pressure let down processes. In the energy industry high pressure amplitude acoustical loadings from pressure let down processes has caused severe fatigue in piping networks, and other mechanical systems, sometimes causing them to fail within hours[1]. Thus, this paper focuses on better understanding the relationships between parallel supersonic jet flows which create severe acoustic emissions.

From an industrial point of view, high acoustical loadings from pressure let down processes has been examined from the aspect of sound transmission and noise generation in the surroundings of piping systems. Carucci and Mueller[1], and, later, Eisinger[2] combined effects of structural fatigue and acoustic loadings within a pipe. As a method to reduce the acoustic emissions, Carucci and Mueller suggested dividing a single jet into multiple smaller jets. Their suggestion was to implement Venturi slots into valves that would create several smaller parallel plane jets out of a single, larger jet.

As reviewed by Tam[5] there are three main mechanisms which describe the total acoustic emissions from individual supersonic jets; turbulent mixing noise, broadband shock associated noise, and narrowband shock associated noise, or screech.

The source of noise from turbulent mixing is generated from the shear layer between the jet and the quiescent medium. The instability wave created from this shear layer is much like a supersonic fluid moving past a wavy wall. The unstable shear layer causes Mach waves to build up and radiate downstream and away from the jet as relatively intense pressure waves.

Broadband shock-associated noise is generated by the formation of oblique shocks, or shock cells, from a supersonic jet. The shock cells mentioned here are formed initially as a result of the expanding fluid of a supersonic jet which creates a shock against the quiescent medium. Due to the high pressure rise of the shock, the jet flow is reflected back into the jet where it then expands again as it moves downstream. These processes can be repeated several times for a supersonic jet. As viewed from the jet flow perspective these shock cells are a disturbance which creates turbulent energy within the flow. This turbulent energy is then translated into acoustic energy which radiates outward and downstream. The first to investigate this noise source were Yu[6] and Harper-Bourne and Fisher[8]. Several others followed up on this research including Seiner and Norum[4], and Tam[5].

The last mechanism is narrowband shock-associated noise, or screech. Screech tones were first investigated by Powell[12] when discrete tones produced from underexpanded supersonic jets were observed. In Raman's[13] review on screech he described screech generation from a feedback loop created from a distinct formation of shocks. These distinct shocks have a vortical structure, either toroidal or helical, which are convected downstream in the near field of the jet. The vortical nature of the shocks causes the jet flow to become unstable and wavy. The

unstable flow in turn cause the shock cells of the jet to interact with the vortical shock waves which then generates a discrete acoustic tone.

Dual jet streams and other multiple jet flow techniques have been used to restrict these mechanisms, particularly screech[13, 17, 18]. As mentioned, the feedback loop which generates screech is dependent upon the existence of vortical shock formations. Such shock formations can be manipulated with the existence of several jets. As reported by Raman[13] in the case of rectangular jets the effects of screech can be minimized with the addition of a second, parallel jet stream. Here the vortical shock formation of the second jet reduces the effects of the first due to a phase mismatch of the two vortical shock formations.

An extension into several axisymmetric jets was performed by Umeda and Ishii[17, 18]. Here they investigated the oscillation modes of two and four axisymmetric jet arrays, as well as a single nozzle jet. Since phase mismatching doesn't work in the same fashion with axisymmetric jets as it does with rectangular jets, they focused their research on the oscillation modes and screech frequencies produced from multiple jets. In this present investigation, instead of the narrowband shock-associated noise, which has been thoroughly investigated, the focus of this paper includes the turbulent mixing noise that radiates from a larger 8x8 jet array.

This paper presents the acoustic emission and shock structure characteristics of several different 8x8 arrays of parallel axisymmetric supersonic jets. The acoustic radiation is characterized in terms of overall sound levels as a function of the net pressure ratio (NPR). The results include a shadowgraph investigation of the formation of shocks from single jets and interacting oblique shocks from multiple jets for different NPR.

3.4 Experiment

A schematic view of an array is provided in Fig. 3.1 .Figures of each jet array can be observed in Appendix A*. The nozzle diameters investigated ranged from 3.2 mm (1/8 in.) to 6.4 mm (1/4 in.). The center-to-center spacing over the nozzle diameter (S/d) ratios investigated ranged from 1.44 to 3. The nozzles were machined in a flat surface which was then fixed onto the exit of a large pressure let down facility. The nozzles are straight cylinders and the nozzle entrances and exits were sharp but with all burrs removed.

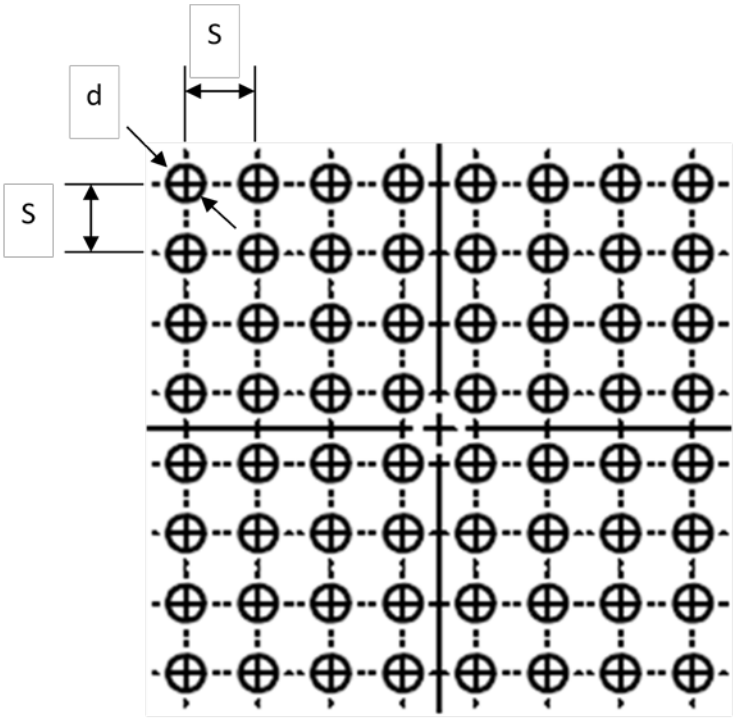

Figure 3.1: Schematic View of a Typical Jet Array.

The NPR values investigated ranged between 2 to 24. This ratio is defined as the static pressure of the flow, acquired upstream of the jet arrays, over the pressure of the quiescent medium, in this case the atmosphere. Static pressure measurements were acquired with an Omega PX309-500G5V pressure transducer and differential pressure measurements were

* Appendices omitted from actual manuscript.

acquired with a pitot tube and an Omega PX409-015WU5V. Temperature measurements were acquired with a type K thermocouple. Table 3.1 shows the full range of nominal NPR values investigated. To provide single jet comparisons, measurements of single hole plates with 3.2 mm and 6.4 mm diameters were also acquired for comparison and are listed in Table 3.2. The 25.4 mm (1 in.) and 50.8 mm (2 in.) diameter single jets represent the total exit area of 3.2 mm and 6.4 mm diameter arrays from Table 3.1, respectively. In summary, fourteen 8x8 arrays and four single jets were investigated for a total of eighteen plates. For each plate, measurements were acquired at approximately 10 NPR values.

Table 3.1: Nominal Net Pressure Ratios Investigated for 8x8 Jet Arrays

Nozzle Spacing over Diameter	*Nozzle Diameters (millimeters)*			
	3.2 (1/8 inch)	***3.7 (18/125 inch)***	***4.0 (5/32 inch)***	***6.4 (1/4 inch)***
1.44	2,3,4,6,8,10, 12,15,20,24	2,3,4,6,8,10, 12,15,20,24	2,3,4,6,8,10, 12,15,20,24	2,3,4,6,8,10, 12,15,20,24
2	2,3,4,6,8,10, 12,15,20,24	*None*	*None*	2,3,4,6,8,10, 12,15,20
2.5	2,3,4,6,8,10, 12,15,20,24	2,3,4,6,8,10, 12,15,20,24	2,3,4,6,8,10, 12,15,20,24	2,3,4,6,8,10, 12,15,20,24
3	2,3,4,6,8,10, 12,15,18,20,24	2,3,4,6,8,10, 12,15,20,24	2,3,4,6,8,10, 12,15,20,24	2,3,4,6,8,10, 12,15,20,24

Table 3.2: Nominal Net Pressure Ratios Investigated for Single Jets

Nozzle Diameters (millimeters)	***3.2 (1/8 inch)***	***6.4 (1/4 inch)***	***25.4 (1 inch)***	***50.8 (2 inches)***
Net Pressure Ratios	2,3,4,6,8,10, 12,15,20,24	2,3,4,6,8,10, 12,15,20,24	2,3,4,6,8,10, 12,15,20,24	2,3,4,6,8,10, 12,15,20,24

Measurements for the fully expanded Mach numbers (M_j) and mass flow rates ($\dot{m}$) display consistent increase with increasing NPR. The values for the 4.0 mm diameter jet arrays will be used as an example in this section. Table 3.3 presents the NPR, fully expanded Mach numbers, and mass flow rates for the 4.0 mm jet arrays. The full compilation of numerical results can be observed in Appendix B*.

Table 3.3: Net Pressure Ratios, Fully Expanded Mach Numbers, and Mass Flow Rates for d = 5/32 in. Jet Arrays.

S/d = 1.44			S/d = 2.5			S/d = 3		
NPR	***M_j***	***$\dot{m}$ (kg/s)***	***NPR***	***M_j***	***$\dot{m}$ (kg/s)***	***NPR***	***M_j***	***$\dot{m}$ (kg/s)***
2.1	1.1	1.3	2.2	1.1	1.4	2.3	1.0	1.5
3.0	1.4	1.8	2.9	1.3	1.7	3.2	1.4	1.9
4.1	1.6	2.7	3.9	1.5	2.4	3.9	1.6	2.5
6.0	1.8	3.6	5.5	1.8	3.3	6.3	1.8	3.6
8.1	2.0	4.5	8.4	2.0	4.8	8.0	2.0	4.2
10.2	2.2	6.2	10.3	2.2	5.7	9.9	2.2	6.0
12.1	2.3	7.6	13.1	2.3	6.2	13.2	2.3	8.0
15.2	2.4	9.5	14.9	2.4	8.4	14.5	2.4	7.4
20.2	2.6	10.9	20.1	2.6	11.6	19.7	2.6	12.4
24.2	2.7	15.3	23.5	2.7	13.2	23.2	2.7	13.8

In the field of supersonic jet noise it is common to relate acoustic parameters to the fully expanded Mach number which takes into account the NPR as well as the density of the supersonic fluid, theoretically, based upon measured parameters. But, since the fully expanded point cannot be determined when the fluid shocks from a jet array interact it would not be appropriate to present a theoretical calculation which does not have a physical representation. Thus, this paper presents acoustic parameters which are based upon the NPR.

* Appendices omitted from actual manuscript.

The facility used to produce the range of NPR values was the high pressure blowdown facility owned by Brigham Young University's Mechanical Engineering Department. This facility has a maximum capacity of 11.0 MPa and a total volume of 24.1 m^3. Flow was released through a control valve which controls the air flow passing through the array. Just downstream of the control valve is 15.2 cm (6 in.) schedule 80 piping that expands to 20.3 cm (8 in.) schedule 80 piping. The plates are mounted at the exit of the 20.3 cm pipe section where shadowgraph images and acoustic measurements were acquired. Figures of the Blowdown Facility can be observed in Appendix A*.

The acoustic emissions were measured with a 6 .4 mm GRAS 40BE free field microphone. The frequency range for this type of microphone is 10 Hz to 100 kHz and has a dynamic range of 40 dB to 170 dB; consistent with the range necessary to measure supersonic jet noise. The microphone was placed at 30° degrees off the centerline axis of the flow, as seen in Figure 3.2, consistent with the research of Yu[6], and Norum and Seiner[4], and at a 1 m radius. Past research has confirmed that at 30° offset from the centerline axis of the flow is the highest acoustic pressure output from a single axisymmetric supersonic jet. Thus, at this position the acoustic emissions from the main noise mechanism being acquired will be turbulent mixing noise[3 - 7] and screech[10 - 19]. At this location there is not a consistent scaled distance, or in other words, ratio of nozzle radius-over-distance (r/D). However, the geometric spreading for the acoustic emissions for 8x8 jet arrays is currently unknown, specifically for when the fluid shocks from the jet arrays interact. Thus, a consistent distance is used for all scenarios in this paper.

* Appendices omitted from actual manuscript.

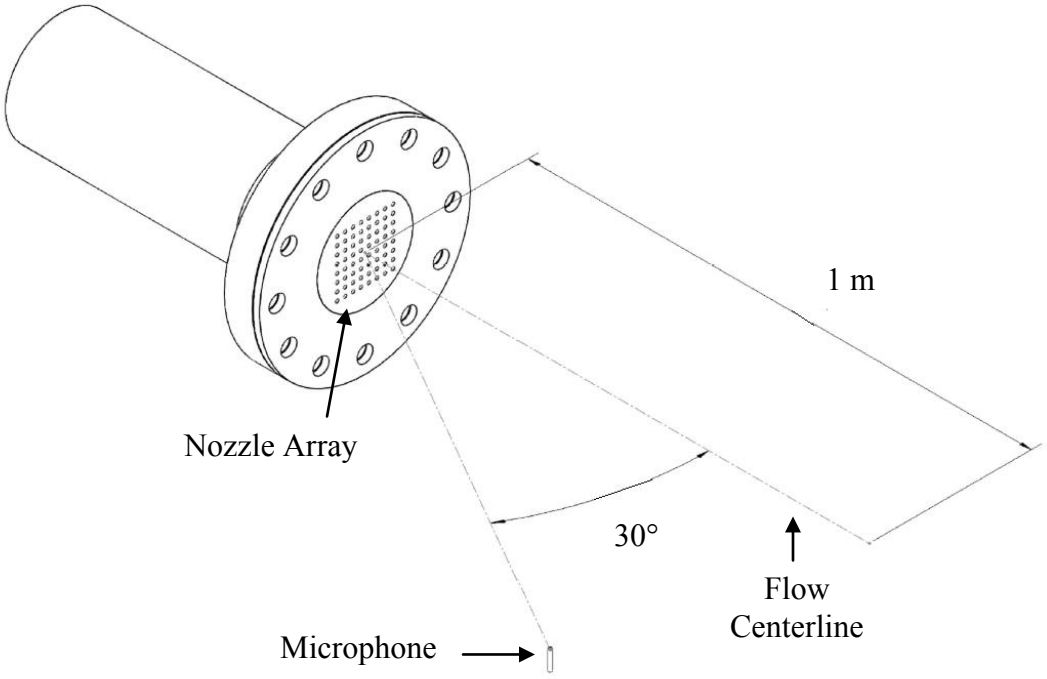

Figure 3.2: Microphone Experimental Setup

Shadowgraph was chosen as the technique to visualize shock cell formations that can be correlated with the trends in overall sound level radiation. The images presented in this paper view the arrays from the side such that eight shock cell structures are evident with the flow from left to right. Shadowgraph images for all the test configurations given in Table 1 were acquired. The trends observed in all the cases were similar, therefore only the shadowgraph images for the 4.0 mm (5/32 inch) diameter jet arrays will be shown in this paper. The full compilation of shadowgraph imagery can be observed in Appendix C*.

* Appendices omitted from actual manuscript.

3.5 Shock Formations

A shadowgraph analysis of the jet flow is useful in examing trends in overall sound radiation as for various jet configurations. Figures 3.3 - 3.5 display shadowgraph images for 4.0 mm diameter jet arrays with S/d ratios of 1.44, 2.5, and 3, respectively. The jets display three stages of shock formations. These shock formations consist of standard shock cells for individual jets as well as shock lattices which form when the shock cells expand large enough to interact with their neighbors. The shock lattices can be observed in Figs. 3.3b – 3.3f, Figs. 3.4c – 3.4d, and Fig. 3.5d.

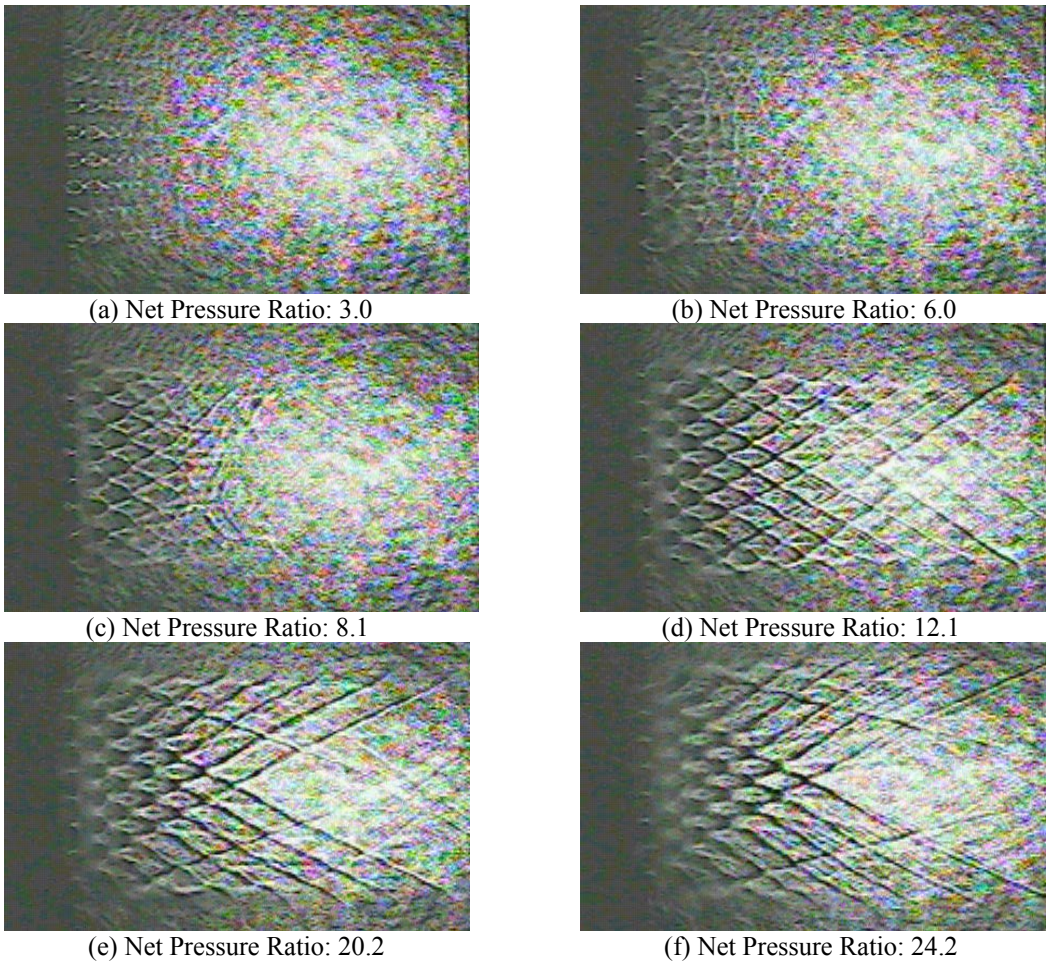

(a) Net Pressure Ratio: 3.0 (b) Net Pressure Ratio: 6.0

(c) Net Pressure Ratio: 8.1 (d) Net Pressure Ratio: 12.1

(e) Net Pressure Ratio: 20.2 (f) Net Pressure Ratio: 24.2

Figure 3.3: Shadowgraph Images for a 4.0 mm Diameter Jet Array and S/d ratio of 1.44 and at NPR values ranging from 3.0 to 24.2.

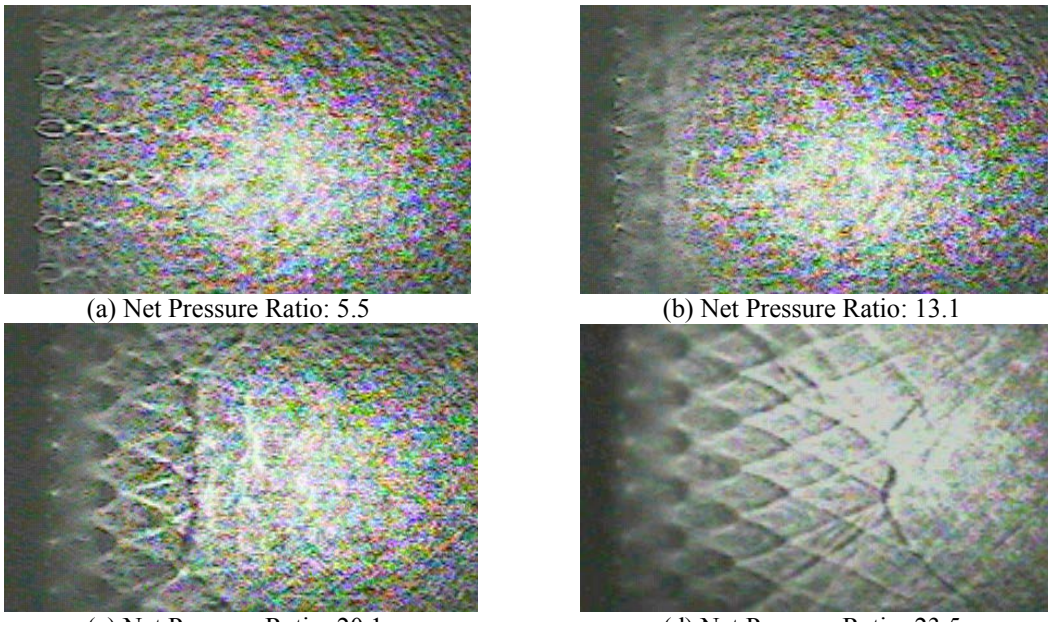

(a) Net Pressure Ratio: 5.5 (b) Net Pressure Ratio: 13.1

(c) Net Pressure Ratio: 20.1 (d) Net Pressure Ratio: 23.5

Figure 3.4: Shadowgraph Images for a 4.0 mm Diameter Jet Array and S/d ratio of 2.5 and at NPR values ranging from 5.5 to 23.5.

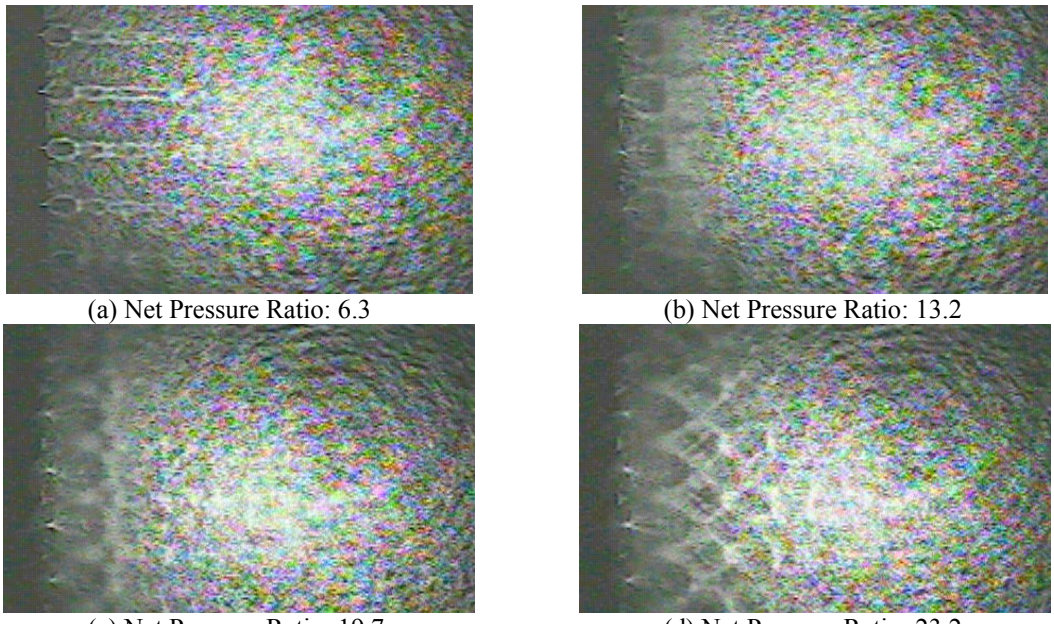

(a) Net Pressure Ratio: 6.3 (b) Net Pressure Ratio: 13.2

(c) Net Pressure Ratio: 19.7 (d) Net Pressure Ratio: 23.2

Figure 3.5: Shadowgraph Images for a 4.0 mm Diameter Jet Array and S/d ratio of 3 and at NPR values ranging from 6.3 to 23.2.

In order to best explain the stages of shock formation Fig. 3.3 is used as an example. Figure 3.3a displays supersonic jet shock formations typical of single jets. Here, the jets are

forming individual shock cells which do not significantly interact with neighboring jets. As the NPR is increased the sizes of the shock cells expand, but do not interact with neighboring shock cells below an NPR of approximately 6. As the NPR is increased further the shock cells of the individual jets expand enough to interact with each other, aside from modest entrainment towards the center of the array. This interaction is defined as shock interaction, where several jets are involved in creating a single shock. When this event occurs in several places it creates a lattice of shockwaves as observed in Figs. 3.3b – 3.3f.

The shock lattices go through two stages of formation; oscillatory and stable. The characteristic of oscillatory shock formation is the unstable nature of the flow; this can be seen in Figs. 3.3b – 3.3c as irregularly shaped, small-scale shock cells that are merging. This unstable nature involves the transient movement of shocks within the shock lattice as well as a flapping motion of the jet just outside of the lattice. The oscillatory shock lattice also somtimes generates screech tones. This is also confirmed by examining the measured pressure spectra observed in Fig. 3.6, as the NPR is increased. The most prominent tone in the spectra can be observed at an NPR of 8.1 which corresponds to the oscillatory shock lattice structure observed in Fig. 3.3c. Although other spectra containing screech tones can also be correlated with oscillatory shock lattices produced by jet arrays a further examination of screech produced by shock lattice formation in jet arrays is beyond the scope of this paper.

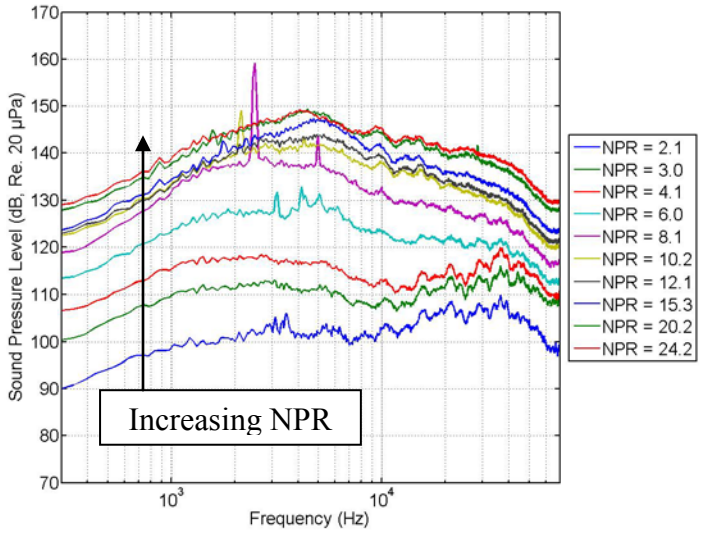

Figure 3.6: Frequency Spectra for a 4.0 mm Diameter Jet Array and S/d ratio of 1.44.

Stable, well defined shock lattice formations occur in Figs. 3.3d -3.32f. They are characterized by their symmetrical formation of oblique shocks about the jet centerline and flow conditions that are non-oscillatory. Figure 3.3d illustrates that the lattice structure is much longer than those occurring at lower NPR values. As the NPR is increased further, the outer oblique shocks shown in Fig. 23.3d are pushed further outward, resulting in a much larger scale, pyramidal shock lattice evident in Figs. 3.3e – 3.3f. It should be noted that once the shock lattice forms these pyramidal type structures there is little change in the structure with increasing NPR.

Comparison of the shadowgraph images from Figs. 3.3 – 3.5 reveal that when the jet spacing is increased the NPR level where interaction between jets first occur also increases. In other words, for constant NPR, a greater separation relative to nozzle diameter results in less jet interaction. In Fig. 3.3 (S/d = 1.44) the initial shock interaction occurs at an NPR of approximately 6. In Fig. 3.4 (S/d = 2.5) shock sharing first occurs at an NPR of approximately 13 to 14, and in Fig. 3.5 (S/d = 3) shock sharing first occurs at an NPR of approximately 20. The images of Figs. 3.4 and 3.5 reveal that weak lattice formations occur at NPR values of ranging

approximately from 20 to 24 for S/d = 2.5, and at an NPR of approximately 24 for S/d = 3. This comparison reveals the mutual importance of S/d and NPR in the transition of the array from multiple individual jets to a merged jet with a stable shock lattice.

3.6 Overall Sound Pressure Levels

The overall sound pressure level (OASPL) is the root mean square of the acoustic signal which is detected by the microphone and translated onto a logarithmic scale as defined by Equation 3.1. Here it is used as a measure of the overall noise emitted from the arrays. The OASPL for the single jet scenarios will first be presented and discussed; then the OASPL for the jet arrays will be presented.

$$OASPL = 20\log\left(\frac{rms(P_{acoustic})}{P_{ref}}\right) \tag{3.1}$$

Figure 3.7 presents the OASPL as a function of the NPR for four single jets with diameters of 3.2, 6.4, 25.4, and 50.8 mm. As discussed previously, all results are for a common measurements location (1 m), which corresponds to different scaled distances. As expected, from a common measurement position the OASPL increases with nozzle diameter for fixed NPR. As shown, between NPR values of approximately 2 - 5 there is a sharp rise in the OASPL for all single jet diameters. After the initial rise, the slopes of the OASPL vs. NPR data decrease and exhibit only modest increase as the NPR increases. Although the scope of this research investigates significantly higher NPR values, the overall behavior of the OASPL seen here for single jets is similar to the results presented by Powell *et al.*[19] and Umeda, and Ishii [17] for single,

two, and four jet arrays. Specifically meaning the steep initial rise in OASPL before an NPR of approximately 5 followed by either only a modest increase, decrease, or leveling off in the data.

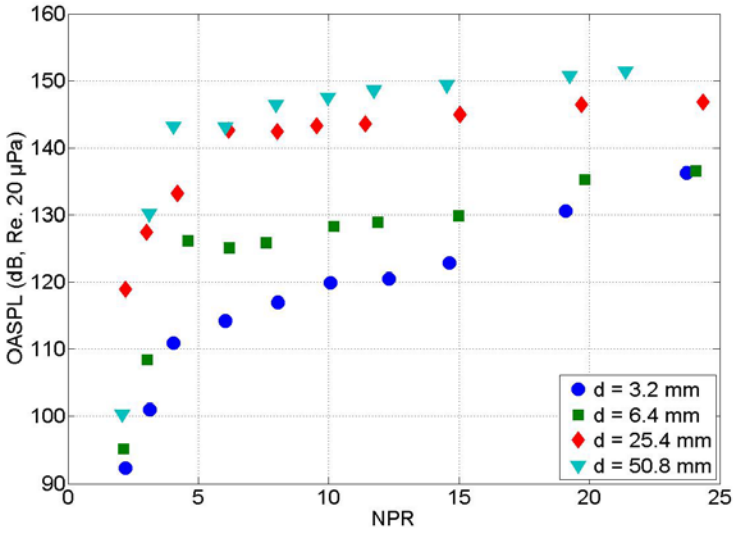

Figure 3.7: Overall Sound Pressure Levels as a function of the NPR for Single Jets of Diameters 3.2 mm, 6.4 mm, 25.4 mm, and 50.8 mm.

Measurements for the OASPL of the 8x8 jet arrays are shown in Figs. 3.8 – 3.11 for S/d = 1.44, 2, 2.5, and 3 respectively. Note that Figs. 3.8 – 3.10 are divided into three regions labeled A, B, and C. Figure 3.11 is also divided, but only into two regions instead of three, labeled A and B. These regions will be used to identify the noise characteristics of the jet arrays as well as correlate the visualizations of shock formations with the measured OASPL.

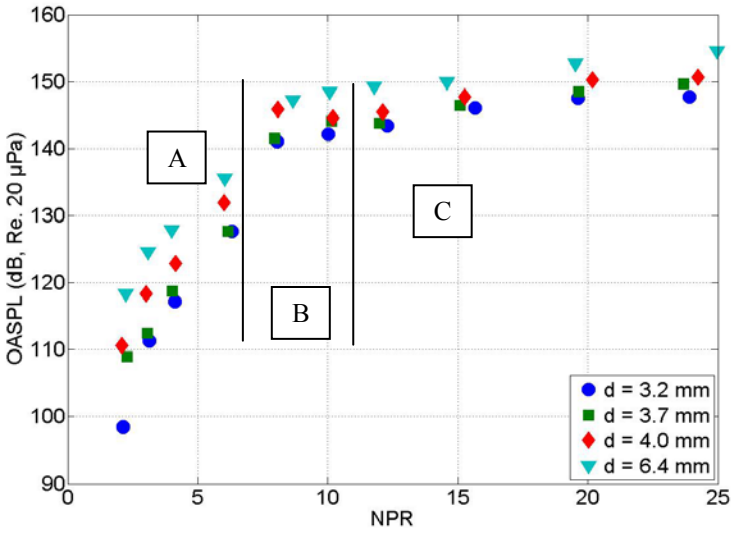

Figure 3.8: Overall Sound Pressure Levels as a function of the NPR for Jet Arrays with S/d ratios of 1.44.

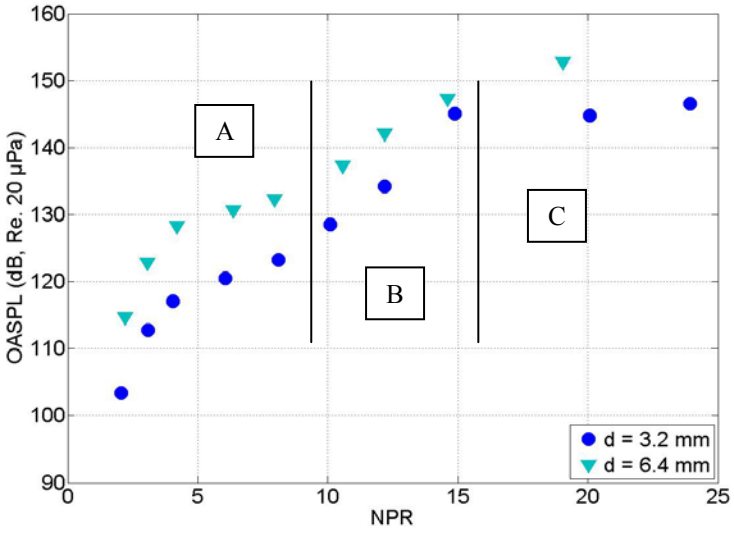

Figure 3.9: Overall Sound Pressure Levels as a function of the NPR for Jet Arrays with S/d ratios of 2.

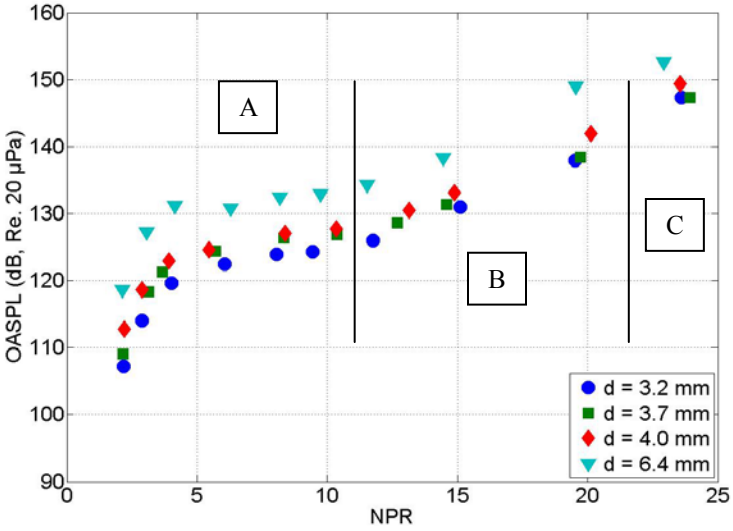

Figure 3.10: Overall Sound Pressure Levels as a function of the NPR for Jet Arrays with S/d ratios of 2.5.

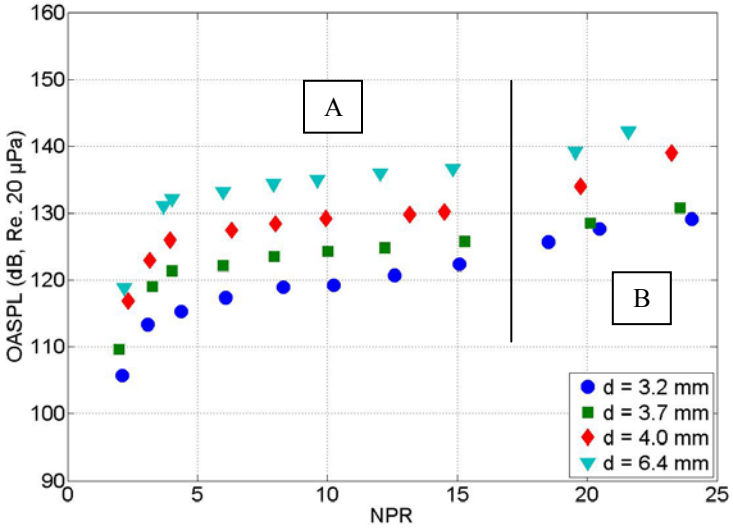

Figure 3.11: Overall Sound Pressure Levels as a function of the NPR for Jet Arrays with S/d ratios of 3.

The OASPL data in region A show characteristics similar to a single jet. In this region the data exhibit a sharp initial rise followed by only a modest increase in the OASPL. This behavior is best illustrated in Figs. 3.8 – 3.11. The data from Figs. 3.9 – 3.11 reveal that region A extends over a smaller range of NPR values as the S/d ratio is reduced. Thus, for S/d = 1.44 (Fig. 3.8),

the OASPL data never level off because region A is so short that region B occurs right after the steep initial rise in the OASPL.

At NPR values above region A, the OASPL for the jet arrays are no longer similar to the single jet noise characteristics. Rather, the data begin to display characteristics unique to that of interacting jet arrays. Figure 3.10 will be used as an example in order to better explain these unique characteristics. Figure 3.10 presents the OASPL for a 4.0 mm diameter jet array with S/d = 2.5. The data in region B in Fig. 3.10 exhibit an upward trend in the OASPL with increasing NPR. This occurs until the OASPL for the jet arrays level off at a higher OSPL level (Region C) as compared to region A. In summary, the OASPL in region A is similar to that of a single jet of the same diameter as one of the array jets. Also, Region C can be viewed as a region where the radiated noise has leveled off to much higher nominal levels as compared to region A. Region B can be viewed as the transition region between these two regimes.

Comparison of region B in Figs. 3.8 – 3.11 shows that the transition regime shifts to higher NPR values as S/d increases. The larger the S/d ratio, the higher the NPR where region B begins. The total NPR range over which region B extends also increases as a function of S/d.

The variation in the OASPL with varying jet diameter also varies with the S/d. As observed in Fig. 3.11 (S/d = 3), the OASPL data for the four jet diameters (3.2 – 6.4 mm) show marked variation. Conversely, when the nozzles are spaced more closely together, as seen in Fig. 3.8 where S/d = 1.44, the OASPL data for each of the four nozzle diameters are clustered more tightly. In general, the data of Figs. 3.8 – 3.11 reveal that for increasing S/d, the OASPL values for the four different nozzle sizes show greater variation. For all S/d, the largest OASPL values correspond to the 6.4 mm diameter jet arrays and the lowest OASPL values correspond to the 3.2 mm diameter arrays. A portion of this increase, but not all, can be attributed to the fact that the

measurements for the larger diameter jet arrays for constant S/d were made at a closer scaled distance.

Figures 3.12 and 3.13 present the OASPL data for the 3.2 and 6.4 mm jet arrays along with corresponding single jet data. Figure 3.12 displays the OASPL for the 3.2 mm diameter jet arrays, a 3.2 mm diameter single jet, and a 25.4 mm diameter single jet with equal total exit area as the 3.2 mm jet array. Likewise, Fig. 3.13 presents the OASPL for 6.4 mm diameter jet arrays, a 6.4 mm diameter single jet, and a 50.8 mm diameter single jet. Again, the 50.8 mm jet represents the same total exit area as the 6.4 mm diameter jet array.

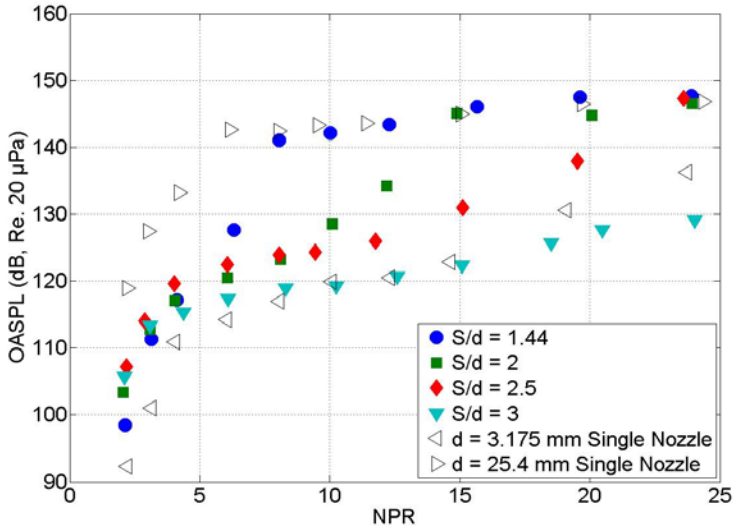

Figure 3.12: Overall Sound Pressure Levels as a function of the NPR for 3.2 mm Diameter Jet Arrays, a 3.2 mm Diameter Single Jet, and a 25.4 mm Diameter Single Jet.

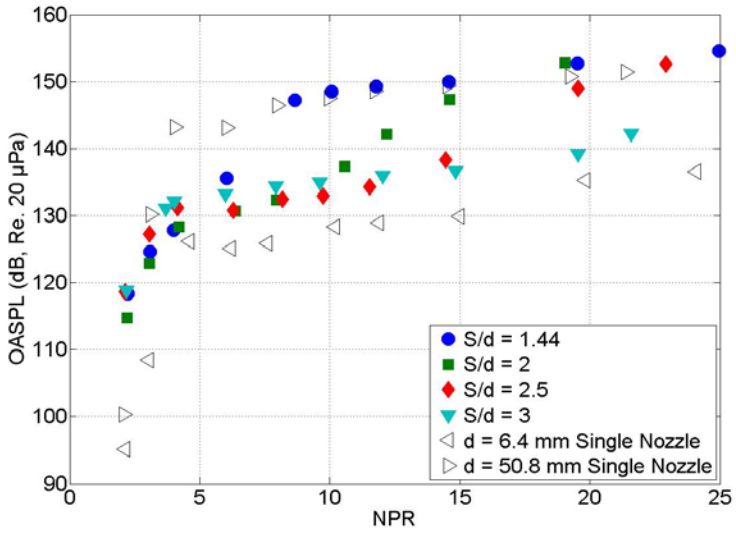

Figure 3.13: Overall Sound Pressure Levels as a function of the NPR for 6.4 mm Diameter Jet Arrays, a 6.4 mm Diameter Single Jet, and a 50.8 mm Diameter Single Jet.

The single jet data from Figs. 3.12 and 3.13 yield approximately an upper (25.4 and 50.8 mm) and lower bound (3.2 and 6.4 mm) about the OASPL data from the jet arrays. Within the bounds formed by the single jet data, the 8x8 jet arrays transition from a point near the lower bound (OASPL level trends equivalent to a single jet, or incoherent sum of multiple single jets) to a point near the upper bound (OASPL levels equivalent to a nozzle with an equal exit area to that of an entire array) as the NPR increases. This transition occurs at different NPR values depending on the S/d ratio for the array. As evidenced by Figs. 3.12 and 3.13, as the S/d increases the transition from the lower bound to the upper bound occurs at higher NPR values.

The bounding behavior of the single jets shown in Figs. 3.12 and 3.13 can also be described in terms of regions A - C. The jet array data which reside near the lower bound, before they transition, correspond to region A. The jet array data which lie near the upper boundary, after they transition, correspond to region C. All the jet array data that lie within the bounds from the single jets are within region B.

3.7 Shock Formations and Overall Sound Pressure Levels

The shock formation structures and OASPL from a supersonic jet array have been shown to be functions of both NPR and S/d. This section correlates the observed shock formations from the shadowgraph images and the OASPL in order to more fully understand the acoustic emissions of jet arrays.

The OASPL plots in Figs. 3.8 – 3.11 were divided above into three regions, A - C. These regions can be correlated with the three stages of shock formations. A Comparison region A from Figs. 3.8 – 3.11 to the shadowgraph images from Figs. 3.3a, 3.4a, and 3.5a reveals that when the array jets are unmerged, the overall levels are similar to that of a single smaller jet (or perhaps the sum of the individual, unshielded jet responses closest to the microphone). Examination of region B from Figs. 3.8 – 3.11 jointly with Figs. 3.3b – 3.3c, 3.4b – 3.4c, and 3.5b – 3.5c reveals that when the shock interaction has begun and an oscillatory, unstable shock lattice has formed the OASPL is transitioning more rapidly from a lower level to a higher level. Finally, a comparison of region C to Figs. 3.3d – 3.3f, and 3.4d reveal that when the jets have formed a lattice of stable shocks, the jets have transitioned to a greater OASPL that is equivalent to a single larger jet of the same total exit area. Thus, it is evident that the acoustic emissions from jet array are similar to the turbulent mixing noise of single jets at lower NPR values. When the jets interact the turbulence increases, which results in increasing the acoustic levels similar to that of a single jet of equivalent exit area to an entire jet array.

The transition of the OASPL from that of a single small jet to a single larger jet is initiated by the interaction and merging of shocks between the multiple small jets of the array. For example, Fig. 3.3b, which displays a shadowgraph image of a 4.0 mm diameter jet array, with S/d = 1.44 at an NPR of 6.0, where there is initial shock interaction, can be correlated with

Fig. 3.8, which displays the OASPL for that array. At this NPR the OSPL from the array has transitioned from region A to region B. Figures 3.4b and 3.10, and Figs. 3.5c and 3.11 also confirm this behavior.

3.8 Conclusion

This paper has reported on an experimental investigation of the acoustic emissions of arrays of parallel supersonic jets. The supersonic jet arrays were observed to produce three types of shock structures, depending upon the NPR. The first shock structure consisted of standard shock cells produced from the individual jets. These shock cells behave similar to single jets up until they expand sufficiently enough to interact with their neighbors. The second shock structure occurs when the shock cells interact with their neighbors and multiple jets are involved in the formation of a single shock; when this occurs in several places a lattice of shocks is produced. The lattice goes through two stages of shock formation; oscillatory and stable. The oscillatory lattice formation is the initial formation and consists of a flapping motion of the overall jet stream and transient motion of shocks within the shock lattice. As the NPR is increased the oscillatory formation stabilizes and there is no longer any transient activity. As the jets within the arrays are spaced farther apart the stages of shock formations occur at higher NPR values.

The radiated OASPL, generated from turbulent energy and narrowband screech tones, also transition between three stages. The first region is similar to that of a single jet; where there is a sharp initial increase below an NPR of approximately 5, and then the slope of the OASPL vs. NPR decreases while exhibiting only modest increase as the NPR increases. The second stage revealed a more rapid increase in OASPL with increasing NPR. The last stage is a region where the slope of the OASPL vs. NPR decreases while still on exhibiting modest increase again. The

transition between the first and final regions occur at higher NPR values as the jet spacing increases.

The OASPL measurements for single jets have been shown to nearly envelope those of the arrays. The lower boundaries of the envelope consists of data for a single jet with a nozzle diameter equal to one of the jets within the array, while the upper boundary consists of data for a jet with an equivalent exit area to the entire array.

The three stages of shock structures correlate well with the three OASPL regions. The first region consists of unmerged shock cells. In the second region an oscillatory shock lattice exists. And in the third region a stable shock lattice forms. Thus, the existence of a shock lattice alters the turbulence of a jet array to a turbulent acoustic response of a larger jet with an exit area equivalent to an entire jet array.

An extension of this investigation can go into the geometric spreading of the acoustic pressure that 8x8 jet arrays exhibit in the near field. Particular interest focuses on the point of sound generating and acoustic lobing before and after jet interaction. Such an investigation would require a larger array of microphones.

A further investigation can go into the characteristic frequency content for 8x8 jet arrays acquired at the same location presented in this investigation. Similar to the idea of geometric spreading, focus would be on the characteristic frequency content before and after jet interaction.

3.9 Acknowledgements

The authors would like to acknowledge Control Components Inc. for their generous support of this research.

Chapter 4. Influence of Nozzle Spacing and Diameter on the Acoustic Emissions of Closely Spaced Supersonic Jets

This chapter is a manuscript to be submitted to the Journal of the Acoustical Society of America. The Formatting of the paper has been modified to meet the stylistic requirements of this thesis.

4.1 Contributing Authors and Affiliations

Ian S. Coltrin, R. Daniel Maynes, Jonathan D. Blotter
Department of Mechanical Engineering, Brigham Young University, Provo, UT 84602

Kent L. Gee
Department of Physics and Astronomy, Brigham Young University, Provo, UT 84602

4.2 Abstract

Acoustic emissions were characterized for 14 8x8 arrays of axisymmetric supersonic jets experimentally. The results were compared to two types of single jets of equivalent flow areas. The nozzle diameters ranged from 3.2 mm (1/8 in.) to 6.4 mm (1/4 in.) and the spacing over diameter ratios ranged from 1.44 to 3. The arrays were tested at several net pressure ratios ranging from 2 to 24. It was found that up to a critical net pressure ratio, the arrays radiated ultrasonic characteristic frequencies. Beyond this critical net pressure ratio the characteristic frequency decreased within audible range. A non-dimensional analysis revealed at the critical net pressure ratio a dramatic reduction in the characteristic Strouhal number; based upon the

characteristic frequency and fully expanded jet diameter and velocity. Small increase in the characteristic acoustic pressure was also observed at net pressure ratios below the critical net pressure ratio and a larger increase was observed at higher net pressure ratios. The critical net pressure ratio appeared to be a linear function of the spacing over diameter ratio for the nozzle arrays. A linear curve fit was applied to the experimental critical net pressure ratio and compared to a developed theoretical model. The experimental results predicted that the critical net pressure ratio occurred at slightly lower net pressure ratios than the theoretical model predicted.

4.3 Introduction

Research into the acoustic emissions from supersonic jets represent an area of significant need. It is important in industries such as aero-acoustics, where jet exhausts have been known to cause structural fatigue of aircraft and overall severe human discomfort, and the energy industry where acoustic loadings created from large pressure drops have been known to cause pipe failure within hours. Thus, this research has been conducted to better understand the acoustic emissions from multiple supersonic jets which are able to create severe acoustic loads.

Methods to predict the acoustic loads from supersonic jets are of great research interest. Models derived by Carucci and Mueller[1], and Eisinger[2] predict acoustic loads caused by high pressure gases in piping networks based upon parameters upstream of the flow. Although these models are used as a standard in most cases they are not able to reduce acoustic emissions. In Carucci and Mueller's paper on flow induced noise they suggest a form of reducing acoustic emissions by implementing Venturi slots within a valve to divide a single larger flow into several smaller parallel plane jets. The research in this paper takes advantage of that concept by investigating the acoustic emissions from arrays of several smaller jets.

An initial investigation into the acoustic emission of several parallel supersonic jet flows was performed by Coltrin *et al.*[*] The goal of their investigation was to apply their results to reduce acoustic loadings by di viding a larger flow into several smaller ones. Coltrin *et al.* investigated several 8x8 array of supersonic jets at relatively high net pressure ratios (NPR), as compared to previous investigations[17 - 19], in order to correlate the shock formations and the overall sound pressure levels (OASPL) emitted from the jet arrays. The point at which Coltrin *et al.* acquired their measurements correlated with the highest sound output from a single axisymmetric jet[4, 6]. At that point the two main noise mechanisms which contributed to the acoustic emissions being acquired were turbulent mixing noise[3 - 7] and screech[10 - 19].

Coltrin *et al.* showed that there are three stages of shock formation which occur from 8x8 jet arrays. The initial formation reveals shock cells for each of the jets of the array which do not interact with each other. The second occurs as the NPR increases and the shock cells expand to the point where they interact with each other and form a lattice of oblique shocks. This stage is defined as the oscillatory stage due to transient oscillations of the shocks within the lattice. The last stage is defined as the stable shock lattice and occurs as the NPR is increased further and the shock lattice stabilizes.

The interaction of shocks was observed to significantly alter the acoustic emission from the jet arrays. Initially, as the shocks are unmerged, the OASPL emitted from the array were similar to that of a single jet within the array. But as the jet arrays formed an oscillatory to stable shock lattice the OASPL transitioned to turbulent noise levels similar to those emitted from a single jet of equivalent exit area to an entire jet array. The interaction of shocks and increased acoustic emissions were shown to be strong functions of the center to center spacing of the 8x8

[*] Reference, "Coltrin *et al.*," refers to Chapter 3: Shockwave Structures and Overall Sound Pressure Levels Emitted From Closely Spaced Supersonic Jet Arrays.

jet arrays over the diameter ratios (S/d). Spacing the jet nozzles farther apart caused shock interaction to occur at high NPR values. This paper extends the investigation performed by Coltrin *et al.* by examining the frequency content as well as the changing acoustic pressures and relating those parameters to the flow regime.

This investigation works off of a principle discovered by Seiner *et al.*[3]. Seiner *et al.* revealed that for a single supersonic axisymmetric jet the characteristic Strouhal number is nominally 0.2. The Strouhal number is a non-dimensional parameter defined as the frequency times a characteristic length scale over the velocity. In the case of jet noise, the frequency is typically the frequency from the acoustic pressure wave, the characteristic length scale is the fully expanded jet diameter, and the velocity is the fully expanded jet velocity. Thus, if a fully expanded jet diameter is reduced while still maintaining an equivalent jet velocity, the characteristic frequency would have to rise.

In this paper research is presented into the acoustic emissions of several supersonic axisymmetric nozzle arrays. This research includes an investigation into the frequency content from the radiating acoustic pressure waves of the jet arrays as well as the change in the acoustic pressures with respect to differing flow regimes. Also, a comparison to two types of single jets is also made. The two single jet types are single jets of the same diameter as those in the arrays and single jets of equivalent flow area as the entire array.

4.4 Experiment

The goal of this research is to characterize the acoustical frequency spectra from 8x8 arrays of supersonic axisymmetric jets. A schematic view of a typical jet array is provided in Fig.

4.1. Figures of the jet arrays can be observed in Appendix A*. In this study the jet diameters investigated ranged from 3.2 mm (1/8 in.) to 6.4 mm (1/4 in.). The S/d ratios investigated ranged from 1.44 to 3. The jets are formed in straight cylindrical holes machined in a flat surface and then fixed to the exit of a large scale pressure let-down facility.

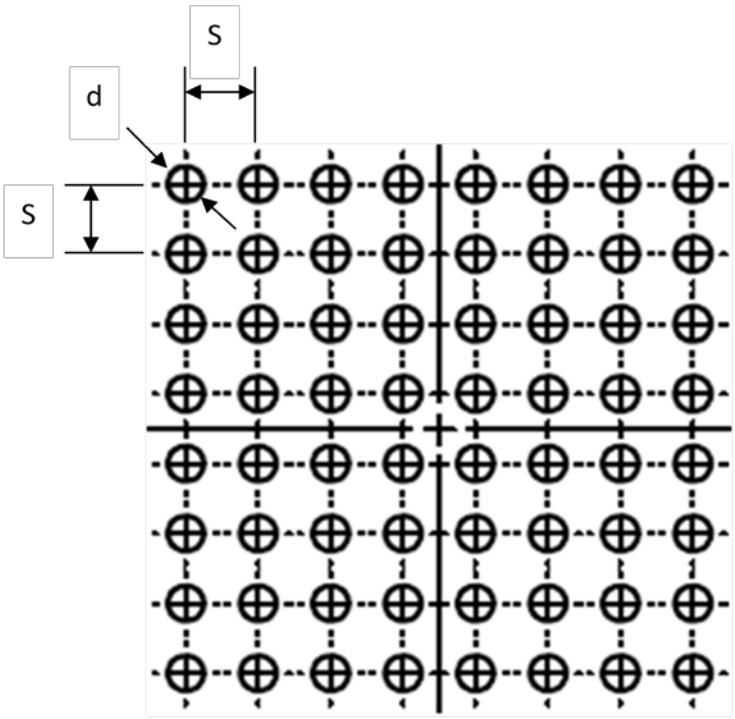

Figure 4.1: Schematic View of a Typical Nozzle Array

The NPR values investigated ranged from 2 to 24. The NPR is defined as the static pressure in a constant diameter pipe upstream of the jet array over the pressure of the quiescent medium the jets are exhausted into, the atmosphere in this case. Static pressure measurements were acquired with an Omega PX309-500G5V pressure transducer and differential pressure measurements were acquired with a pitot tube and an Omega PX409-015WU5V differential pressure transducer. Temperature measurements were acquired with a type K thermocouple. Table 4.1 presents the array configurations and nominal NPR values investigated. Single jet measurements were also acquired for comparison and are listed in Table 4.2. The 3.2 mm and 6.4

* Appendices omitted in actual manuscript.

mm diameter single jets from Table 4.2 represent a jet with the same diameter as those in the 3.2 mm and 6.4 mm diameter jet arrays from Table 4.1, respectively. The 25.4 mm (1 in.) and 50.8 mm (2 in.) diameter jets from Table 4.2 exhibit the same exit area as that of entire jet arrays for 3.2 mm and 6.4 mm diameter jets from Table 4.1, respectively. In summary, 14 8x8 jet arrays and 4 single jet plates were tested. For each jet configuration noise and flow data were acquired at approximately 10 NPR values.

Table 4.1: Nominal Net Pressure Ratios Investigated for 8x8 Jet Arrays

Nozzle Spacing over Diameter	*Nozzle Diameters (millimeters)*			
	3.2 (1/8 inch)	***3.7 (18/125 inch)***	***4.0 (5/32 inch)***	***6.4 (1/4 inch)***
1.44	2,3,4,6,8,10, 12,15,20,24	2,3,4,6,8,10, 12,15,20,24	2,3,4,6,8,10, 12,15,20,24	2,3,4,6,8,10, 12,15,20,24
2	2,3,4,6,8,10, 12,15,20,24	*None*	*None*	2,3,4,6,8,10, 12,15,20
2.5	2,3,4,6,8,10, 12,15,20,24	2,3,4,6,8,10, 12,15,20,24	2,3,4,6,8,10, 12,15,20,24	2,3,4,6,8,10, 12,15,20,24
3	2,3,4,6,8,10, 12,15,18,20,24	2,3,4,6,8,10, 12,15,20,24	2,3,4,6,8,10, 12,15,20,24	2,3,4,6,8,10, 12,15,20,24

Table 4.2: Nominal Net Pressure Ratio Investigated for Single Jets

Nozzle Diameters (millimeters)	***3.2 (1/8 inch)***	***6.4 (1/4 inch)***	***25.4 (1 inch)***	***50.8 (2 inches)***
Net Pressure Ratios	2,3,4,6,8,10, 12,15,20,24	2,3,4,6,8,10, 12,15,20,24	2,3,4,6,8,10, 12,15,20,24	2,3,4,6,8,10, 12,15,20,24

The facility used to provide the supply pressure was the high pressure blowdown facility owned by Brigham Young University's Mechanical Engineering Department. This facility has a maximum capacity of 11.0 MPa and a total volume of 24.1 m^3. Figures of the blowdown facility

can be observed in Appendix A*. The flow was released through a control valve that controlled the total supply pressure for a jet array. The control valve feeds into a 15.2 cm (6 in.) schedule 80 pipe that was expanded to a 20.3 cm (8 in.) schedule 80 pipe. The plates were then attached to the end of the 20.3 cm pipe section where acoustic measurements were acquired.

Acoustic measurements were acquired with a 6.4 mm (1/4 in.) GRAS 40BE free field microphone. This microphone has a dynamic range of 40 dB to 170 dB and a frequency range between 10 Hz to 100 kHz, consistent with the ranges necessary to measure the acoustic emissions of supersonic jets. The microphone was placed at 30° off the centerline axis of the flow, consistent with research done by Coltrin *et al.*, Yu[3], and Norum and Seiner[1], and at a 1 m radius as seen in Fig. 4.2. Coltrin *et al.* used this point to measure the acoustic emissions due to the maximum pressure output of supersonic axisymmetric jets emitted at approximately 30° off the centerline axis of the flow. At this angle the acoustic emissions from the main noise mechanisms of supersonic jets are turbulent mixing noise[3 - 7] and screech[10 - 19]. The acoustic measurements were sampled at 200 kHz.

* Appendices omitted from actual manuscript.

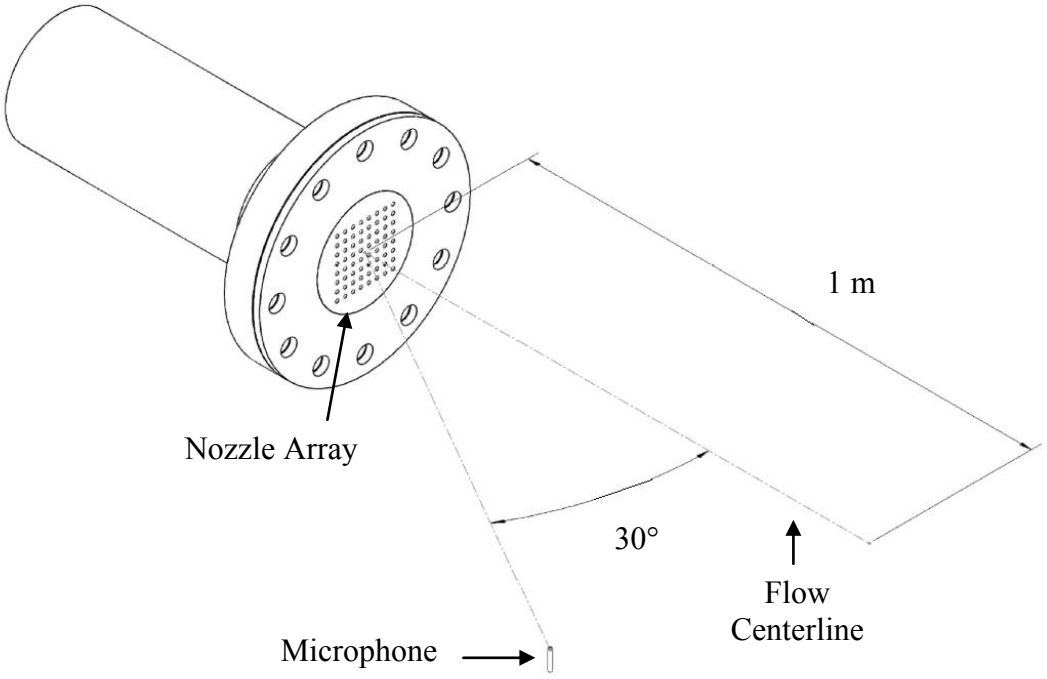

Figure 4.2: Microphone Experimental Setup

4.5 Results

4.5.1 Single Jets

Figures 4.3 and 4.4 present the acoustic pressure generated from turbulent mixing and screech in the frequency domain for the 3.2 mm and 25.4 mm diameter single jets, respectively. The characteristic sound pressure levels (SPL) from each of the nozzles displays a range of approximately 80 dB to 130 dB for the 3.2 mm diameter jet and 110 dB to 145 dB for the 25.4 mm diameter jet. Because screech tones only exist in some spectra they will be ignored, as well as their harmonics, when determining characteristic values. Examples of such screech tones are pointed out in Figs. 4.3 and 4.4. Comparing the spectra from the two figures reveals that there is a consistent increase in SPL with respect to increasing NPR for both nozzle diameters. The

amount of increase is dependent upon the diameter of the jet, with the smaller jet exhibiting characteristic SPL values that are initially quieter, however the SPL increases more dramtically with increasing NPR.

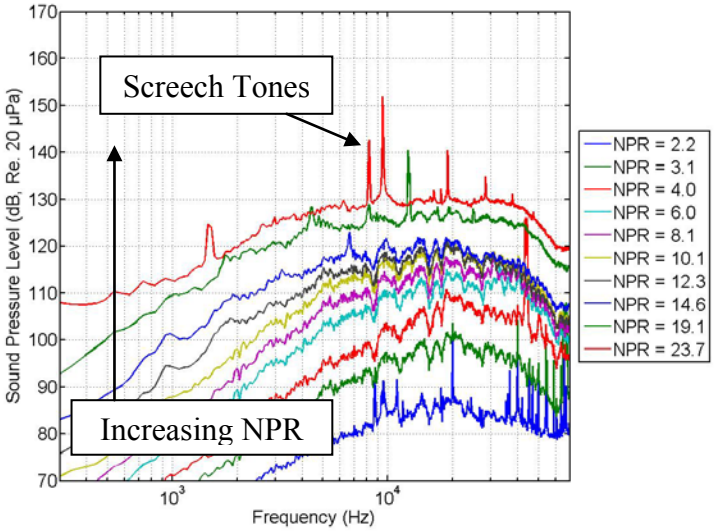

Figure 4.3: Frequency Spectra for a Single 3.2 mm Diameter Nozzle Jet and NPR Ranging From 2.2 to 23.7.

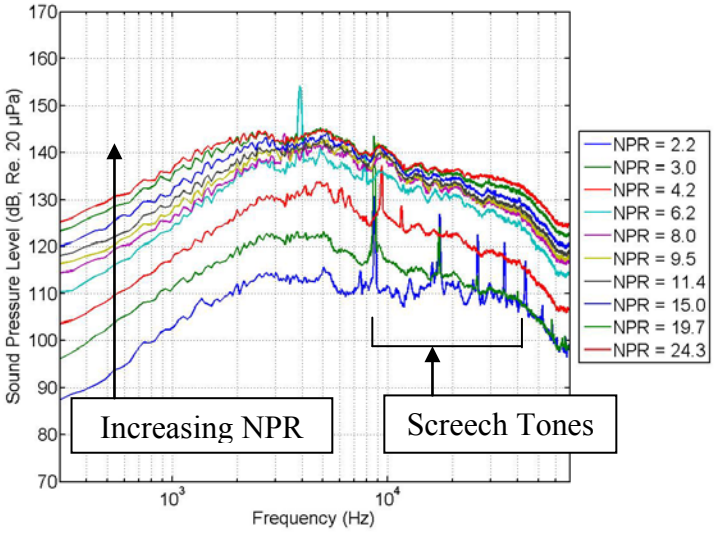

Figure 4.4: Frequency Spectra for a Single 25.4 mm Diameter Nozzle Jet and NPR Ranging From 2.2 to 24.3.

Ignoring screech tones, the characteristic frequencies for the jets represented in Figs. 4.3 and 4.4 are dependent upon nozzle size. For the 3.2 mm diameter jet (Fig. 4.3) the maximum

characteristic frequency is approximately 20 kHz for all NPR. For the 25.4 mm diameter jet (Fig. 4.4) the characteristic frequency is approximately 4 kHz for all NPR explored.

4.5.2 Jet Arrays

The results from the jet arrays revealed that the characteristics of interest were mainly functions of the S/d ratios and NPR. Since the results for the different jet diameters were similar, only the results for just the 4.0 mm diameter jet arrays are presented in this paper. The full compilation of frequency spectra can be observed in Appendix C*. Figures 4.5 – 4.7 present the acoustic pressure spectra generated from turbulent mixing and screech in the frequency domain for 4.0 mm diameter jet arrays with S/d ratios of 1.44, 2.5, and 3, respectively.

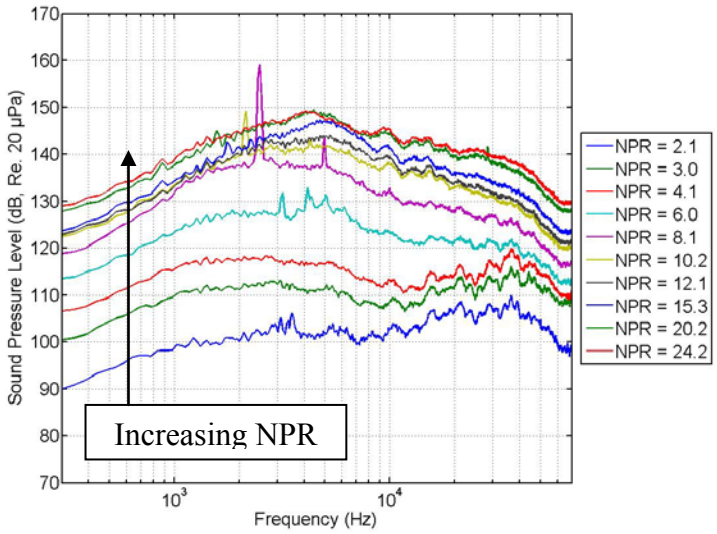

Figure 4.5: Frequency Spectra for a 4.0 mm Diameter Jet Array of S/d = 1.44 and NPR ranging from 2.1 to 24.2

* Appendices omitted in actual manuscript.

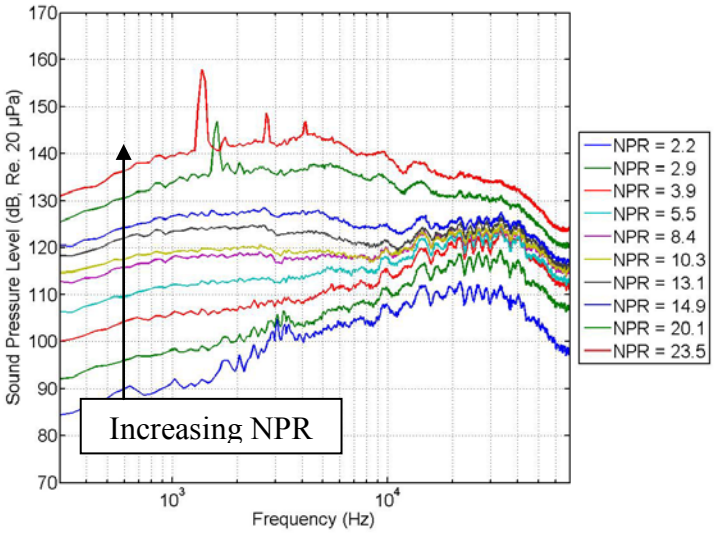

Figure 4.6: Frequency Spectra for a 4.0 mm Diameter Jet Array of S/d = 2.5 and NPR Ranging From 2.2 to 23.5

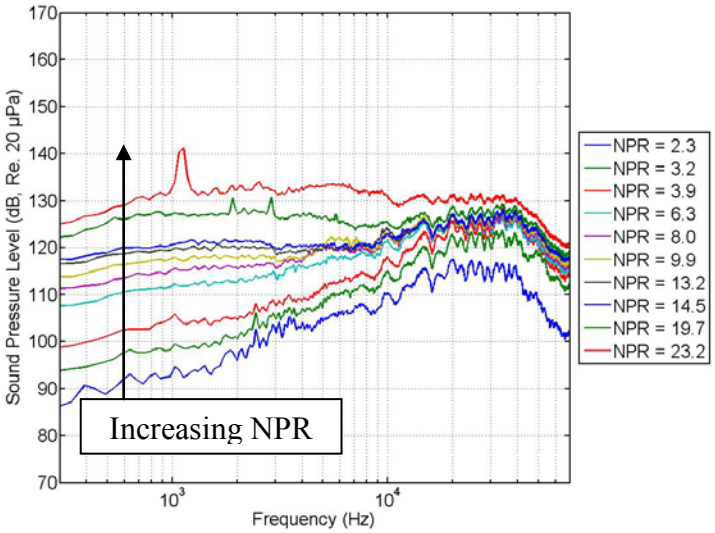

Figure 4.7: Frequency Spectra for a 4.0 mm Diameter Jet Array of S/d = 3 and NPR Ranging From 2.3 to 23.2.

Figures 4.5 – 4.7 reveal an interesting and important transition in characteristic frequencies for jet arrays, ignoring screech tones. At lower NPR values, the characteristic frequencies occur at approximately 40 kHz. However, as the NPR increases the characteristic frequencies shift to lower values. Comparing Figs. 4.5 – 4.7 reveal that the shift in characteristic frequency, from high to low, occurs at increased NPR values for increased S/d ratios. For S/d =

1.44 (Fig. 4.5) the shift occurs $4.1 \leq NPR \leq 6.0$; for S/d = 2.5 (Fig. 5) the shift occurs at $14.9 \leq NPR \leq 20.1$; and for S/d = 3 (Fig. 6) the shift occurs at $19.7 \leq NPR \leq 23.2$. Comparing Figs. 4.5 – 4.7 with Figs. 4.3 and 4.4 reveal that at lower NPR values the characteristic frequency for an entire jet array is similar to the spectra observed for the turbulent mixing noise of a jet with the same diameter as a jet within a jet array. However, at higher NPR values the characteristic frequency shifts to a value similar to the spectra observed for the turbulent mixing noise of a jet with an equivalent exit area to an entire jet array.

4.6 Analysis

One of the goals of this investigation is to characterize the acoustic emissions of an 8x8 jet array with the flow regime. This section of the paper applies non-dimensional analysis to combine the characteristic parameters which define both the acoustics and the flow. The acoustic parameters of interest include the frequency and sound pressure. The flow parameters of interest include the jet diameter, the jet velocity, and the jet density. Other parameters that have already been mentioned include the NPR, which describes the total pressure decrease of the system, and the S/d ratio, which describes the geometry of the arrays.

By combining the parameters of interest two non-dimensional parameters are generated; the Strouhal number, a common non-dimensional number used in jet noise[3], and the ratio of the acoustic pressure over the dynamic pressure (ADP). The definition of the Strouhal number can be found in Equation 4.1. The definition of the ADP ratio can be found in Equation 4.2.

$$St = \frac{f \cdot d_j}{u_j} \tag{4.1}$$

$$ADP = \frac{P_{acoustic}}{\frac{1}{2}\rho_j {u_j}^2} \tag{4.2}$$

In Equation 4.1, f represents the acoustic frequency, d represents the jet diameter, and u represents the jet velocity. In Equation 4.2, $P_{acoustic}$ represents the acoustic pressure, and ρ represents the jet density. The subscript j represents when the jet is fully expanded; or when the jet has expanded to its greatest cross sectional area just outside of the nozzle. The fully expanded jet velocity and density were determined from isentropic expansion relationships for a perfect gas. Using stagnation, or total, property ratios the point where a flow has the greatest velocity can be determined. In the case of underexpanded jets, this occurs when a supersonic fluid exits the nozzle and expands to its greatest cross sectional area; the fully expanded point. In order to define the fully expanded density and velocity the total pressure ratio (P_0/P_{atm}) is first defined in Equation 4.3 and the fully expanded Mach number (M_j) is defined in Equation 4.4. The fully expanded density, temperature, and velocity are defined by Equations 4.5 - 4.7.

$$\frac{P_0}{P_{atm}} = NPR + \frac{P_{differential}}{P_{atm}} \tag{4.3}$$

$$M_j = \sqrt{\frac{1}{\gamma - 1}\left[\left(\frac{P_0}{P_{atm}}\right)^{\frac{\gamma-1}{\gamma}} - 1\right]} \tag{4.4}$$

$$\frac{\rho_0}{\rho_j} = \left(\frac{P_0}{P_{atm}}\right)^{\frac{1}{\gamma}} \tag{4.5}$$

$$\frac{T_j}{T_0} = 1 + \frac{k-1}{2} {M_j}^2 \tag{4.6}$$

$$u_j = M_j \sqrt{\gamma R T_j} \tag{4.7}$$

In Equation 4.3 – 4.5, P_0 represents the total pressure of the flow, and P_{atm} represents the atmospheric pressure. In Equation 4.3, $P_{differential}$ represents the dynamic pressure of the flow acquired at the same point as the static pressure. In Equations 4.4 and 4.7, γ represents the ratio of specific heats for the fluid. In Equation 4.5, ρ_0 represents the total density of the fluid. In Equation 4.6, T_j represents the fully expanded temperature, and T_0 represents the total temperature. In Equation 4.7, u_j represents the fully expanded velocity, and R represents the ideal gas constant.

The fully expanded jet diameter was modeled analytically by employing the Method of Characteristics[20]. The Method of Characteristics involves solving for flow properties by dividing the expansion and compression waves within a shock cell into finite regions. The lines which divide the flow are referred to as characteristic lines. How the Method of Characteristics was employed is described in this section. A schematic of an underexpanded supersonic jet is shown in Fig. 4.8. Due to symmetry, only half of the jet expansion is depicted.

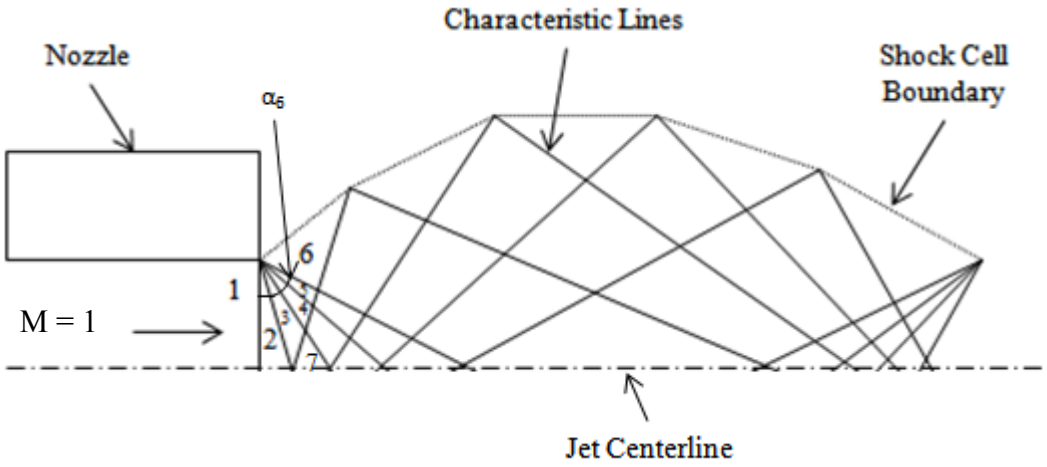

Figure 4.8: Diagram of Characteristic Lines Forming an Underexpanded Supersonic Jet Shock Cell with Labeled Regions 1 - 7.

As observed in Fig. 4.8, a Prandtl-Meyer expansion fan forms at the nozzle lip in the figure and has been divided into regions by characteristic lines[20]. For the purpose of explanation six regions are defined in the figure. Region 1 consists of the flow within the nozzle. Since the cylindrical holes which comprise the nozzles within the jet arrays create choked flow the Mach number at the nozzle exit will always be unity and the turning angle (ν) will always be zero, assuming no loses within the nozzle[20]. Region 6 represents the point where the jet is completely expanded. The pressure in region 6 is equal to the ambient pressure and thus total pressure ratio can be solved for. This pressure ratio is shown in Equation 4.8. The Mach number in region six is then be determined assuming isentropic relations[20]. The flow angle (α) at region 6, determined from the Mach number and classical Prandtl-Meyer expansion, is then divided by four to determine the turning angle, Mach numbers, and Mach line angles (μ) for regions 2 – 5.

$$\left(\frac{P_6}{P_1}\right)\left(\frac{P_1}{P_0}\right) = \left(\frac{P_{atm}}{P_1}\right)\left(\frac{P_1}{P_0}\right) = \frac{P_6}{P_0} \tag{4.8}$$

Continuing downstream the flow interacts with characteristic lines reflected from the jet centerline of the edge of the jet and exhibits either a positive or negative slope. The characteristic lines with a negative slope are labeled as Type I waves and those with a positive slope are labeled as Type II waves. When crossing over a Type I wave the change in turning angle (Δν) is equal to the change in flow angle (Δα). When crossing over a Type II wave the change in turning angle is equal to a negative change in flow angle (-Δα). Also, due to symmetry the turning angle at the centerline is always zero[20]. Thus, moving from region 5 to 7 a Type II wave is crossed. Knowing that the flow angle for region 7 is zero, because it shares a boundary with the centerline, the turning angle for region 7 can be determined by Equation 4.9.

$$\nu_7 = \nu_5 - \alpha_5 \tag{4.9}$$

From the turning angle, the Mach number, and Mach line angle for region 7 are determined. This process is repeated until all the turning, flow angles, and Mach line angles can be determined for each region of interest. The slopes ($m_{I,II}$) of the Type I and II waves are then determined using equations 4.10 and 4.11[20].

$$m_I = tan\left[\frac{(\alpha - \mu)_A + (\alpha - \mu)_C}{2}\right] \tag{4.10}$$

$$m_{II} = tan\left[\frac{(\alpha + \mu)_B + (\alpha + \mu)_C}{2}\right] \tag{4.11}$$

In Equations 4.10 and 4.11, the subscripts *A* and *B*, represent the regions before crossing either the Type I or Type II waves, respectively. The subscript *C*, represents the region after, or the region of interest.

Starting at the nozzle lip and the centerline axis of the flow, the points, in Cartesian coordinates (*x*, *y*), where the Type I and II waves intersect can be determined using Equations 4.12 - 4.14[20].

$$y_P = y_D + m_I(x_P - x_D) \tag{4.12}$$

$$y_P = y_E + m_{II}(x_P - x_E) \tag{4.13}$$

$$x_P = \frac{y_D - y_E + m_{II}x_E - m_I x_D}{m_{II} - m_I} \tag{4.14}$$

In Equations 4.12 – 4.14, the subscript *P* represents the point of interest. The subscript *D* represents the point upstream of the Type I wave creating the intersection. The subscript *E* represents the point upstream of the Type II wave creating the intersection.

The schematic of the jet shock cell from Fig. 4.8 is given in Fig. 4.9 to demonstrate how to further employ the Method of Characteristics in order to determine the size of a shock cell after the slopes of the characteristics have been determined. Points 1 – 4 determine where characteristic lines intersect either other characteristic lines or the jet centerline. Knowing the slopes of the characteristic lines and that the position of points 1 and 2 are (0,R) and (0,0), respectively (where R is the radius of the nozzle), points 3 then 4 can be determined using

Equations 4.12 – 4.14. Equations 4.12 – 4.14 are then repeatedly used moving downstream, centerline to shock cell boundary, point to point, to determine the positions of the remainder of the characteristic line intersections. The maximum y coordinate at the shock cell boundary determined from this method is the fully expanded radius.

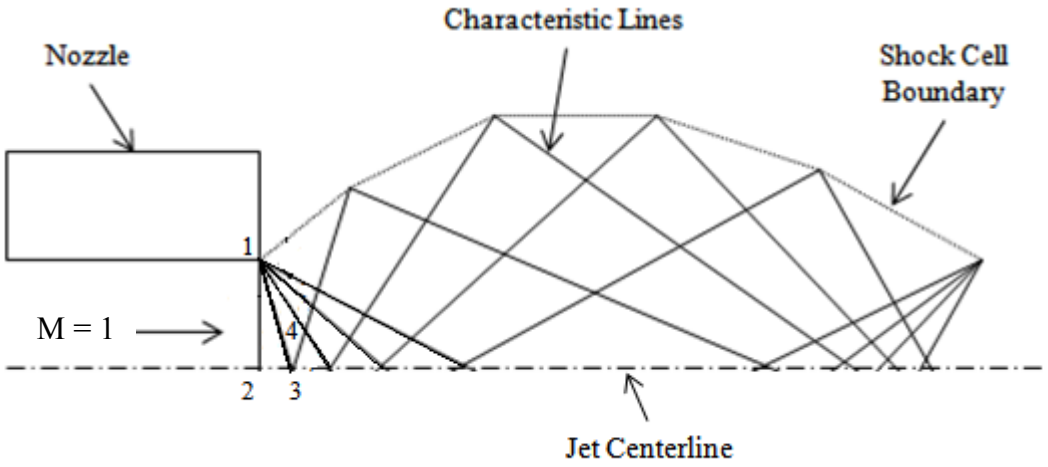

Figure 4.9: Diagram of Characteristic Lines Forming an Underexpanded Supersonic Jet Shock Cell with Labeled Points 1 - 4.

This example initially applied five characteristic lines which expanded off of the nozzle lip. Increasing the number of characteristic lines increases the accuracy of this method. It was determined that the accuracy converged at eight characteristic lines, and for this investigation 30 characteristic lines were used. The Matlab code used to employ the Method of Characteristics for this investigation can be observed in Appendix F*.

* Appendices omitted in actual manuscript.

4.6.1 Non-Dimensional Spectra

Figures 4.3 – 4.7 display the acoustic pressure in the frequency domain for single jets and nozzle arrays. Applying Equations 4.1 and 4.2 the frequency in those spectra are replaced with the Strouhal number and the SPL are replaced with the ADP ratio to form non-dimensional spectra.

4.6.1.1 Single Jets

Figures 4.10 and 4.11 are non-dimensional forms of Figs. 4.3 and 4.4. F igure 4.10 presents the non-dimensional spectra for a 3.2 mm diameter jet and Fig. 4.11 presents the non-dimensional spectra for a 25.4 mm diameter jet. Both figures reveal a characteristic Strouhal number at approximately 0.2 for both jets (0.15 for the 3.2 mm jet and 0.25 for the 25.4 mm jet), consistent with the investigation performed by Seiner *et al.*[3]. The only difference in the two figures is the magnitude in the characteristic ADP amplitude. The spectra observed in Fig. 4.11 reveal that for the larger diameter jet a larger percentage of flow energy is converted to acoustic emissions than for the smaller diameter jet, as observed in Fig. 4.10.

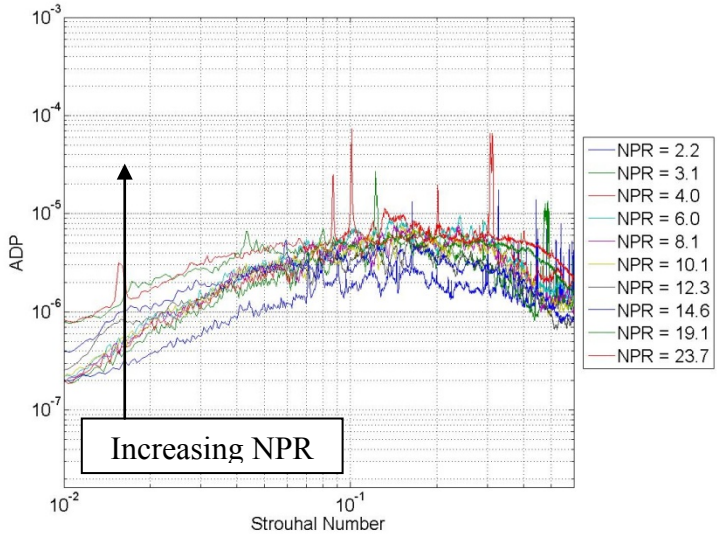

Figure 4.10: Non-Dimensional Spectra for a 3 .2 mm Diameter Single Nozzle Jet and NPR Ranging From 2.2 to 23.7.

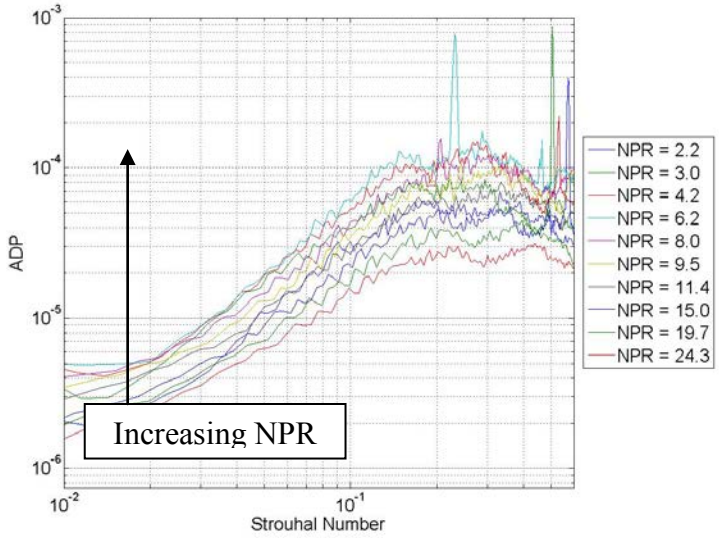

Figure 4.11: Non-Dimensional Spectra for a 25.4 mm Diameter Single Nozzle Jet and NPR Ranging From 2.2 to 23.7.

4.6.1.2 Jet Arrays

Figures 4.12 – 4.14 present non-dimensional spectra for 4.0 mm diameter jet arrays with S/d ratios of 1.44, 2.5, and 3, respectively. The full compilation of non-dimensional spectra can

be observed in Appendix E*. The non-dimensional spectra reveal an important shift in the characteristic Strouhal with increasing NPR. The first characteristic Strouhal number is approximately 0.2 at lower NPR values, consistent with a single jet[3]. Furthermore, at lower NPR values, as the NPR increases the characteristic ADP decreases. The second characteristic Strouhal number resides at approximately 0.04 at higher NPR values; after which the characteristic ADP increases with increasing NPR. The shift in characteristic Strouhal number is strongly dependent upon the S/d of the jet array; consistent with the shift in characteristic frequency seen in Figs. 4.5 – 4.7. Also, comparing Figs. 4.12 – 4.14 with Figs. 4.10 and 4.11 reveal that the characteristic Strouhal number is only similar to a single jet of equivalent size to a single jet within an array at lower NPR values before the characteristic Strouhal number shifts at higher NPR values.

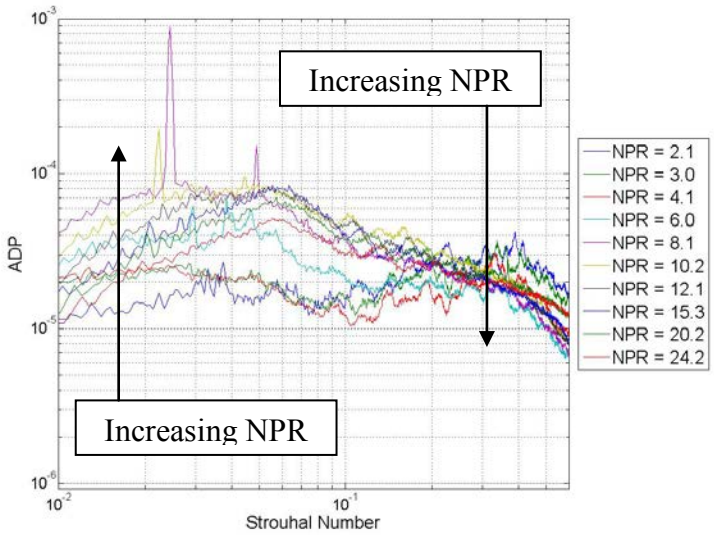

Figure 4.12: Non-Dimensional Spectra for a 4.0 mm Diameter Jet Array of S/d = 1.44 and NPR Ranging From 2.1 to 24.2.

* Appendices omitted in actual manuscript.

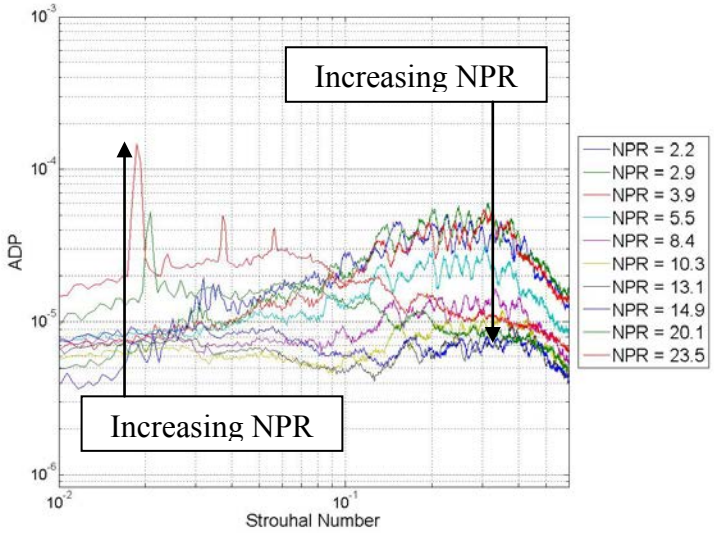

Figure 4.13: Non-Dimensional Spectra for a 4.0 mm Diameter Jet Array of S/d = 2.5 and NPR Ranging From 2.2 to 23.5.

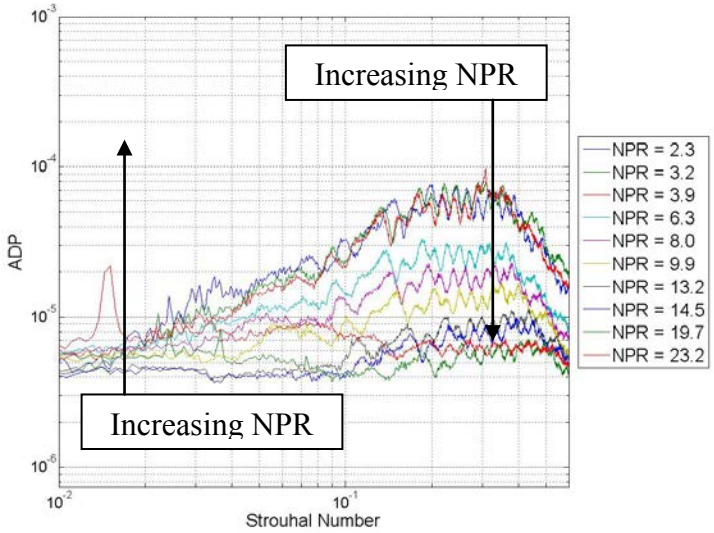

Figure 4.14: Non-Dimensional Spectra for a 4.0 mm Diameter Jet Array of S/d = 3 and NPR Ranging From 2.3 to 23.2.

4.6.2 Characteristic Values

An important factor in characterizing the acoustic emissions of a jet array is the shift in the characteristic Strouhal number. Figures 4.15 – 4.18 present the characteristic Strouhal numbers as a function of the NPR values for jet arrays with S/d ratios of 1.44, 2, 2.5, and 3,

respectively. The characteristic Strouhal numbers were taken from the non-dimensional spectra for each nozzle array at the point of maximum acoustic pressure over dynamic pressure amplitude; ignoring any screech tones. The shift in characteristic Strouhal number observed in Figs. 4.12 – 4.14 can be readily identified in Figs. 4.15 – 4.18 as the lowest NPR where the characteristic Strouhal number lies below 0.2.

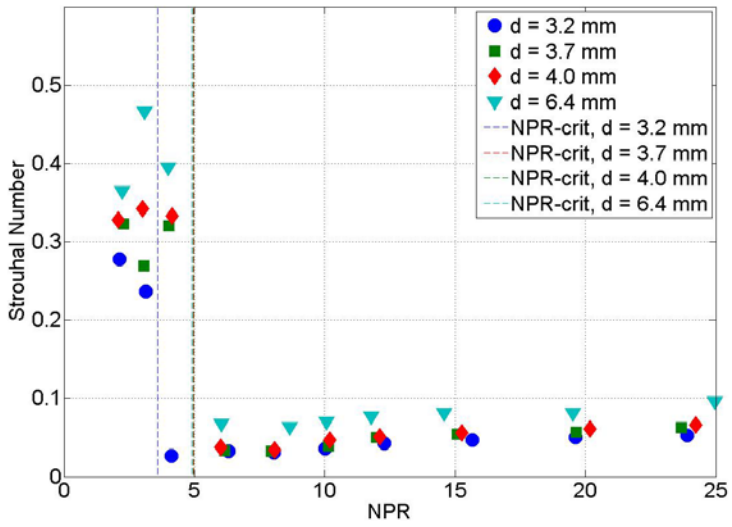

Figure 4.15: Characteristic Strouhal Numbers for Jet Arrays of S/d = 1.44.

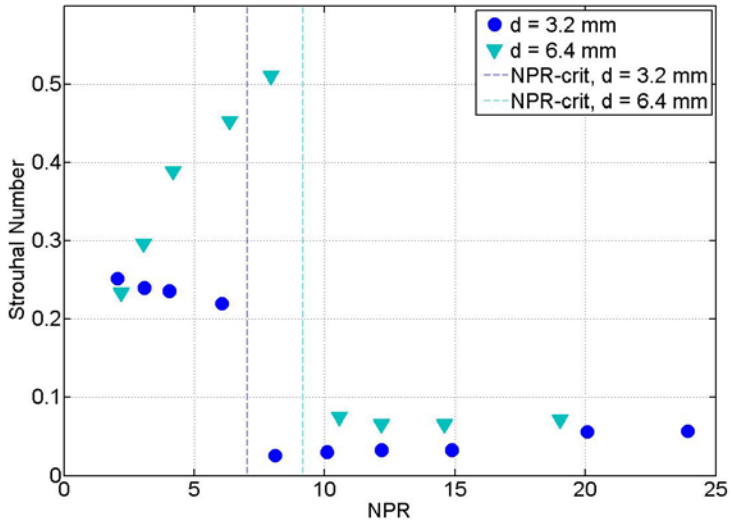

Figure 4.16: Characteristic Strouhal Numbers for Jet Arrays of S/d = 2.

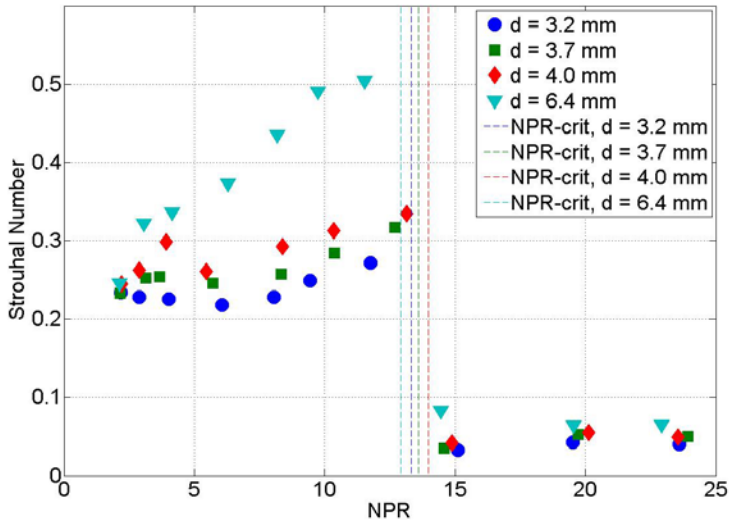

Figure 4.17: Characteristic Strouhal Numbers for Jet Arrays of S/d = 2.5.

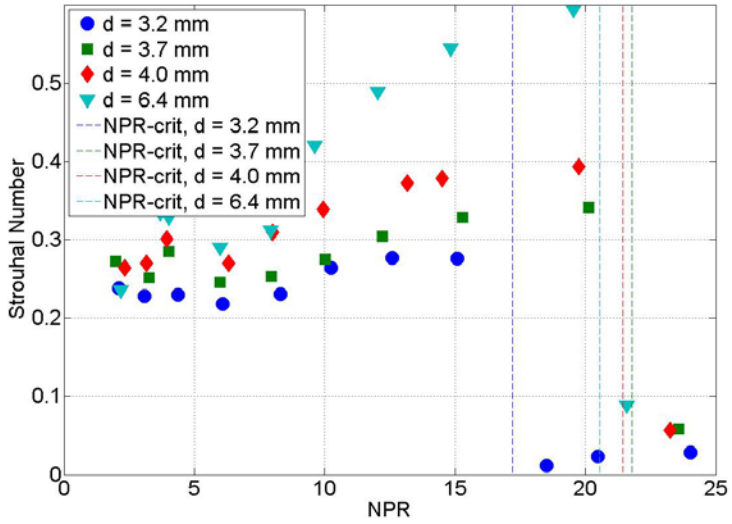

Figure 4.18: Characteristic Strouhal Numbers for Jet Arrays of S/d = 3.

Shown in Figs. 4.15 – 4.18 are vertical dashed lines indicating Critical NPR values (NPR-crit). The Critical NPR is defined as the NPR at which the characteristic Strouhal number shifts from a value similar to that of a single jet (approximately St = 0.2) to a lower value and is used to identify the shift in characteristic frequency and the NPR at which jet interaction occurs. The Critical NPR is an average of the NPR values for the characteristic Strouhal numbers just

before and just after the shift. They can be viewed in Figs. 4.14 – 4.17 as vertical lines for each nozzle diameter; blue for 3.2 mm, green for 3.7 mm, red for 4.0 mm, and teal for 6.4 mm.

Another important factor in characterizing the acoustic emissions of a nozzle array is the change in the acoustic pressure. The characteristic ADP ratios were also extracted from the non-dimensional spectra and can be observed in Figs. 4.19 – 4.22 as a function of NPR for S/d ratios of 1.44, 2, 2.5, and 3, respectively. Also plotted in Fig. 4.19 – 4.22 are the Critical NPR values that were determined from Figs. 4.15 – 4.18.

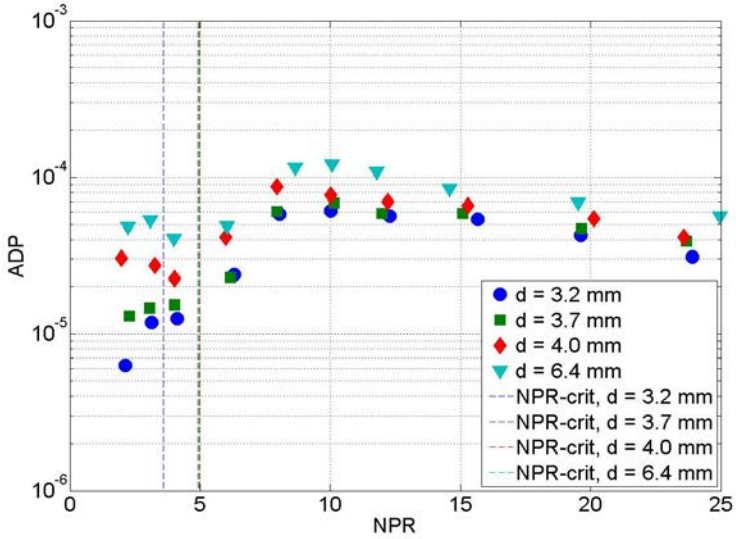

Figure 4.19: Characteristic ADP for Jet Arrays of S/d = 1.44.

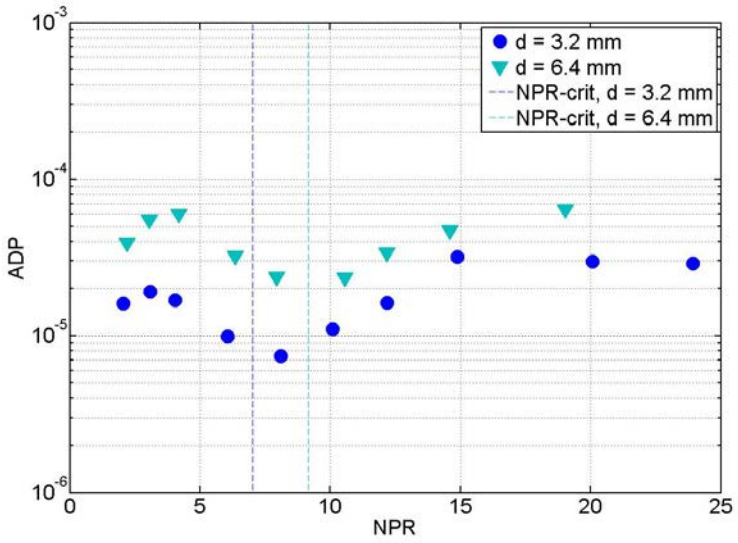

Figure 4.20: Characteristic ADP for Jet Arrays of S/d = 2.

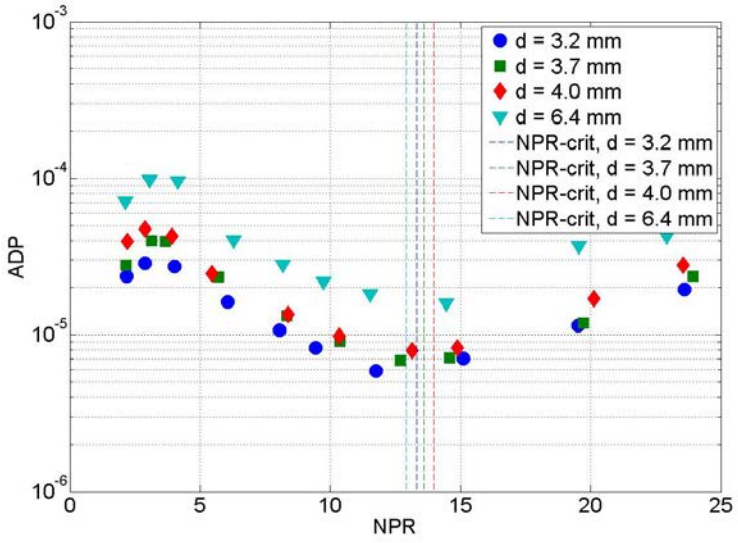

Figure 4.21: Characteristic ADP for Jet Arrays of S/d = 2.5.

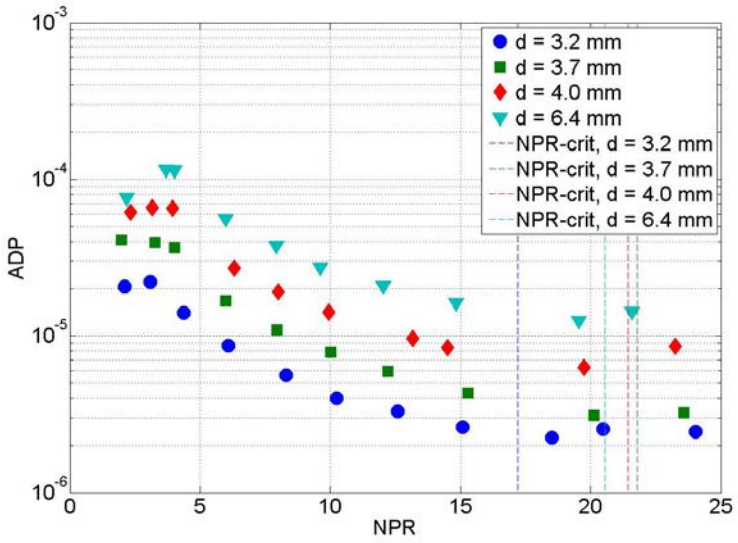

Figure 4.22: Characteristic ADP for Jet Arrays of S/d = 3.

Figures 4.19 – 4.22 reveal important characteristics in the Critical NPR values. The data in Figs. 4.18 – 4.21 show a positive slope in the ADP vs. NPR below an NPR of approximately 5, followed by a negative slope before the Critical NPR values are attained. This can best be seen in Fig. 4.20 – 4.22. At NPR values higher than the Critical NPR the slope of ADP vs. NPR is again positive. Thus, since the ADP ratio is a measure of the acoustic pressure with respect to the dynamic pressure of the flow, the data shown in Figs. 4.19 – 4.22 reveal that before the Critical NPR there are relatively small changes in the acoustic pressure with respect to increasing NPR. However, at NPR values larger than the Critical NPR the acoustic pressure increases more than the dynamic pressure with respect to increasing NPR; indicating increased turbulent energy from the turbulent mixing noise. Also, since the Critical NPR occurs sooner for jet arrays with smaller S/d ratios, the ADP data seen in Fig.4.19 (S/d = 1.44) never experience a negative slope before the Critical NPR is reached. While ignoring the initial increases in ADP, an important characteristic seen in Figs. 4.19 – 4.22 reveal that the Critical NPR indicates when the ADP is at a minimum.

For comparative purposes, the characteristic ADP values for single nozzles have been plotted with the ADP values for corresponding jet arrays. Figures 4.23 and 4.24 present the characteristic ADP ratios for jet arrays with nozzle diameters of 3.2 mm and 6.4 mm, respectively. Also plotted in Figs. 4.23 and 4.24 are the characteristic ADP ratios for single jets with nozzle diameters of 3.2 mm and 25.4 mm diameters (Fig. 4.23), and 6.4 mm and 50.8 mm diameters (Fig.4.24). The smaller diameter nozzles, 3.2 mm and 6.4 mm, represent a single nozzle within a jet array while the larger diameter nozzles, 25.4 mm and 50.8 mm, represent a single jet with an equivalent exit area to an entire array.

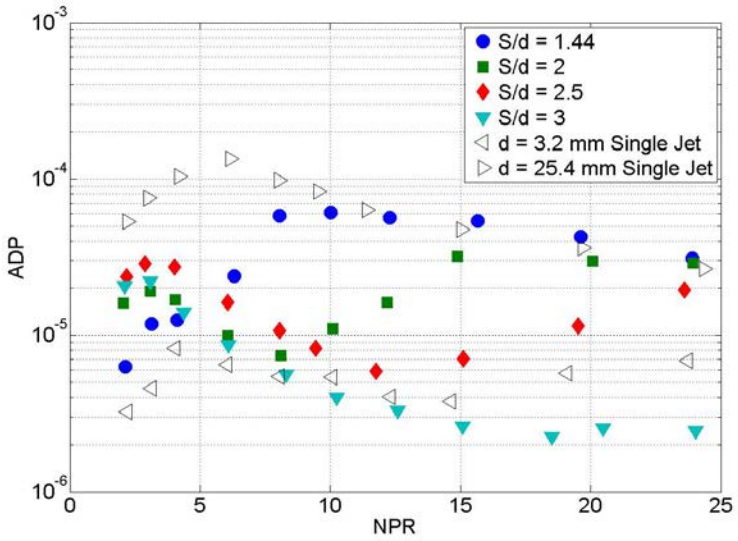

Figure 4.23: Characteristic ADP for 3.2 mm Diameter Jet Arrays and 3.2 mm and 25.4 mm Diameter Single Nozzle Jets.

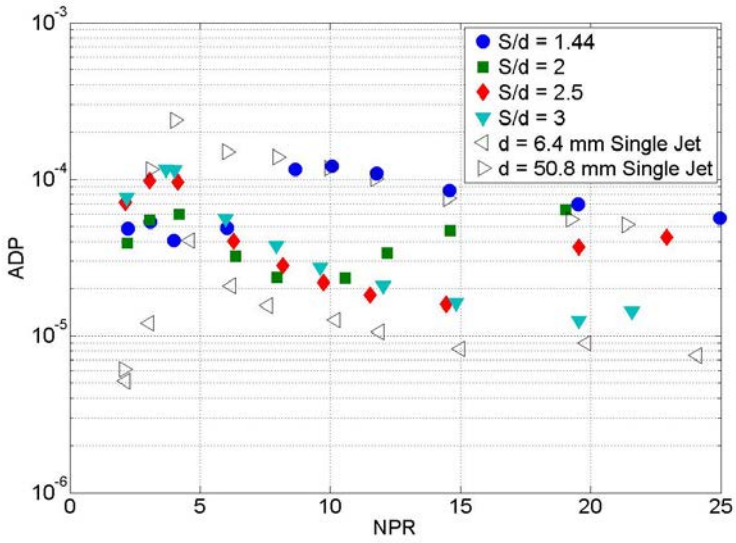

Figure 4.24: Characteristic ADP for 6.4 mm Diameter Jet Arrays and 6.4 mm and 50.8 mm Diameter Single Nozzle Jets.

The data from the single nozzles yield nominally an upper bound (25.4 mm and 50.8 mm diameters) and lower bound (3.2 mm and 6.4 mm diameters) about the data for the jet arrays. Comparing Figs. 4.19 and 4.22 with Figs. 4.23 and 4.24 reveal that at the Critical NPR the ADP ratio for the jet arrays shift from the lower boundary to the upper boundary. Also shown, as the S/d ratio for the jet arrays is increased this shift occurs at higher NPR values. Thus, at NPR values higher than the Critical NPR the turbulent mixing noise shifts to levels similar to that of a single jet with equivalent exit area to an entire array.

4.6.3 Critical Net Pressure Ratio

The Critical NPR is the NPR at which the acoustic emissions from a jet array are significantly altered. When the pressure across a jet array approaches the Critical NPR the characteristic frequency of the jet flow shifts from ultrasonic levels to audible levels. Also, at pressure ratios lower than the Critical NPR there is little change in the acoustic pressure with

respect to the increasing dynamic pressure, but as the NPR is increased to NPR values greater than the Critical NPR the change in acoustic pressure increases at a higher rate than the dynamic pressure with respect to increasing NPR.

The Critical NPR has been shown to be a strong function of the S/d ratio; where the Critical NPR occurs at higher NPR values for higher S/d ratios. Figure 4.25 presents the Critical NPR values for each nozzle diameter as a function of the S/d ratios. Also plotted along with the experimental results are the results from a theoretical model. The theoretical model was determined by assuming that the acoustic emissions were altered when the shock cells from the individual jets within an array expanded large enough to interact with their neighbors. Or, in other words, when the fully expanded radius of a shock cell is equal to half of the center-to-center spacing distance between jets. Using the Method of Characteristics the shock cell sizes were theoretically determined using the experimental NPR values and temperatures. The theoretical Critical NPR values were determined from when the fully expanded radius of a shock cell reached half of the spacing distance. This was done for every jet array iteration.

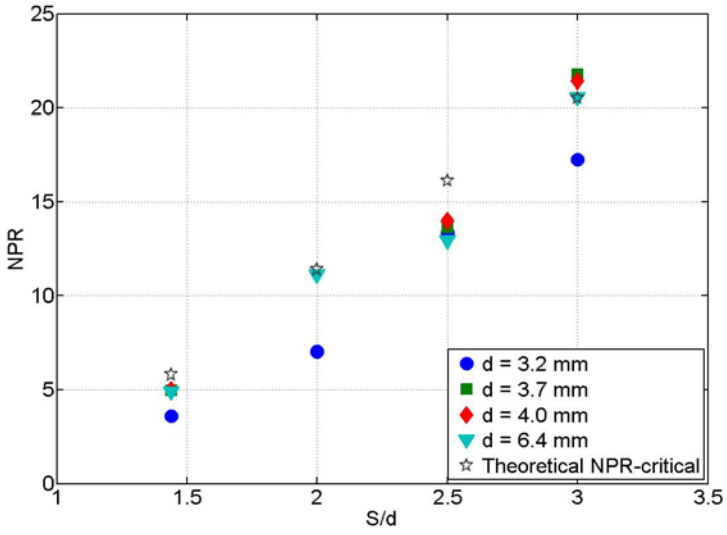

Figure 4.25: Critical Net Pressure Ratios.

Figure 4.26 presents the average of the experimental Critical NPR values for each S/d ratio, along with the theoretical values. Also shown in Fig. 4.26 are linear curve fits to both the experimental and theoretical models. The equations for the curve fits are given in Equations 4.15 and 4.16 for the experimental and theoretical results, respectively. The coefficients of determination for the experimental and theoretical curve fits are 0.9726 and 0.9994, respectively.

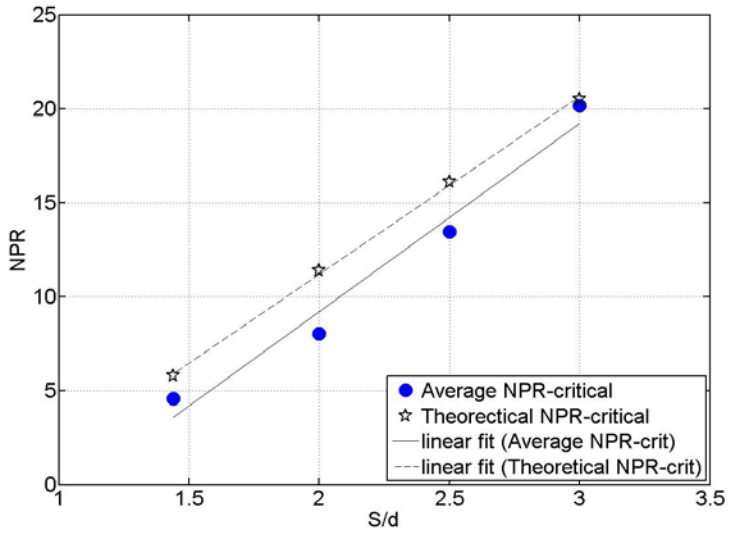

Figure 4.26: Averaged Critical Net Pressure Ratios.

$$NPR_{critical-experimental} = 10.0\frac{S}{d} - 10.9 \tag{4.15}$$

$$NPR_{critical-theoretical} = 9.5\frac{S}{d} - 7.7 \tag{4.16}$$

Comparing the experimental and theoretical models suggest that the acoustic emissions are altered before the individual jets theoretically merge. Coltrin *et al.*'s shadowgraph images of the shock formations showed entrainment of the outer jet by the inner jets of a nozzle array, lending to cause shock interaction sooner than predicted by the theoretical model. Thus,

entrainment of the outer jets would cause the Critical NPR to occur at lower NPR values than theoretically predicted; which is what the data of Fig. 4.26 show.

The goal of this paper was to investigate the acoustic emissions of a jet array in order to reduce them. Using the experimental model seen in Equation 4.15, the Critical NPR can be determined for a jet array of a certain spacing and nozzle diameter. By maintaining the NPR below the Critical NPR the acoustic emissions are reduced by sustaining high characteristic frequencies and low changes in the acoustic pressure. At NPR values higher than the Critical NPR, however, the characteristic frequency of the flow reduces and the change in acoustic pressure increases.

4.7 Conclusion

This paper has reported on an experimental investigation of arrays of parallel supersonic jets. Unlike single supersonic jets, which contain a single characteristic frequency throughout increasing NPR values, nozzle arrays have two. The nozzle arrays investigated here produced ultrasonic characteristic frequencies at lower NPR values and then shifted to audible frequencies at higher NPR values. This shift in characteristic frequency was shown to be mainly a function of the S/d ratio for the nozzle arrays. The shift in characteristic frequency occurred at higher NPR values for higher S/d ratios.

A non-dimensional analysis was performed which related the flow characteristics to the acoustic emissions of the jet arrays. The same shifting behavior was observed when the frequency spectrum was transformed to the Strouhal number spectrum. Seiner *et al.*[3] reported that for a single jet the characteristic Strouhal number is nominally 0.2. For a jet array this held true until a Critical NPR; after which the characteristic Strouhal number shifted to approximately

0.04. Also, the Critical NPR indicated a minimum in the ADP for all jet arrays. Thus, at NPR values lower than the Critical NPR there is a small percentage of flow energy being converted into acoustical emissions. However, at NPR values higher than the critical NPR, there is a significant increase in flow energy being converted into acoustical emissions.

The Critical NPR predicts when the acoustic emissions of a nozzle array are altered. This investigation showed that before the Critical NPR a nozzle array emitted ultrasonic characteristic frequencies and produced small changes in acoustic pressure with respect to increasing NPR values. For NPR values higher than the Critical NPR the characteristic frequency dropped within audible levels and the change in acoustic pressure increased.

The Critical NPR was shown to be mainly a function of the S/d ratio for the jet arrays; increasing linearly with increasing S/d. A theoretical model, based upon the assumption that when the shock cells from the individual jets of an array would merge would alter the acoustic emissions, predicted that the Critical NPR would occur at slightly higher NPR values than experimentally determined. A previous investigation revealed that the inner jets of the nozzle array entrained the outer jets, causing the shocks to interact at lower NPR values[17]. Applying the experimental model with a n ozzle array can reduce the acoustic emissions produced from supersonic jets by sustaining ultrasonic frequencies and lower changes in acoustic pressures with increasing NPR values.

4.8 Acknowledgments

The authors would like to acknowledge Control Components Inc. for their generous support of this research.

Chapter 5. Conclusion

5.1 Summary

The noise radiated from supersonic jets has been known to cause severe fatigue in industry involving high pressure reducing processes. A method to reduce the acoustic emissions of supersonic jets is to divide the single, larger flow into several, smaller ones. Current research into multiple supersonic jets is mainly involved with manipulating the oscillation modes involved in screech tones. This research does not constrain itself to a single noise mechanism but characterizes the overall noise emitted from several closely spaced supersonic jets as well as the flow regime.

This investigation characterized the acoustic emissions with the flow regime for 14 8x8 arrays of parallel axisymmetric jets. The nozzle diameters ranged from 3.2 mm (1/8 in.) to 6.4 mm (1/4 in.) and the S/d values ranged from 1.44 to 3. Comparative investigations were also done on single nozzles of equivalent sizes of 3.2 mm (1/8in.), 6.4 mm (1/4 in.), 25.4 mm (1 in.), and 50.8 mm (2 in.). The smaller nozzles (1/8 and 1/4 in.) represented a single nozzle from a 1/8 and 1/4 in. diameter jet arrays, respectively. The 1 and 2 in. nozzles represented an equivalent exit area to 1/8 and 1/4 in. diameter jet arrays, respectively. Each jet array iteration was tested at NPR vales ranging from approximately 2 to 24.

The acoustic emissions were acquired 30° off the centerline axis of the flow, consistent with the greatest sound pressure output for a single axisymmetric jet. At this position the noise

mechanisms being emitted are the turbulent mixing noise and narrowband shock associated noise. The microphone acquired samples at 200 kHz.

The flow regime included the pressures and temperatures of the fluid as well as shock formations. Differential, static, and temperature data were acquired upstream of the jet arrays. Shadowgraph images were acquired at the nozzle exits for the jet arrays, allowing observation of the shock formations not only as the shock cells expanded independently, but as the shock cells interacted, forming oblique shock lattices. Figures of the experimental setup can be viewed in Appendix A including the pressure transducers, temperature probe, and the experimental setup for the shadowgraph imagery method. Numerical results acquired and analyzed can be observed in Appendix B.

The shock formations showed to form individual shock cells for the jets within the jet arrays as well as oblique shock lattices formed when the NPR increases enough for the shock cells of the jets to expand and interact with each other. The non-interacting shock cells formed initially at lower NPR values. These shock cells are similar to standard shock cells formed from single supersonic jets. The shock lattices formed as the NPR increased past a critical NPR. The oblique shock lattices also showed to go through two stages of formation; oscillatory at first and then stable as the NPR continued to increase. The oscillatory shock lattice displayed a slight flapping motion in the jet stream as well as transient oscillations in the oblique shocks which comprise the shock lattice. As the NPR increases the transient effects of oscillatory shock lattices are reduced and stabilize into a stable shock lattice. The NPR at which the jets interacted showed to be a strong function of the S/d for all nozzle diameters. In general, as the S/d increased the jet interaction occurred at higher NPR values. The shadowgraph images for each jet array iteration can be observed in Appendix C.

The OASPL emitted from the jet arrays showed to have a strong correlation to the shock formations. Initially, when the jets do not interact, the OASPL was similar to a single jet, including a steep initial rise in the OASPL data followed by a leveling off in the slope with only modest increase in the OASPL as the NPR increased. As the jets interacted the OASPL transitioned from lower to higher levels. The shadowgraph imagery revealed that as the OASPL was transitioning the jet arrays experienced an oscillatory shock lattice and as the lattice transitioned to a stable lattice the OASPL leveled off at higher levels with still modest increase as the NPR increased. A comparative investigation into single nozzles revealed that before the jet interacted the OASPL was similar to the turbulent mixing noise of a single nozzle of equivalent size to a single nozzle within a jet array. The OASPL then transitioned, as the shock lattices formed, to similar levels for turbulent mixing noise of a single nozzle of equivalent exit area to an entire jet array.

The characteristic frequency's emitted from the arrays revealed a shift when jet interaction occurred. The characteristic frequency being examined is generated from turbulent mixing noise. There were screech tones present when observing the frequency spectra but the generation of screech tones only randomly occurred during oscillatory shock lattice formations for unknown reasons. Initially the characteristic frequency was similar to a single jet within a jet array. In the scope of this investigation the diameter of the jets caused that frequency to be ultrasonic or nearly ultrasonic (above 20 kHz). As soon as the shocks interacted and initially formed shock lattices the characteristic frequency shifted within audible levels (between 20 Hz to 20 kHz). The sound pressure observed in the frequency domain for each jet array iteration can be observed in Appendix D.

The parameters of interest which showed to contribute to the acoustic emissions of 8x8 jet arrays include the NPR, S/d, acoustic frequency, acoustic pressure, and fully expanded jet velocity, diameter, and density. NPR and S/d are non-dimensional parameters. The other parameters were combined also to form two more non-dimensional parameters. The first is the Strouhal number, defined as the acoustic frequency times the fully expanded jet diameter over the fully expanded jet velocity. The second parameter is the ADP ratio and is defined as the acoustic pressure over the dynamic pressure. The dynamic pressure is defined as one half times the fully expanded jet density times the fully expanded jet velocity squared.

ADP vs. Strouhal spectra revealed initially the characteristic Strouhal is approximately 0.2, similar to a single jet. As the NPR is increased and the shocks from the jets interact the characteristic Strouhal number reduces nearly an order of magnitude; not comparable to any other type of single jet. The Strouhal spectra for the jet arrays can be observed in Appendix E.

Plots of the characteristic Strouhal number against NPR revealed the shift in the acoustic emissions of a jet array when the characteristic Strouhal number reduced below 0.2. Averages of the NPR values just before and just after the shift in the characteristic Strouhal number are defined as the Critical NPR. Plots of the characteristic ADP values reveal that at pressure ratios below the Critical NPR the acoustic pressure is changing less than the dynamic pressure with respect to increasing NPR. However, at NPR values larger than the Critical NPR the acoustic pressure showed to change more than the dynamic pressure with increasing NPR.

The Critical NPR is shown to be a strong function of S/d. Plotting the Critical NPR against the S/d for each nozzle diameter revealed that as the S/d increased the Critical NPR increased linearly. A theoretical model indicated that the shocks interact and the acoustic emissions shift at Critical NPR values slightly lower than predicted. The theoretical model

applies the Method of Characteristics to theoretically determine the maximum radius of a shock cell. At the NPR when the maximum radius equals one half a spacing distance is defined as a theoretical Critical NPR. The Matlab code written and applied for this model can be observed in Appendix F.

Applying the experimental model for determining the Critical NPR at a certain S/d identifies shifting flow and acoustic characteristics from an 8x8 jet array. Maintaining an NPR below the Critical NPR restricts the shock cells from the jets in a jet array from interacting. Restricting shock interaction maintains a characteristic frequency at high levels as well as reducing the acoustic pressure output emitted from turbulent mixing noise. But, increasing the NPR higher than the Critical NPR causes the shocks to interact and form oscillatory to stable shock lattices. When the jets interact the characteristic frequency reduces and the increased turbulent energy causes high acoustic pressure levels.

5.2 Recommendations for Future Work

This research investigated the acoustic emissions from several 8x8 arrays of axisymmetric parallel jets. The limitations of this research include the following:

1) Only eight by eight arrays of axisymmetric jets.

2) Nozzle diameters ranging between 1/8 inch to 1/4 inch.

3) Spacing over nozzle diameter ratios between 1.44 to 3.

4) Nozzle arrays machined onto flat surfaces.

Practical applications for nozzle arrays include implementation into a valve; similar to the design proposed by Carruci and Mueller[1]. Such a design may require a larger radial nozzle array. For these types of applications it is recommended that a similar investigation into radial nozzle arrays be conducted. A radial jet array is a jet array machined onto the side of a cylinder causing the jets exhaust parallel to any radial vector. Other practical application would be to investigate a triangular array of axisymmetric jets as well as rectangular nozzles. Also, extending this investigation beyond the four points noted above.

References

[1] Carucci, V.A., & Mueller R.T., *Acoustically Induced Piping Vibration in High Capacity Pressure Reducing Systems*, ASME Paper No. 82-WA/PVP-8

[2] Eisinger, F.L., *Designing Piping Systems Against Acoustically Induced Structural Fatigue*, J. Pressure Vessel Tech., Vol. 119, pp. 379-383

[3] Seiner, J., & McLaughlin, D.K., & Liu, C.H., *Supersonic Jet Noise Generated by Large-Scale Instabilities*, NASA TP-2072, 1982

[4] Norum, T.D., & Seiner, J.M. (1982a), *Measurements of Static Pressure and Far Field Acoustics of Shock-Containing Supersonic Jets*, NASA TM 84521

[5] Tam, C.K.W., *Supersonic Jet Noise*, Annual Review of Fluid Mechanics, Vol 27, pp. 17-43

[6] Yu, J.C., *Investigations of the Noise Fields of Supersonic Axisymmetric Jet Flow*, Ph.D. Thesis, Syracuse University, 1971

[7] Tanna, H.K., *An Experimental Study of Jet Noise, Part I: Turbulent Mixing Noise*, J. Sound Vib., Vol. 50, pp. 405-444

[8] Oertel, H., *Modern Developments in Shock Tube Research,* Shock Tube Research Society, Japan, 1975

[9] Tadatomo, K., *Study on Structure of Pseudo-Shock Waves in Under-Expanded Jet*, J. Visual. Soc. Japan, Vol. 23, pp. 53 – 56

[10] Harper-Bourne, M., & Fisher, M.J., *The Noise From Shock Waves in Supersonic Jets*, AGARD-CP-131, Mar. 1974

[11] Tanna, H.K., *An Experimental Study of Jet Noise, Part II: Shock Associated Noise*, J. Sound Vib., Vol 50, pp. 405-444

[12] Powell, A. (1953b), *On the Mechanism of Chocked Jet Noise*, Proc. Phys. Soc. London, Vol 66, pp. 1039-1056

[13] Raman, G., *Advances in Understanding Supersonic Jet Screech: Review and Perspective*, Prog. Aerospace Sci., Vol. 34, pp. 45-106

[14] Sherman, P.M., & Glass, D.R., & Duleep, K.G., *Jet Flow Field During Screech*, Appl. Sci. Res., Vol. 32,pp. 283-303

[15] Norum, T.D., *Screech Suppression in Supersonic Jets*, AI AA J., Vol. 21, pp. 235-240

[16] Massey, K., & Ahuja, K.K., & Jones III, R., & Tam, C.K.W., *Screech Tones of Supersonic Heated Free Jets*, AI AA, paper 94-0141

[17] Umeda, Y., & Ishii, R., *Oscillation Modes of Supersonic Multijets*, J. Acoust. Soc. Am., Vol. 101, pp. 3353-3360

[18] Umeda, Y., & Ishii, R., *Oscillation Modes of Supersonic Multijets Exhausting From Very Adjacent Multiple Nozzles*, J. Acoust. Soc. Am., Vol. 110, pp. 1873-1877

[19] Powell, A., Umeda, Y., Ishii, R., *Observations of the Oscillation Modes of Chocked Circular Jets*, J. Acoust. Soc. Am., Vol. 92, pp. 2823-2836

[20] John, F.E., & Keith, T.G., *Gas Dynamics*, 3rd ed., Pearson Prentice Hall, 2006

Appendix A: Experimental Setup

Appendix A includes figures and images which detail the experimental setup used to measure the flow regime and acoustic emissions of 8x8 arrays of parallel supersonic axisymmetric jets on the blowdown facility owned by Brigham Young University's Mechanical Engineering Department. This Appendix includes figures and images of the blowdown facility, pressure transducers, thermocouple, jet array plates tested, as well as a schematic of the shadowgraph imagery method and microphone placement.

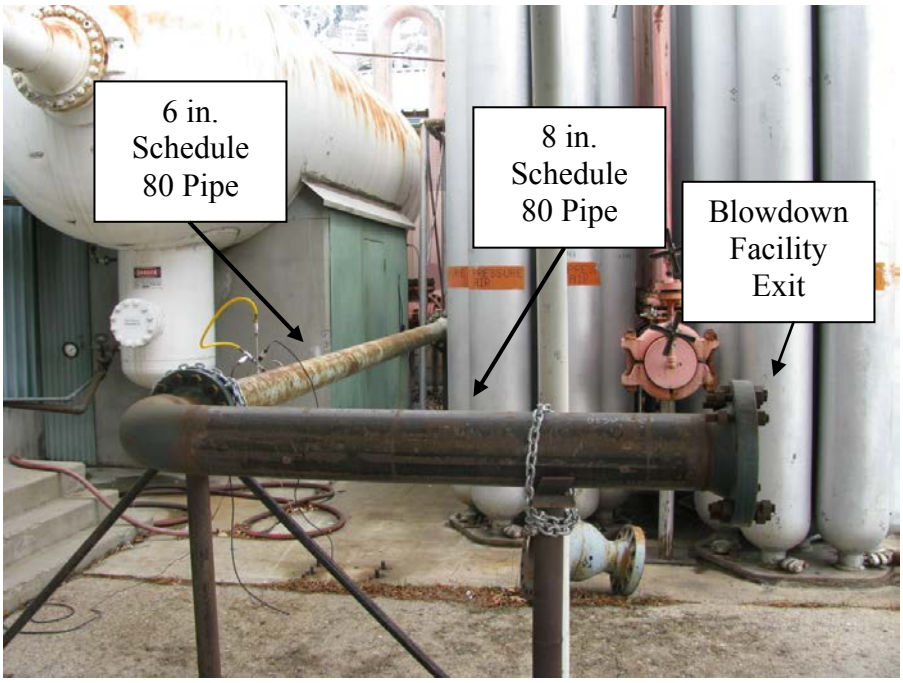

Figure A.1: Blowdown Facility Piping Network.

Figure A.2: Blowdown Facility Exit.

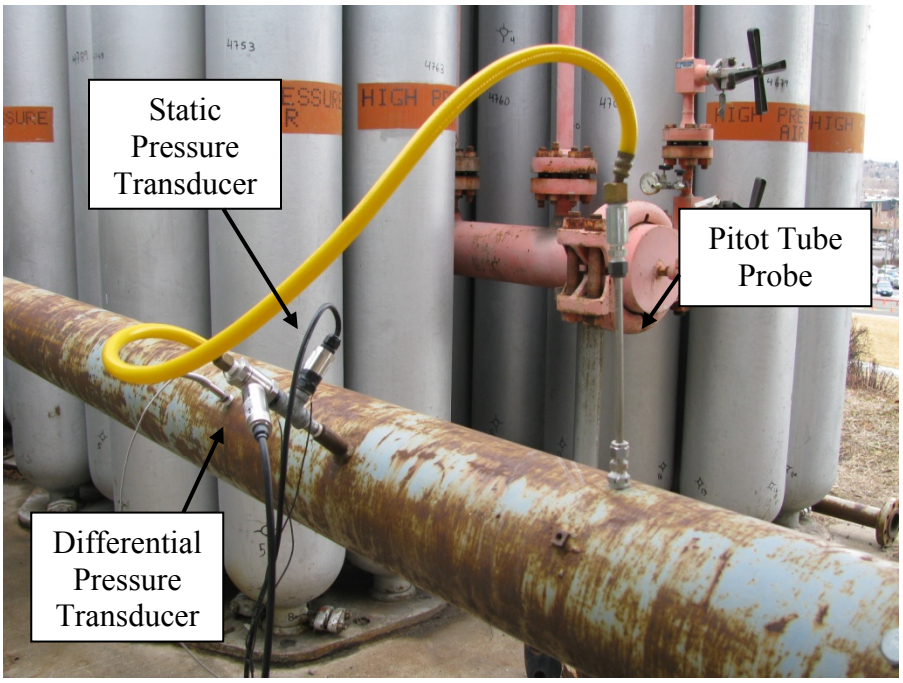

Figure A.3: Pressure Transuders with Pitot Tube Probe.

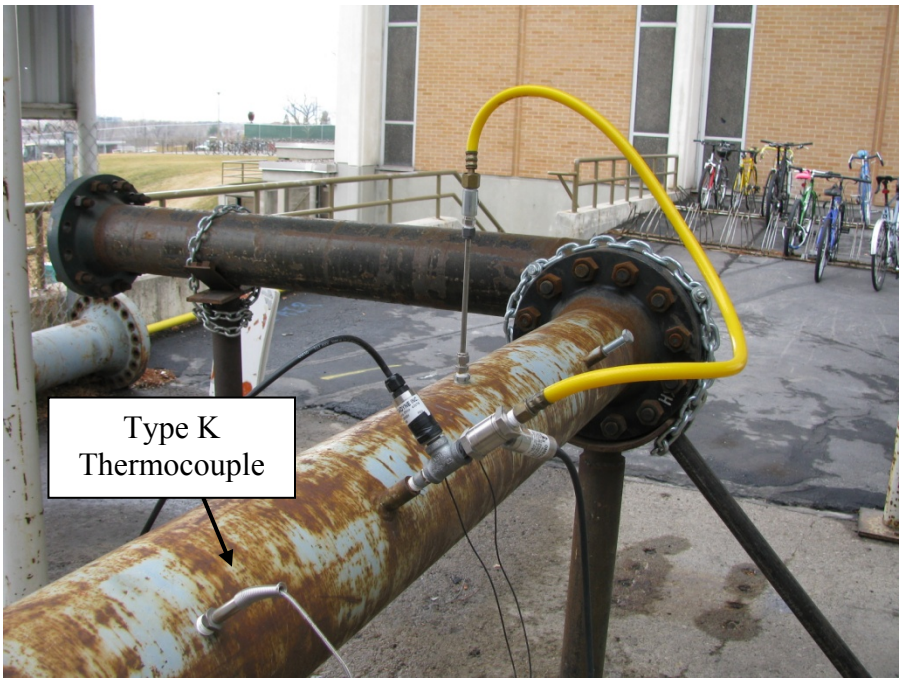

Figure A.4: Thermocouple, Pressure Transducers, and Pitot Tube Probe.

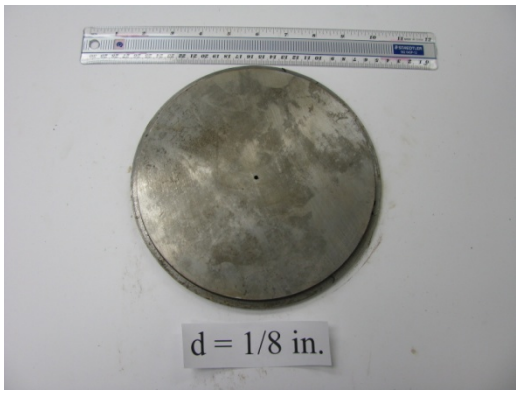

(a) d = 1/8 in.

(b) d = 1/4 in.

(c) d = 1 in.

(d) d = 2 in.

Figure A.5: Single Nozzles.

(a) d = 1/8 in.

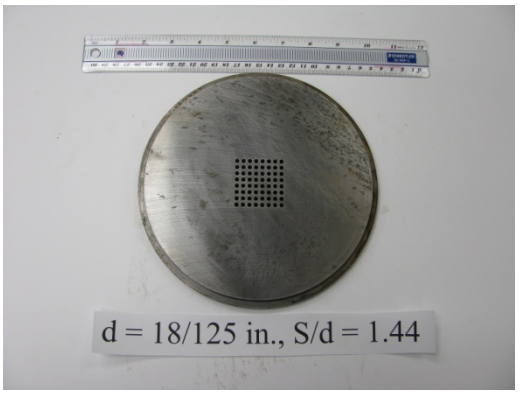

(b) d = 18/125 in.

(c) d = 5/32 in.

(d) d = 1/4 in.

Figure A.6: 8x8 Jet Arrays at S/d = 1.44.

(a) d = 1/8 in.

(b) d = 1/4 in.

Figure A.7: 8x8 Jet Arrays at S/d = 2.

(a) d = 1/8 in.

(b) d = 18/125 in.

(c) d = 5/32 in.

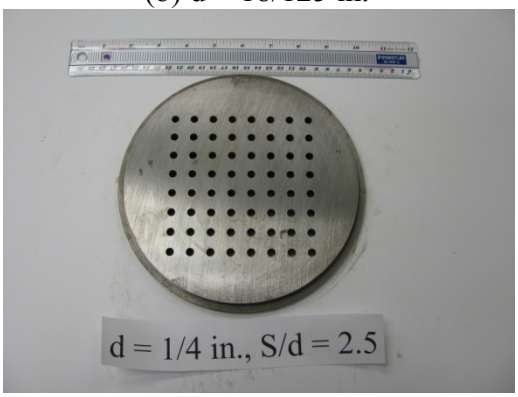

(d) d = 1/4 in.

Figure A.8: 8x8 Jet Arrays at S/d = 2.5.

(a) d = 1/8 in.

(b) d = 18/125 in.

(c) d = 5/32 in.

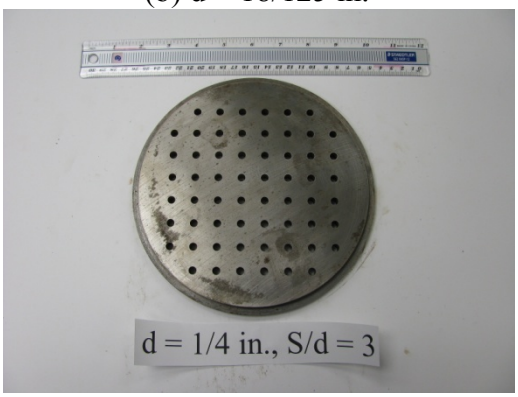

(d) d = 1/4 in.

Figure A.9: 8x8 Jet Arrays at S/d = 3.

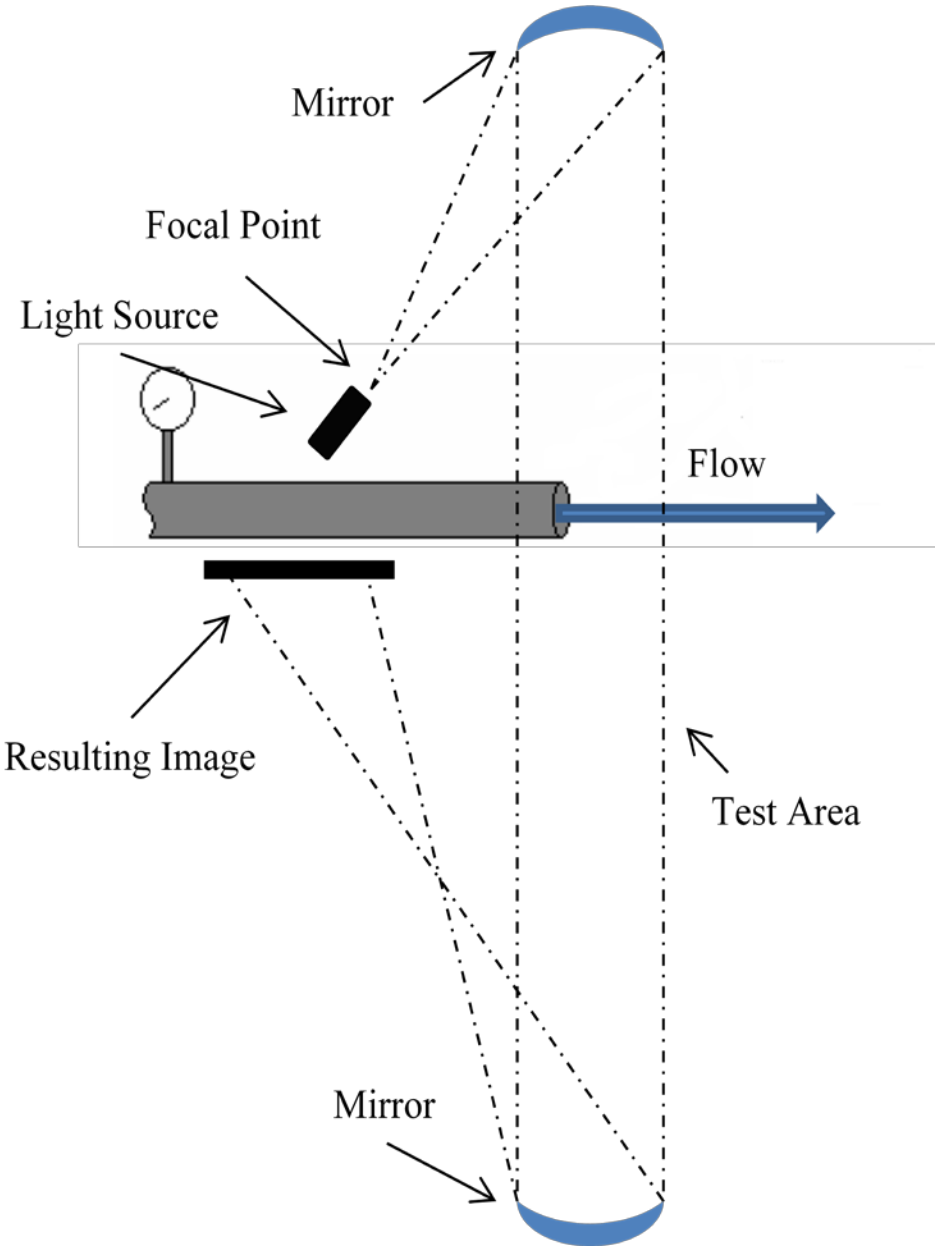

Figure A.10: Shadowgraph Imagery Method Experimental Setup.

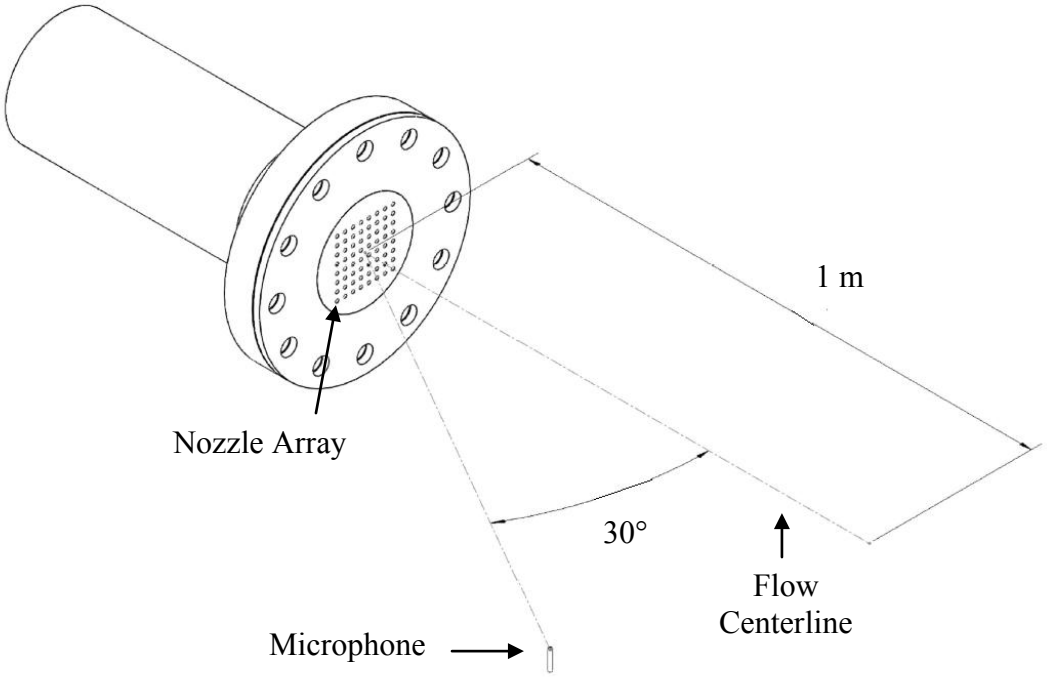

Figure A.11: Microphone Experimental Setup.

Appendix B: Numerical Results

Appendix B displays the numerical results acquired from the pressure transducers, thermocouples, and microphone as well as analyzed data. The values presented here include the net pressure ratio (*NPR*), temperature (*T*), mass flow rate ($\dot{m}$), overall sound pressure level (*OASPL*), fully expanded jet diameter, velocity, and density (d_j, u_j, ρ_j), fully expanded jet Mach number (M_j), characteristic Strouhal number (*St*), and characteristic acoustic pressure over the dynamic pressure ratio (*AP/DP*).

Table B.1: Numerical and Analytical Results From a 1/8 inch Diameter Single Jet.

NPR	***T* (°C)**	**$\dot{m}$ (kg/s)**	***OASPL* (dB, ref. 20 μPa)**	**d_j (in.)**	**u_j (m/s)**	**ρ_j (kg/m^3)**	**M_j**	***St***	***AP/DP***
2.2	33.6	1.4	92.3	0.1	395.5	1.3	1.2	0.82	3.2E-06
3.1	33.6	1.7	101.0	0.1	487.3	1.4	1.5	0.18	4.6E-06
4.0	33.8	1.9	110.9	0.2	549.6	1.5	1.7	0.30	8.3E-06
6.0	34.4	2.2	114.2	0.2	644.0	1.7	1.9	0.22	6.5E-06
8.1	35.3	2.5	117.0	0.2	710.6	1.8	2.1	0.18	5.5E-06
10.1	36.5	2.7	120.0	0.2	762.7	1.9	2.3	0.18	5.4E-06
12.3	36.0	2.9	120.5	0.3	807.3	2.0	2.4	0.15	4.0E-06
14.6	36.4	3.0	122.8	0.3	846.7	2.1	2.6	0.14	3.8E-06
19.1	35.2	5.2	130.6	0.3	905.1	2.3	2.7	0.13	5.7E-06
23.7	34.0	8.8	136.3	0.4	952.8	2.5	2.9	0.11	6.9E-06

Table B.2: Numerical and Analytical Results From a 1/4 inch Diameter Single Jet.

NPR	*T (°C)*	*ṁ (kg/s)*	*OASPL (dB, ref. 20 µPa)*	d_j *(in.)*	u_j *(m/s)*	ρ_j *(kg/m^3)*	M_j	*St*	*AP/DP*
2.1	32.8	1.3	95.2	0.3	383.6	1.2	1.2	0.16	5.1E-06
3.0	33.6	1.6	108.5	0.3	479.2	1.4	1.4	0.16	1.2E-05
4.6	34.8	1.8	126.2	0.3	580.9	1.5	1.8	0.27	4.1E-05
6.2	34.9	2.1	125.1	0.4	649.8	1.7	2.0	0.27	2.1E-05
7.6	34.4	2.3	125.9	0.4	696.5	1.8	2.1	0.23	1.6E-05
10.2	34.6	2.5	128.3	0.5	763.1	1.9	2.3	0.19	1.3E-05
11.9	34.6	2.7	128.9	0.5	797.4	2.0	2.4	0.17	1.1E-05
15.0	34.3	3.3	129.9	0.6	849.0	2.2	2.6	0.14	8.3E-06
19.8	32.4	6.6	135.2	0.7	909.5	2.4	2.7	0.16	9.0E-06
24.1	31.9	9.6	136.6	0.8	952.8	2.5	2.9	0.17	7.5E-06

Table B.3: Numerical and Analytical Results From a 1 inch Diameter Single Jet.

NPR	*T (°C)*	*ṁ (kg/s)*	*OASPL (dB, ref. 20 µPa)*	d_j *(in.)*	u_j *(m/s)*	ρ_j *(kg/m^3)*	M_j	*St*	*AP/DP*
2.2	29.4	2.2	118.9	1.0	393.5	1.3	1.2	0.42	5.3E-05
3.0	28.7	3.2	127.4	1.1	473.2	1.4	1.4	0.31	7.5E-05
4.2	27.3	4.6	133.3	1.2	553.4	1.5	1.7	0.27	1.0E-04
6.2	26.8	7.0	142.7	1.5	640.5	1.7	1.9	0.27	1.3E-04
8.0	25.7	9.3	142.4	1.7	698.8	1.9	2.1	0.32	9.8E-05
9.5	24.3	11.2	143.3	1.9	735.2	2.0	2.2	0.33	8.3E-05
11.4	22.5	13.5	143.6	2.1	772.5	2.1	2.3	0.34	6.3E-05
15.0	19.8	18.1	145.0	2.4	829.5	2.3	2.5	0.36	4.7E-05
19.7	19.2	11.0	146.4	2.8	888.2	2.5	2.7	0.37	3.6E-05
24.3	20.0	10.8	146.8	3.2	936.6	2.6	2.8	0.39	2.7E-05

Table B.4: Numerical and Analytical Results From a 2 inch Diameter Single Jet.

NPR	*T (°C)*	*ṁ (kg/s)*	*OASPL (dB, ref. 20 µPa)*	d_j *(in.)*	u_j *(m/s)*	ρ_j *(kg/m^3)*	M_j	*St*	*AP/DP*
2.1	32.6	2.0	100.3	2.0	376.6	1.2	1.1	1.03	6.1E-06
3.1	30.0	3.3	130.2	2.2	484.0	1.4	1.5	0.56	1.2E-04
4.0	28.2	4.4	143.2	2.4	544.9	1.5	1.6	0.44	2.4E-04
6.0	23.8	6.9	143.1	2.9	632.7	1.7	1.9	0.77	1.5E-04
8.0	20.9	9.3	146.5	3.4	691.5	1.9	2.1	0.63	1.4E-04
10.0	20.6	11.8	147.5	3.8	740.2	2.0	2.2	0.62	1.2E-04
11.7	20.7	14.0	148.6	4.2	776.4	2.1	2.3	0.61	1.0E-04
14.5	20.9	17.4	149.4	4.8	823.6	2.2	2.5	0.62	7.6E-05
19.2	20.7	23.2	150.7	5.6	885.2	2.4	2.6	0.68	5.6E-05
21.4	20.6	25.9	151.5	6.0	908.5	2.5	2.7	0.69	5.1E-05

Table B.5: Numerical and Analytical Results From a 1/8 inch Diameter Jet Array with S/d of 1.44.

NPR	*T (°C)*	$\dot{m}$ (kg/s)	*OASPL (dB, ref. 20 µPa)*	d_j *(in.)*	u_j *(m/s)*	ρ_j *(kg/m^3)*	M_j	*St*	*AP/DP*
2.1	19.0	1.7	98.5	0.1	375.2	1.3	1.1	0.28	6.3E-06
3.1	18.9	2.1	111.3	0.1	476.9	1.5	1.4	0.24	1.2E-05
4.1	18.3	2.5	117.1	0.2	539.8	1.6	1.6	0.03	1.2E-05
6.3	16.3	3.7	127.7	0.2	635.0	1.8	1.9	0.03	2.4E-05
8.1	15.9	4.3	141.1	0.2	687.9	1.9	2.0	0.03	5.8E-05
10.0	14.4	4.9	142.2	0.2	733.7	2.1	2.2	0.04	6.1E-05
12.3	14.0	6.0	143.4	0.3	777.3	2.2	2.3	0.04	5.6E-05
15.7	13.8	7.6	146.1	0.3	830.0	2.4	2.4	0.05	5.4E-05
19.6	13.7	9.7	147.5	0.4	879.0	2.5	2.6	0.05	4.3E-05
23.9	14.1	9.2	147.7	0.4	923.0	2.7	2.7	0.05	3.1E-05

Table B.6: Numerical and Analytical Results From a 18/125 inch Diameter Jet Array with S/d of 1.44.

NPR	*T (°C)*	$\dot{m}$ (kg/s)	*OASPL (dB, ref. 20 µPa)*	d_j *(in.)*	u_j *(m/s)*	ρ_j *(kg/m^3)*	M_j	*St*	*AP/DP*
2.3	27.1	1.8	108.9	0.1	401.2	1.3	1.2	0.32	1.3E-05
3.1	26.2	2.1	112.4	0.2	476.8	1.4	1.4	0.27	1.5E-05
4.0	24.1	2.5	118.7	0.2	539.9	1.5	1.6	0.32	1.5E-05
6.2	23.2	3.5	127.6	0.2	636.7	1.7	1.8	0.03	2.3E-05
7.9	21.3	4.2	141.6	0.2	691.2	1.9	2.0	0.03	6.0E-05
10.1	18.5	6.0	144.1	0.3	741.3	2.0	2.2	0.04	6.8E-05
12.0	17.0	6.9	143.7	0.3	776.1	2.2	2.3	0.05	5.8E-05
15.1	15.8	8.5	146.4	0.4	824.7	2.3	2.4	0.05	5.9E-05
19.6	14.2	11.6	148.4	0.4	880.0	2.5	2.6	0.06	4.7E-05
23.7	13.6	12.5	149.7	0.5	920.2	2.6	2.7	0.06	3.9E-05

Table B.7: Numerical and Analytical Results From
a 5/32 inch Diameter Jet Array with S/d of 1.44.

NPR	*T* (°C)	$\dot{m}$ (kg/s)	*OASPL* (dB, ref. 20 µPa)	d_j (in.)	u_j (m/s)	ρ_j (kg/m^3)	M_j	*St*	*AP/DP*
2.1	24.8	1.3	110.6	0.2	373.5	1.3	1.1	0.33	3.0E-05
3.0	24.3	1.8	118.3	0.2	469.9	1.4	1.4	0.34	2.7E-05
4.1	23.3	2.7	122.8	0.2	546.4	1.6	1.6	0.33	2.3E-05
6.0	21.8	3.6	131.9	0.2	630.1	1.7	1.8	0.04	4.1E-05
8.1	20.0	4.5	145.8	0.3	693.2	1.9	2.0	0.03	8.8E-05
10.2	18.4	6.2	144.5	0.3	742.4	2.0	2.2	0.05	7.7E-05
12.1	17.3	7.6	145.5	0.3	778.7	2.2	2.3	0.05	7.0E-05
15.3	16.8	9.5	147.7	0.4	828.4	2.3	2.4	0.06	6.6E-05
20.2	17.1	10.9	150.2	0.5	890.3	2.5	2.6	0.06	5.4E-05
24.2	17.9	15.3	150.6	0.5	932.2	2.6	2.7	0.07	4.1E-05

Table B.8: Numerical and Analytical Results From
a 1/4 inch Diameter Jet Array with S/d of 1.44.

NPR	*T* (°C)	$\dot{m}$ (kg/s)	*OASPL* (dB, ref. 20 µPa)	d_j (in.)	u_j (m/s)	ρ_j (kg/m^3)	M_j	*St*	*AP/DP*
2.2	31.0	1.8	118.4	0.3	396.8	1.3	1.1	0.36	4.9E-05
3.1	29.0	2.5	124.6	0.3	479.9	1.4	1.4	0.47	5.4E-05
4.0	24.8	3.2	127.8	0.3	538.8	1.5	1.6	0.39	4.1E-05
6.0	21.7	4.7	135.6	0.4	630.2	1.7	1.8	0.07	4.9E-05
8.7	20.8	7.0	147.2	0.4	709.8	1.9	2.1	0.06	1.2E-04
10.1	20.5	7.8	148.5	0.5	742.7	2.0	2.2	0.07	1.2E-04
11.8	20.6	9.5	149.2	0.5	777.1	2.1	2.3	0.08	1.1E-04
14.6	21.5	10.7	150.0	0.6	825.1	2.2	2.4	0.08	8.5E-05
19.5	14.5	14.5	152.8	0.7	879.1	2.5	2.6	0.08	6.9E-05
25.0	7.0	18.4	154.5	0.8	921.0	2.8	2.7	0.10	5.7E-05

Table B.9: Numerical and Analytical Results From
a 1/8 inch Diameter Jet Array with S/d of 2.

NPR	*T (°C)*	$\dot{m}$ (kg/s)	*OASPL (dB, ref. 20 µPa)*	d_j *(in.)*	u_j *(m/s)*	ρ_j *(kg/m^3)*	M_j	*St*	*AP/DP*
2.1	25.9	2.0	103.4	0.1	370.6	1.3	1.1	0.25	1.6E-05
3.1	25.8	3.3	112.7	0.1	478.1	1.4	1.4	0.24	1.9E-05
4.0	25.3	4.4	117.1	0.2	542.4	1.5	1.6	0.24	1.7E-05
6.1	25.1	6.9	120.5	0.2	635.1	1.7	1.8	0.22	9.9E-06
8.1	23.6	9.4	123.3	0.2	698.7	1.9	2.0	0.03	7.4E-06
10.1	22.3	11.9	128.5	0.2	745.3	2.0	2.2	0.03	1.1E-05
12.2	20.7	14.5	134.2	0.3	784.5	2.1	2.3	0.03	1.6E-05
14.9	19.8	17.8	145.0	0.3	827.3	2.3	2.4	0.03	3.2E-05
20.1	18.5	24.3	144.8	0.4	891.5	2.5	2.6	0.06	3.0E-05
23.9	18.0	29.1	146.6	0.4	929.6	2.6	2.7	0.06	2.9E-05

Table B.10: Numerical and Analytical Results From
a 1/4 inch Diameter Jet Array with S/d of 2.

NPR	*T (°C)*	$\dot{m}$ (kg/s)	*OASPL (dB, ref. 20 µPa)*	d_j *(in.)*	u_j *(m/s)*	ρ_j *(kg/m^3)*	M_j	*St*	*AP/DP*
2.2	28.2	2.1	114.8	0.3	390.7	1.3	1.1	0.23	3.9E-05
3.1	27.1	3.2	122.8	0.3	476.9	1.4	1.4	0.30	5.5E-05
4.2	25.8	4.6	128.3	0.3	551.4	1.5	1.6	0.39	6.0E-05
6.4	21.6	7.3	130.7	0.4	642.4	1.8	1.9	0.45	3.2E-05
8.0	19.7	9.3	132.3	0.4	689.6	1.9	2.0	0.51	2.4E-05
10.6	18.7	12.6	137.4	0.5	751.1	2.1	2.2	0.07	2.3E-05
12.2	18.5	14.6	142.2	0.5	781.6	2.2	2.3	0.06	3.4E-05
14.6	18.9	17.5	147.4	0.6	821.9	2.3	2.4	0.06	4.7E-05
19.0	14.3	23.2	152.8	0.7	873.4	2.5	2.6	0.07	6.4E-05
2.2	28.2	2.1	114.8	0.3	390.7	1.3	1.1	0.23	3.9E-05

Table B.11: Numerical and Analytical Results From
a 1/8 inch Diameter Jet Array with S/d of 2.5.

NPR	*T* (°C)	$\dot{m}$ (kg/s)	*OASPL* (dB, ref. 20 μPa)	d_j (in.)	u_j (m/s)	ρ_j (kg/m^3)	M_j	*St*	*AP/DP*
2.2	15.6	1.5	107.2	0.1	379.4	1.3	1.1	0.23	2.4E-05
2.9	14.7	1.8	114.0	0.1	451.9	1.5	1.3	0.23	2.9E-05
4.0	13.8	2.2	119.6	0.2	531.1	1.6	1.6	0.23	2.7E-05
6.1	13.4	3.3	122.4	0.2	622.8	1.8	1.8	0.22	1.6E-05
8.0	12.3	4.1	124.0	0.2	683.5	1.9	2.0	0.23	1.1E-05
9.4	10.8	4.7	124.3	0.2	715.9	2.1	2.1	0.25	8.3E-06
11.7	11.2	5.9	126.0	0.3	763.9	2.2	2.3	0.27	5.9E-06
15.1	10.8	7.7	130.9	0.3	817.9	2.4	2.4	0.03	7.0E-06
19.5	12.7	10.1	137.9	0.4	876.4	2.5	2.6	0.04	1.1E-05
23.6	13.4	12.2	147.3	0.4	919.2	2.7	2.7	0.04	2.0E-05

Table B.12: Numerical and Analytical Results From
a 18/125 inch Diameter Jet Array with S/d of 2.5.

NPR	*T* (°C)	$\dot{m}$ (kg/s)	*OASPL* (dB, ref. 20 μPa)	d_j (in.)	u_j (m/s)	ρ_j (kg/m^3)	M_j	*St*	*AP/DP*
2.2	29.6	1.5	109.0	0.1	387.2	1.3	1.1	0.23	2.8E-05
3.1	26.0	1.8	118.3	0.2	481.0	1.4	1.4	0.25	4.0E-05
3.7	23.1	2.1	121.2	0.2	518.0	1.5	1.5	0.25	3.9E-05
5.7	19.9	3.4	124.4	0.2	616.3	1.7	1.8	0.25	2.3E-05
8.3	16.2	4.9	126.4	0.3	695.6	1.9	2.0	0.26	1.3E-05
10.4	14.7	5.3	126.8	0.3	741.3	2.1	2.2	0.28	9.1E-06
12.7	11.7	6.7	128.7	0.3	781.4	2.2	2.3	0.32	6.9E-06
14.6	10.4	8.3	131.4	0.3	809.3	2.3	2.4	0.03	7.2E-06
19.7	9.8	11.2	138.5	0.4	874.0	2.5	2.6	0.05	1.2E-05
23.9	11.5	14.7	147.3	0.5	919.2	2.7	2.7	0.05	2.4E-05

Table B.13: Numerical and Analytical Results From
a 5/32 inch Diameter Jet Array with S/d of 2.5.

NPR	*T* (°C)	$\dot{m}$ (kg/s)	*OASPL* (dB, ref. 20 μPa)	d_j (in.)	u_j (m/s)	ρ_j (kg/m^3)	M_j	*St*	*AP/DP*
2.2	22.3	1.4	112.7	0.2	389.0	1.3	1.1	0.25	4.0E-05
2.9	21.4	1.7	118.7	0.2	456.4	1.4	1.3	0.26	4.7E-05
3.9	20.0	2.4	122.9	0.2	529.7	1.5	1.5	0.30	4.3E-05
5.5	17.8	3.3	124.6	0.2	603.7	1.7	1.8	0.26	2.5E-05
8.4	16.1	4.8	127.1	0.3	696.7	2.0	2.0	0.29	1.4E-05
10.3	14.7	5.7	127.7	0.3	740.9	2.1	2.2	0.31	9.9E-06
13.1	13.6	6.2	130.5	0.4	791.3	2.2	2.3	0.33	8.0E-06
14.9	12.8	8.4	133.1	0.4	817.3	2.3	2.4	0.04	8.3E-06
20.1	13.8	11.6	142.0	0.5	884.8	2.5	2.6	0.06	1.7E-05
23.5	15.2	13.2	149.4	0.5	921.4	2.6	2.7	0.05	2.8E-05

Table B.14: Numerical and Analytical Results From
a 1/4 inch Diameter Jet Array with S/d of 2.5.

NPR	*T* (°C)	$\dot{m}$ (kg/s)	*OASPL* (dB, ref. 20 μPa)	d_j (in.)	u_j (m/s)	ρ_j (kg/m^3)	M_j	*St*	*AP/DP*
2.1	19.0	1.8	118.7	0.3	376.0	1.3	1.1	0.25	7.1E-05
3.1	17.0	2.4	127.3	0.3	468.4	1.5	1.4	0.32	9.8E-05
4.1	15.5	3.2	131.1	0.3	539.0	1.6	1.6	0.34	9.6E-05
6.3	10.8	7.0	130.8	0.4	627.6	1.8	1.9	0.37	4.0E-05
8.2	8.5	6.6	132.4	0.4	682.2	2.0	2.0	0.43	2.8E-05
9.8	6.5	7.9	133.0	0.5	717.7	2.1	2.1	0.49	2.2E-05
11.5	5.5	8.9	134.3	0.5	752.1	2.2	2.2	0.50	1.8E-05
14.5	5.9	13.2	138.3	0.6	801.2	2.4	2.4	0.08	1.6E-05
19.5	9.7	14.5	149.0	0.7	872.0	2.5	2.6	0.06	3.7E-05
22.9	8.8	18.4	152.6	0.8	905.4	2.7	2.7	0.07	4.3E-05

Table B.15: Numerical and Analytical Results From
a 1/8 inch Diameter Jet Array with S/d of 3.

NPR	*T* (°C)	$\dot{m}$ (kg/s)	*OASPL* (dB, ref. 20 µPa)	d_j (in.)	u_j (m/s)	ρ_j (kg/m^3)	M_j	*St*	*AP/DP*
2.1	7.0	0.9	105.7	0.1	368.9	1.4	1.1	0.24	2.1E-05
3.1	1.2	2.9	113.3	0.1	461.9	1.5	1.4	0.23	2.2E-05
4.4	6.8	2.2	115.3	0.2	548.2	1.7	1.7	0.23	1.4E-05
6.1	3.2	3.3	117.4	0.2	617.5	1.9	1.9	0.22	8.7E-06
8.3	5.3	4.3	118.9	0.2	687.4	2.0	2.1	0.23	5.6E-06
10.3	-0.8	5.9	119.2	0.2	724.7	2.2	2.2	0.26	4.0E-06
12.6	1.0	7.8	120.7	0.3	770.9	2.3	2.3	0.28	3.3E-06
15.1	0.9	10.1	122.3	0.3	809.2	2.4	2.4	0.28	2.6E-06
18.5	0.2	29.1	125.7	0.3	851.9	2.6	2.6	0.01	2.3E-06
20.5	0.8	42.6	127.7	0.4	874.5	2.7	2.6	0.02	2.5E-06
24.0	1.0	49.1	129.1	0.4	909.3	2.8	2.7	0.03	2.5E-06

Table B.16: Numerical and Analytical Results From
a 18/125 inch Diameter Jet Array with S/d of 3.

NPR	*T* (°C)	$\dot{m}$ (kg/s)	*OASPL* (dB, ref. 20 µPa)	d_j (in.)	u_j (m/s)	ρ_j (kg/m^3)	M_j	*St*	*AP/DP*
2.0	9.7	0.8	109.6	0.1	348.9	1.3	1.0	0.27	4.1E-05
3.3	9.6	1.4	119.0	0.2	477.9	1.5	1.4	0.25	4.0E-05
4.0	8.9	2.0	121.3	0.2	526.6	1.6	1.6	0.29	3.6E-05
6.0	8.1	3.3	122.2	0.2	613.8	1.8	1.8	0.25	1.7E-05
7.9	7.1	4.7	123.5	0.2	674.5	2.0	2.0	0.25	1.1E-05
10.0	6.2	6.2	124.3	0.3	723.2	2.1	2.2	0.28	7.9E-06
12.2	5.6	7.4	124.8	0.3	764.5	2.3	2.3	0.30	6.0E-06
15.3	5.4	7.3	125.7	0.4	812.5	2.4	2.4	0.33	4.3E-06
20.1	6.0	9.3	128.5	0.4	872.6	2.6	2.6	0.34	3.1E-06
23.6	7.0	13.8	130.7	0.5	908.6	2.7	2.7	0.06	3.2E-06

Table B.17: Numerical and Analytical Results From
a 5/32 inch Diameter Jet Array with S/d of 3.

NPR	*T* (°C)	$\dot{m}$ (kg/s)	*OASPL* (dB, ref. 20 µPa)	d_j (in.)	u_j (m/s)	ρ_j (kg/m^3)	M_j	*St*	*AP/DP*
2.3	29.1	1.5	116.9	0.2	408.0	1.3	1.2	0.26	6.2E-05
3.2	27.1	1.9	122.9	0.2	485.4	1.4	1.4	0.27	6.6E-05
3.9	26.4	2.5	126.0	0.2	536.9	1.5	1.5	0.30	6.5E-05
6.3	23.6	3.6	127.5	0.2	643.1	1.8	1.9	0.27	2.7E-05
8.0	23.3	4.2	128.4	0.3	695.0	1.9	2.0	0.31	1.9E-05
9.9	21.3	6.0	129.2	0.3	740.5	2.0	2.2	0.34	1.4E-05
13.2	20.1	7.9	129.8	0.4	800.6	2.2	2.3	0.37	9.6E-06
14.5	20.2	7.4	130.2	0.4	822.3	2.3	2.4	0.38	8.4E-06
19.7	21.1	12.4	134.0	0.4	891.5	2.5	2.6	0.39	6.3E-06
23.2	22.1	13.8	139.0	0.5	929.6	2.6	2.7	0.06	8.6E-06

Table B.18: Numerical and Analytical Results From
a 1/4 inch Diameter Jet Array with S/d of 3.

NPR	*T* (°C)	$\dot{m}$ (kg/s)	*OASPL* (dB, ref. 20 µPa)	d_j (in.)	u_j (m/s)	ρ_j (kg/m^3)	M_j	*St*	*AP/DP*
2.2	24.8	1.9	118.8	0.3	387.3	1.3	1.1	0.24	7.6E-05
3.7	21.7	2.9	131.1	0.3	517.1	1.5	1.5	0.33	1.2E-04
4.0	20.5	3.2	132.1	0.3	536.4	1.6	1.6	0.33	1.1E-04
6.0	16.6	7.7	133.2	0.4	622.9	1.8	1.8	0.29	5.6E-05
7.9	14.0	5.6	134.4	0.4	681.9	1.9	2.0	0.31	3.8E-05
9.6	12.5	7.5	135.0	0.5	722.1	2.1	2.1	0.42	2.7E-05
12.0	12.2	9.2	136.0	0.5	770.4	2.2	2.3	0.49	2.1E-05
14.8	13.1	11.4	136.7	0.6	816.9	2.3	2.4	0.54	1.6E-05
19.6	12.9	14.5	139.2	0.7	877.0	2.5	2.6	0.59	1.3E-05
21.6	11.4	15.1	142.2	0.8	896.4	2.6	2.7	0.09	1.4E-05

Appendix C: Shadowgraph Imagery

Appendix B displays shadowgraph images for all of the 8x8 jet array iterations. The shadowgraph images reveal shock waves emitted from the supersonic jets individually and as they interact. The jet arrays are observed from the side of the array such that the images reveal the flow moving left to right. The Figures begin with jet arrays with S/d = 1.44 and conclude at jet arrays with S/d = 3.

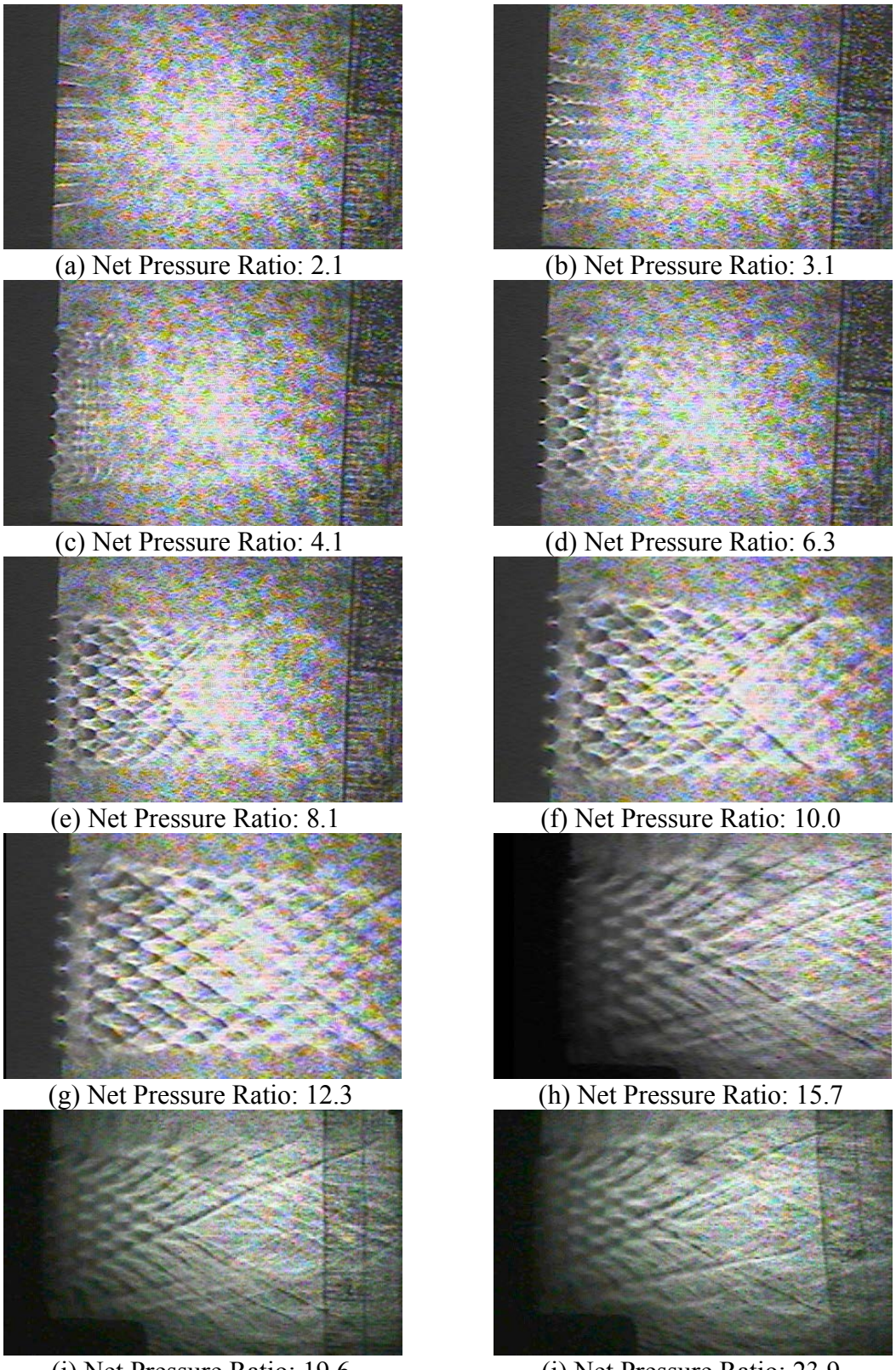

(a) Net Pressure Ratio: 2.1
(b) Net Pressure Ratio: 3.1
(c) Net Pressure Ratio: 4.1
(d) Net Pressure Ratio: 6.3
(e) Net Pressure Ratio: 8.1
(f) Net Pressure Ratio: 10.0
(g) Net Pressure Ratio: 12.3
(h) Net Pressure Ratio: 15.7
(i) Net Pressure Ratio: 19.6
(j) Net Pressure Ratio: 23.9

Figure C.1: Shadowgraph Images for a 1/8 inch Diameter Jet Array with S/d Ratio of 1.44 and at NPR Values Ranging From 2.1 to 23.9.

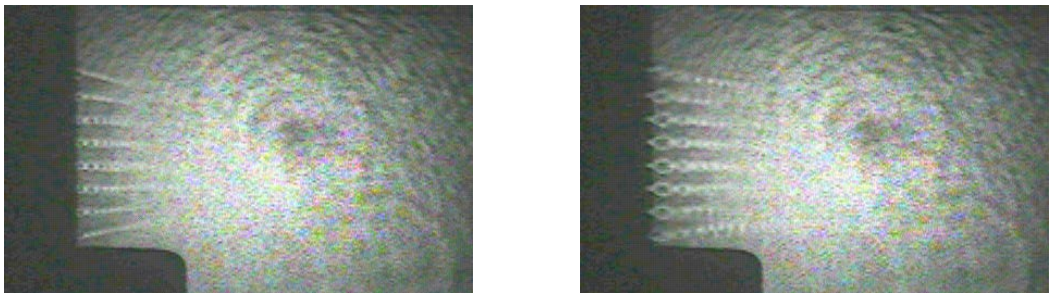

(a) Net Pressure Ratio: 2.3 (b) Net Pressure Ratio: 3.1

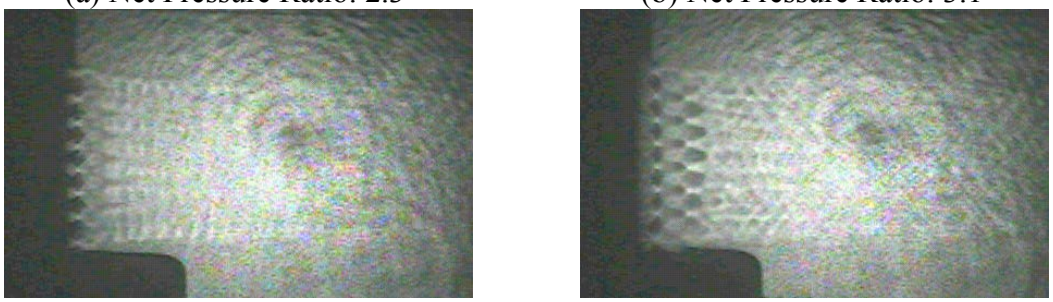

(c) Net Pressure Ratio: 4.0 (d) Net Pressure Ratio: 6.2

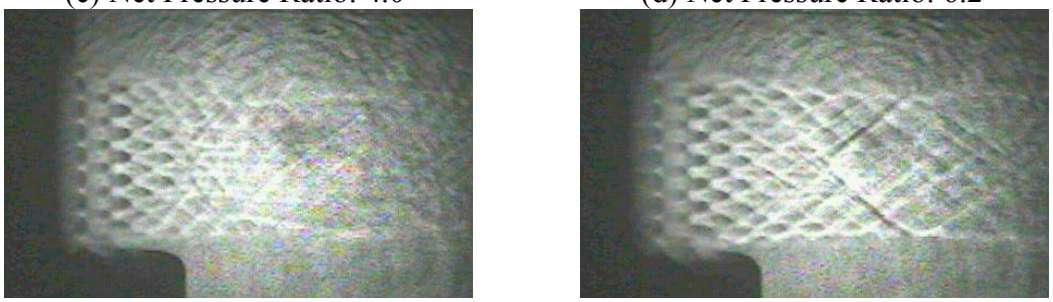

(e) Net Pressure Ratio: 7.9 (f) Net Pressure Ratio: 10.1

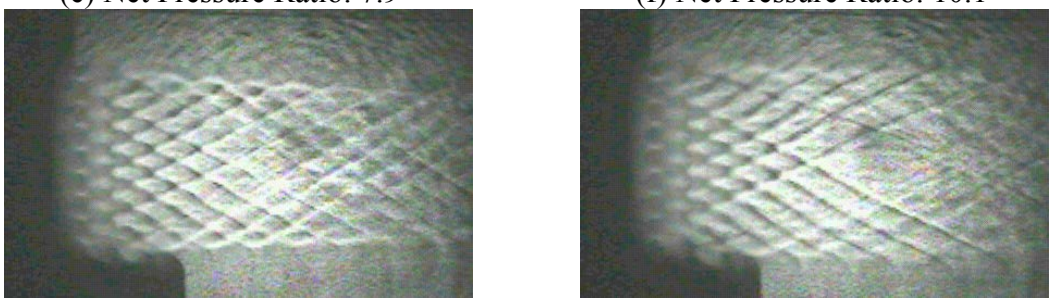

(g) Net Pressure Ratio: 12.0 (h) Net Pressure Ratio: 15.1

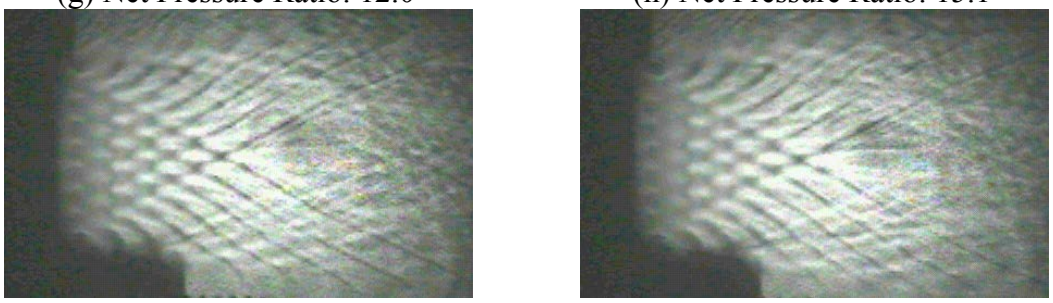

(i) Net Pressure Ratio: 19.6 (j) Net Pressure Ratio: 23.7

Figure C.2: Shadowgraph Images for a 18/125 inch Diameter Jet Array with S/d Ratio of 1.44 and at NPR Values Ranging From 2.3 to 23.7.

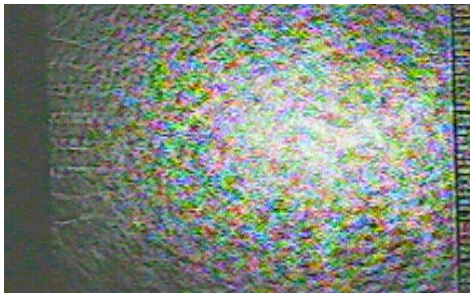

(a) Net Pressure Ratio: 2.1

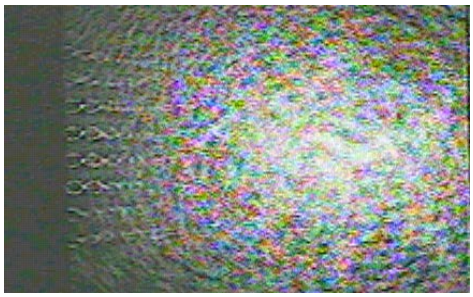

(b) Net Pressure Ratio: 3.0

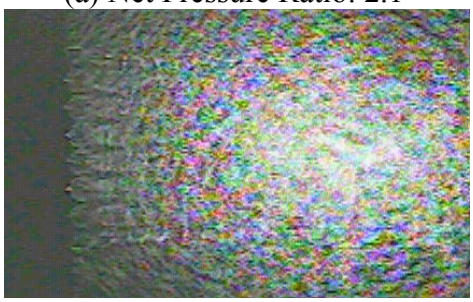

(c) Net Pressure Ratio: 4.1

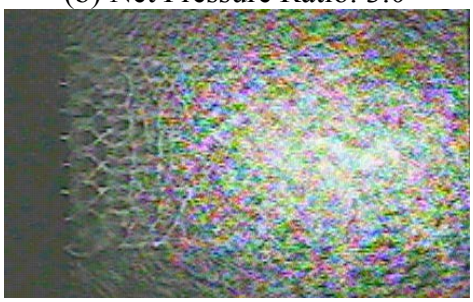

(d) Net Pressure Ratio: 6.0

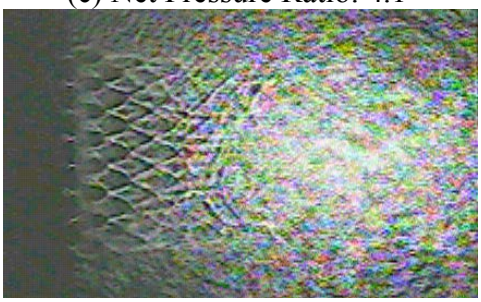

(e) Net Pressure Ratio: 8.1

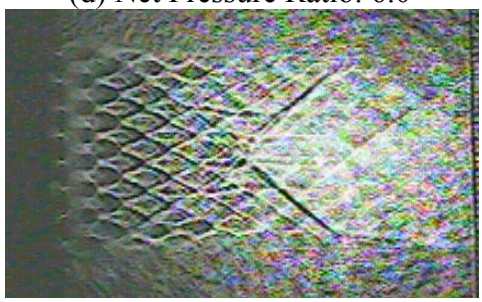

(f) Net Pressure Ratio: 10.2

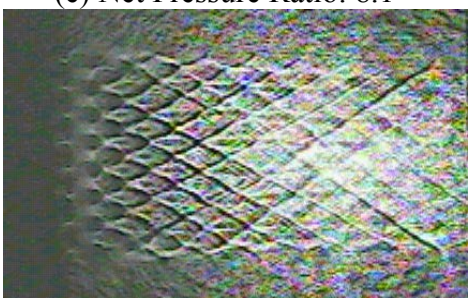

(g) Net Pressure Ratio: 12.1

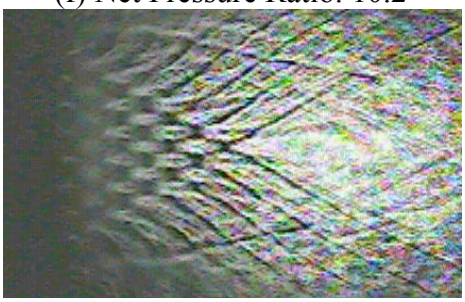

(h) Net Pressure Ratio: 15.3

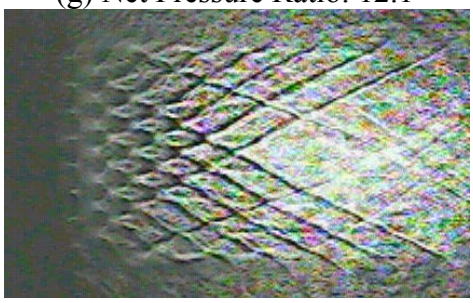

(i) Net Pressure Ratio: 20.2

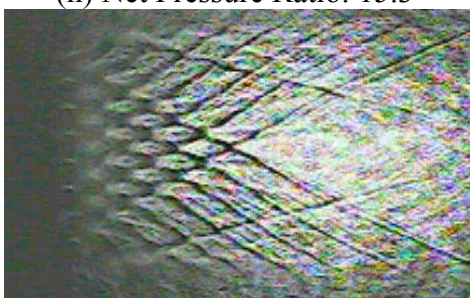

(j) Net Pressure Ratio: 24.2

Figure C.3: Shadowgraph Images for a 5/32 inch Diameter Jet Array with S/d Ratio of 1.44 and at NPR Values Ranging From 2.1 to 24.2.

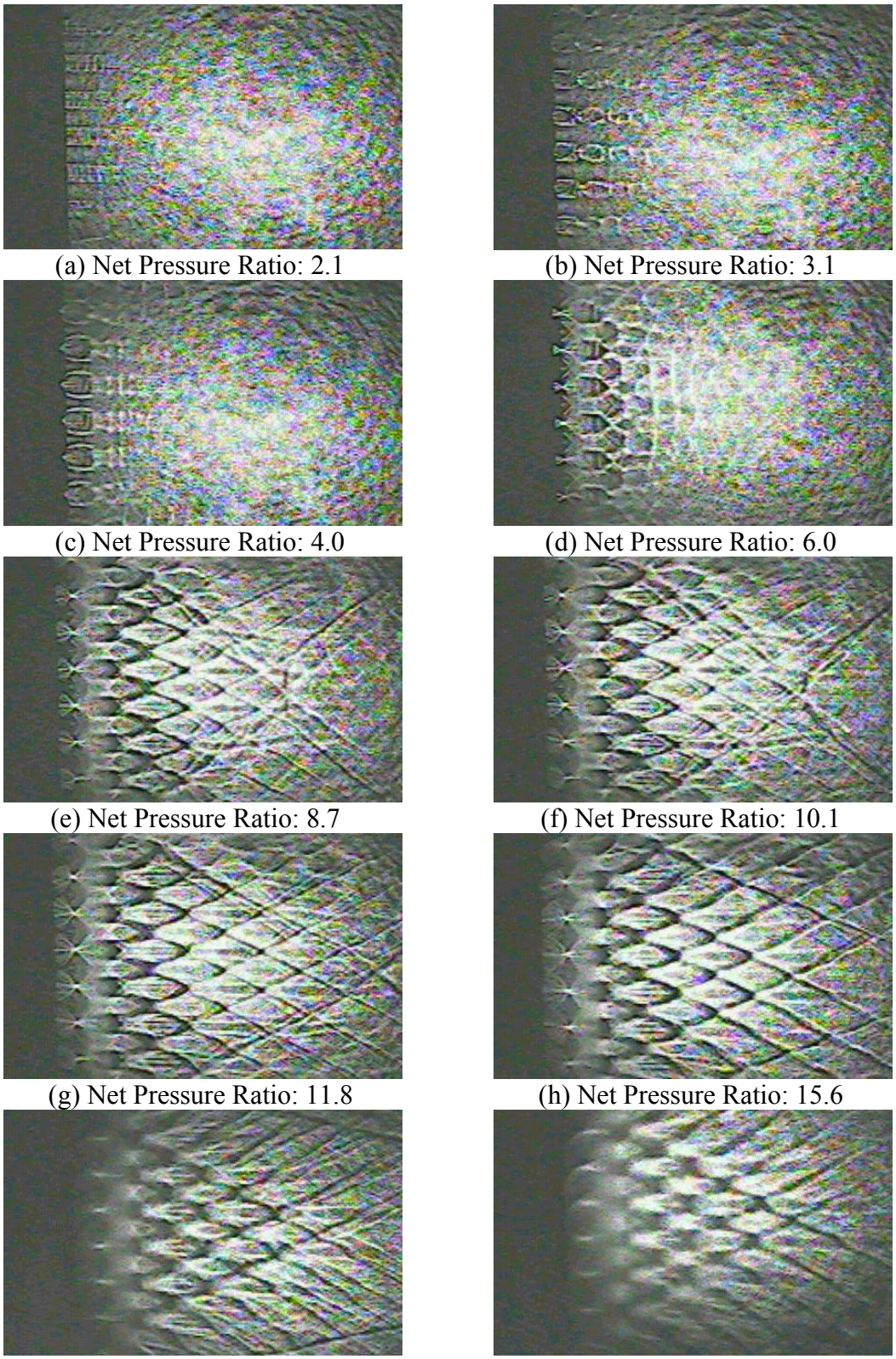

(a) Net Pressure Ratio: 2.1
(b) Net Pressure Ratio: 3.1
(c) Net Pressure Ratio: 4.0
(d) Net Pressure Ratio: 6.0
(e) Net Pressure Ratio: 8.7
(f) Net Pressure Ratio: 10.1
(g) Net Pressure Ratio: 11.8
(h) Net Pressure Ratio: 15.6
(i) Net Pressure Ratio: 19.5
(j) Net Pressure Ratio: 25.0

Figure C.4: Shadowgraph Images for a 1/4 inch Diameter Jet Array with S/d Ratio of 1.44 and at NPR Values Ranging From 2.1 to 25.0.

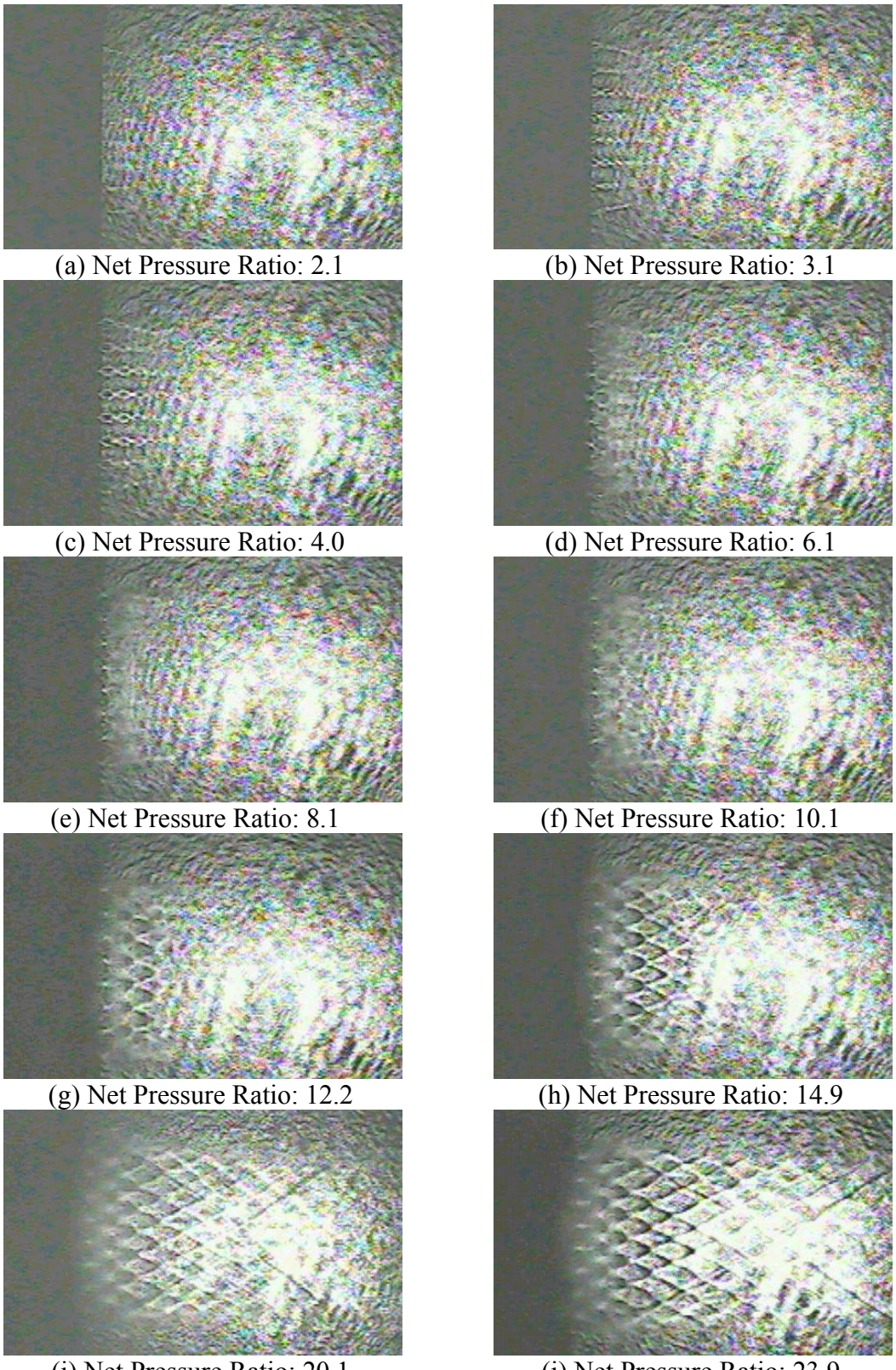

(a) Net Pressure Ratio: 2.1 (b) Net Pressure Ratio: 3.1

(c) Net Pressure Ratio: 4.0 (d) Net Pressure Ratio: 6.1

(e) Net Pressure Ratio: 8.1 (f) Net Pressure Ratio: 10.1

(g) Net Pressure Ratio: 12.2 (h) Net Pressure Ratio: 14.9

(i) Net Pressure Ratio: 20.1 (j) Net Pressure Ratio: 23.9

Figure C.5: Shadowgraph Images for a 1/8 inch Diameter Jet Array with S/d Ratio of 2 and at NPR Values Ranging From 2.1 to 23.9.

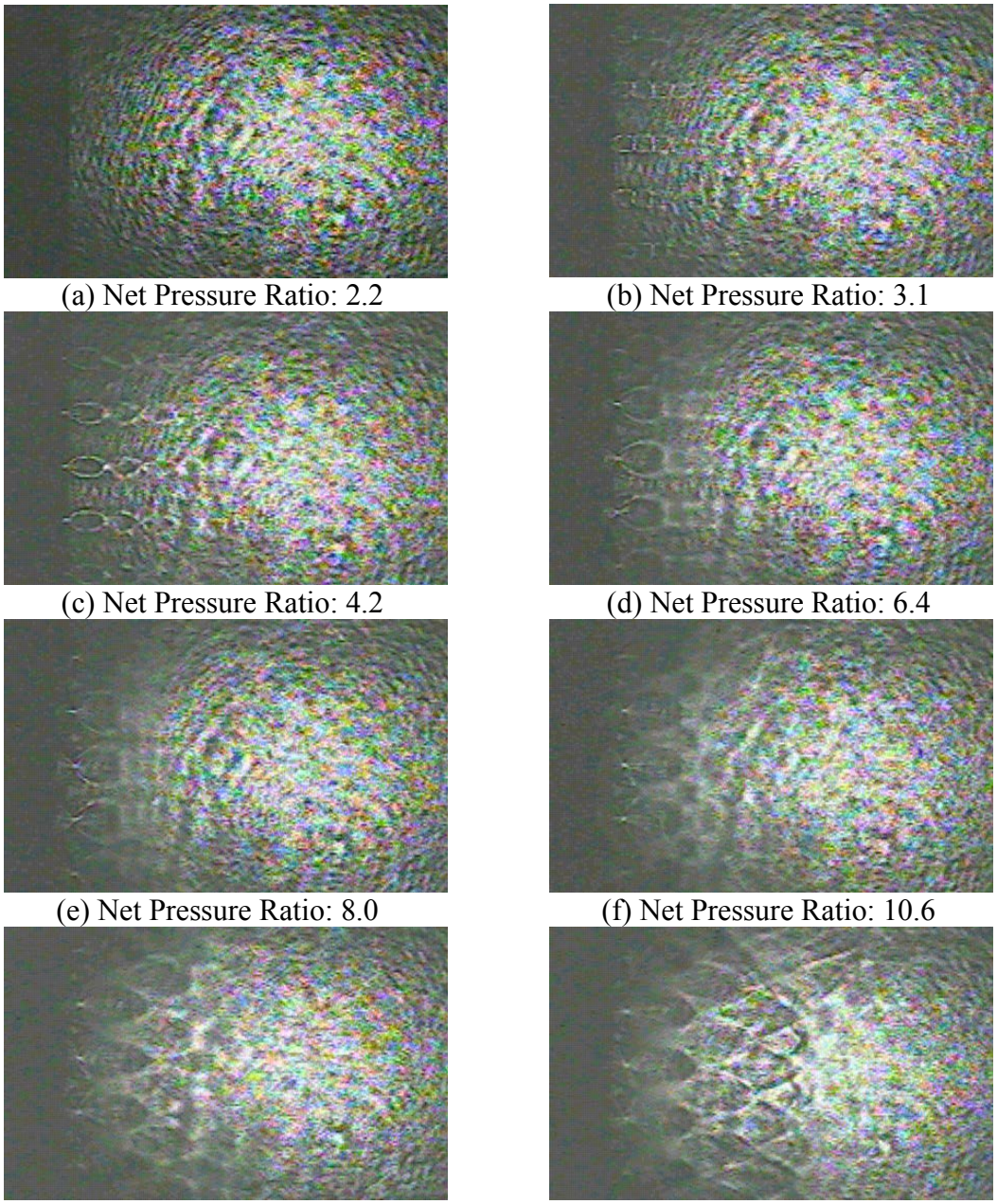

(a) Net Pressure Ratio: 2.2 (b) Net Pressure Ratio: 3.1

(c) Net Pressure Ratio: 4.2 (d) Net Pressure Ratio: 6.4

(e) Net Pressure Ratio: 8.0 (f) Net Pressure Ratio: 10.6

(g) Net Pressure Ratio: 12.2 (h) Net Pressure Ratio: 14.6

Figure C.6: Shadowgraph Images for a 1/4 inch Diameter Jet Array with S/d Ratio of 2 and NPR Values Ranging From 2.2 to 14.6.

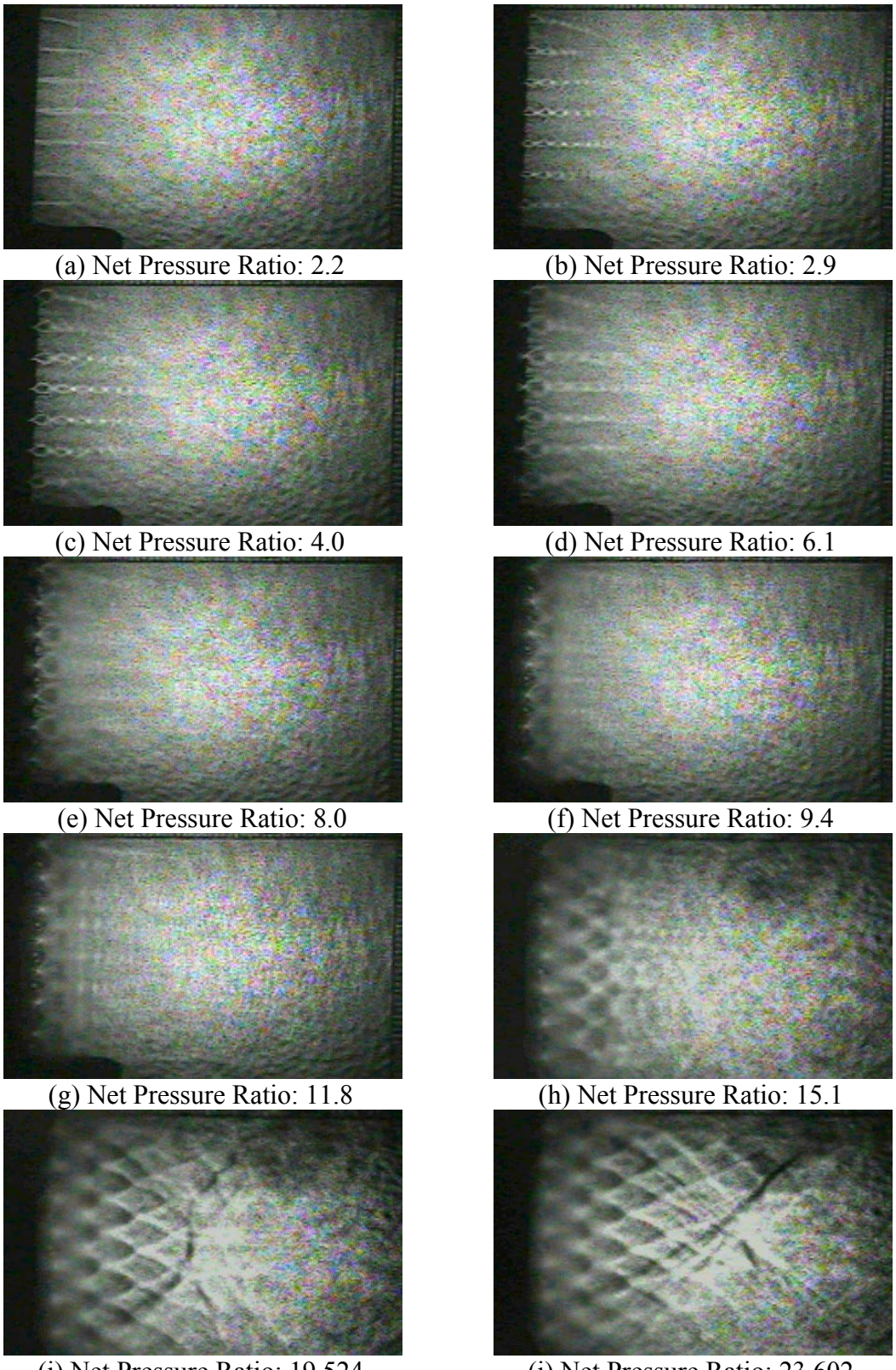

(a) Net Pressure Ratio: 2.2
(b) Net Pressure Ratio: 2.9
(c) Net Pressure Ratio: 4.0
(d) Net Pressure Ratio: 6.1
(e) Net Pressure Ratio: 8.0
(f) Net Pressure Ratio: 9.4
(g) Net Pressure Ratio: 11.8
(h) Net Pressure Ratio: 15.1
(i) Net Pressure Ratio: 19.524
(j) Net Pressure Ratio: 23.602

Figure C.7: Shadowgraph Images for a 1/8 inch Diameter Jet Array with S/d Ratio of 2.5 and NPR Values Ranging From 2.2 to 23.6.

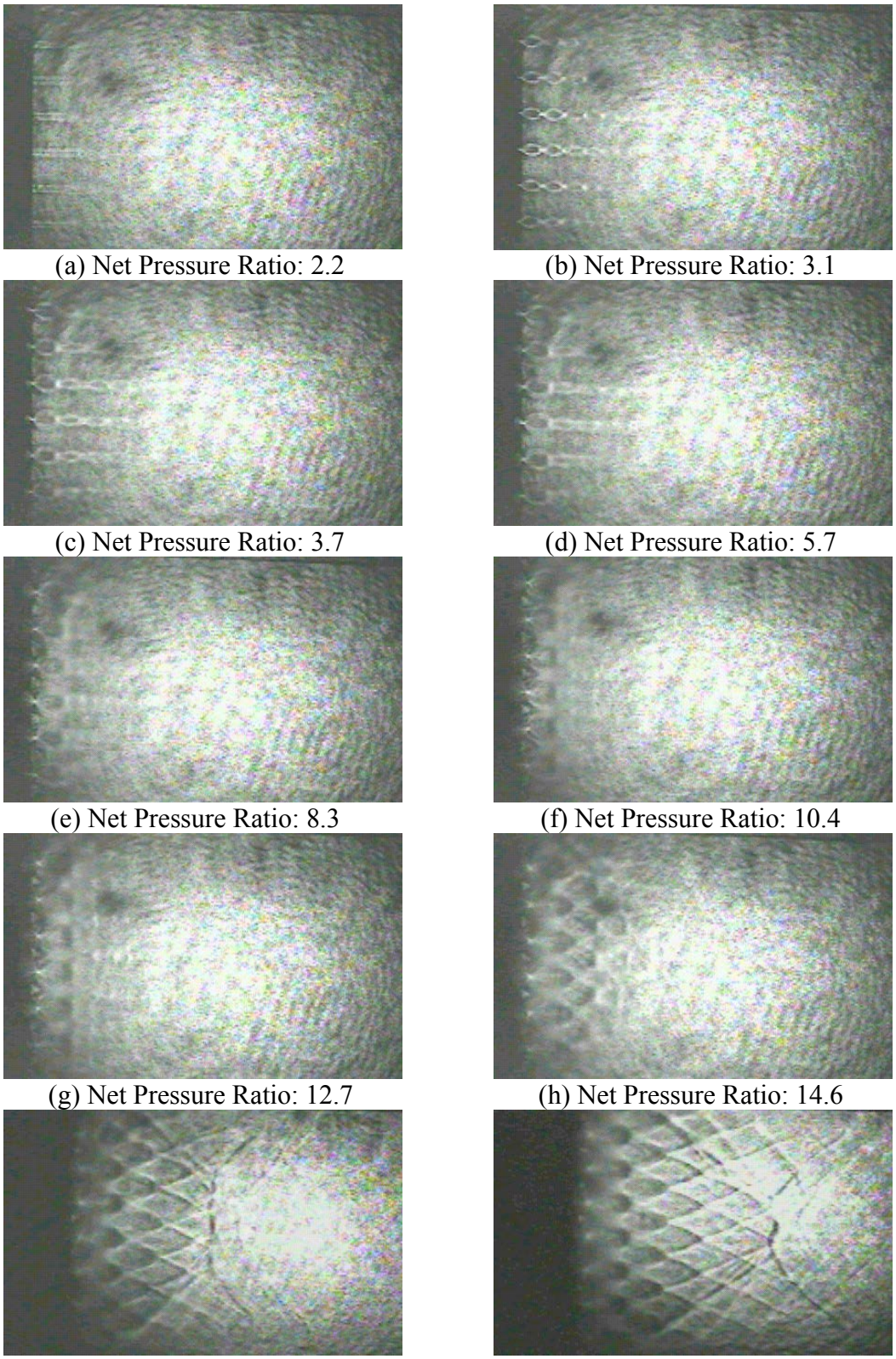

(a) Net Pressure Ratio: 2.2
(b) Net Pressure Ratio: 3.1
(c) Net Pressure Ratio: 3.7
(d) Net Pressure Ratio: 5.7
(e) Net Pressure Ratio: 8.3
(f) Net Pressure Ratio: 10.4
(g) Net Pressure Ratio: 12.7
(h) Net Pressure Ratio: 14.6
(i) Net Pressure Ratio: 19.7
(j) Net Pressure Ratio: 23.9

Figure C.8: Shadowgraph Images for a 18/125 inch Diameter Jet Array with S/d Ratio of 2.5 and at NPR Values Ranging From 2.2 to 23.9

(a) Net Pressure Ratio: 2.2

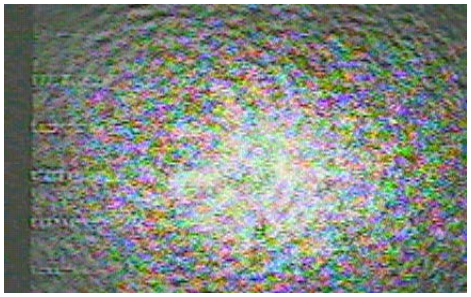

(b) Net Pressure Ratio: 2.9

(c) Net Pressure Ratio: 3.9

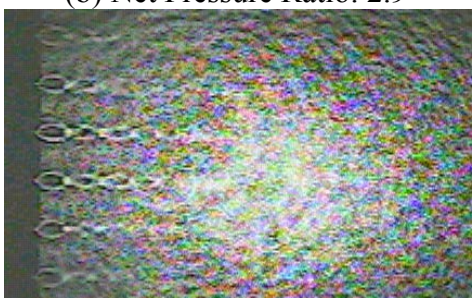

(d) Net Pressure Ratio: 5.5

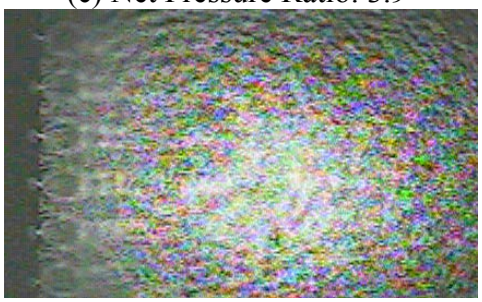

(e) Net Pressure Ratio: 8.4

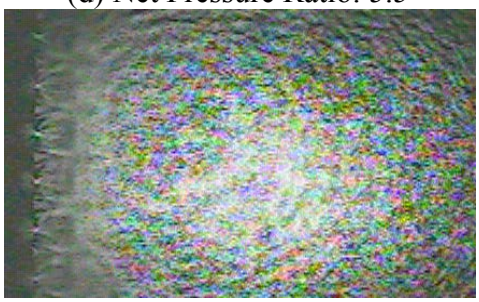

(f) Net Pressure Ratio: 10.3

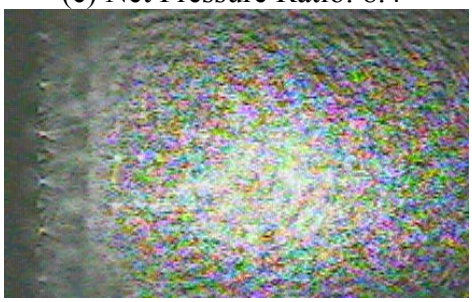

(g) Net Pressure Ratio: 13.1

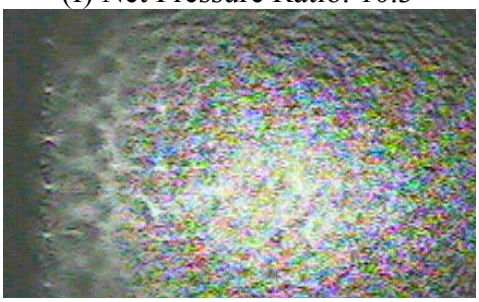

(h) Net Pressure Ratio: 14.9

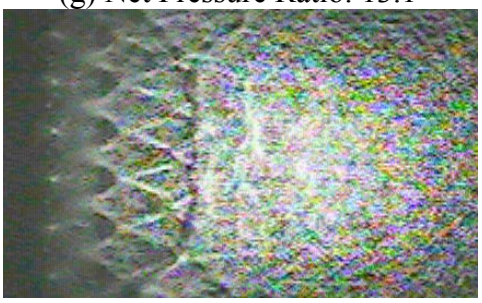

(i) Net Pressure Ratio: 20.1

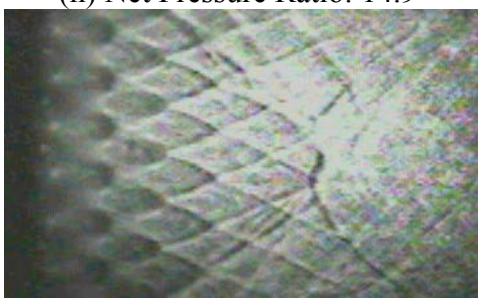

(j) Net Pressure Ratio: 23.5

Figure C.9: Shadowgraph Images for a 5/32 inch Diameter Jet Array with S/d Ratio of 2.5 and at NPR Values Ranging From 2.2 to 23.5.

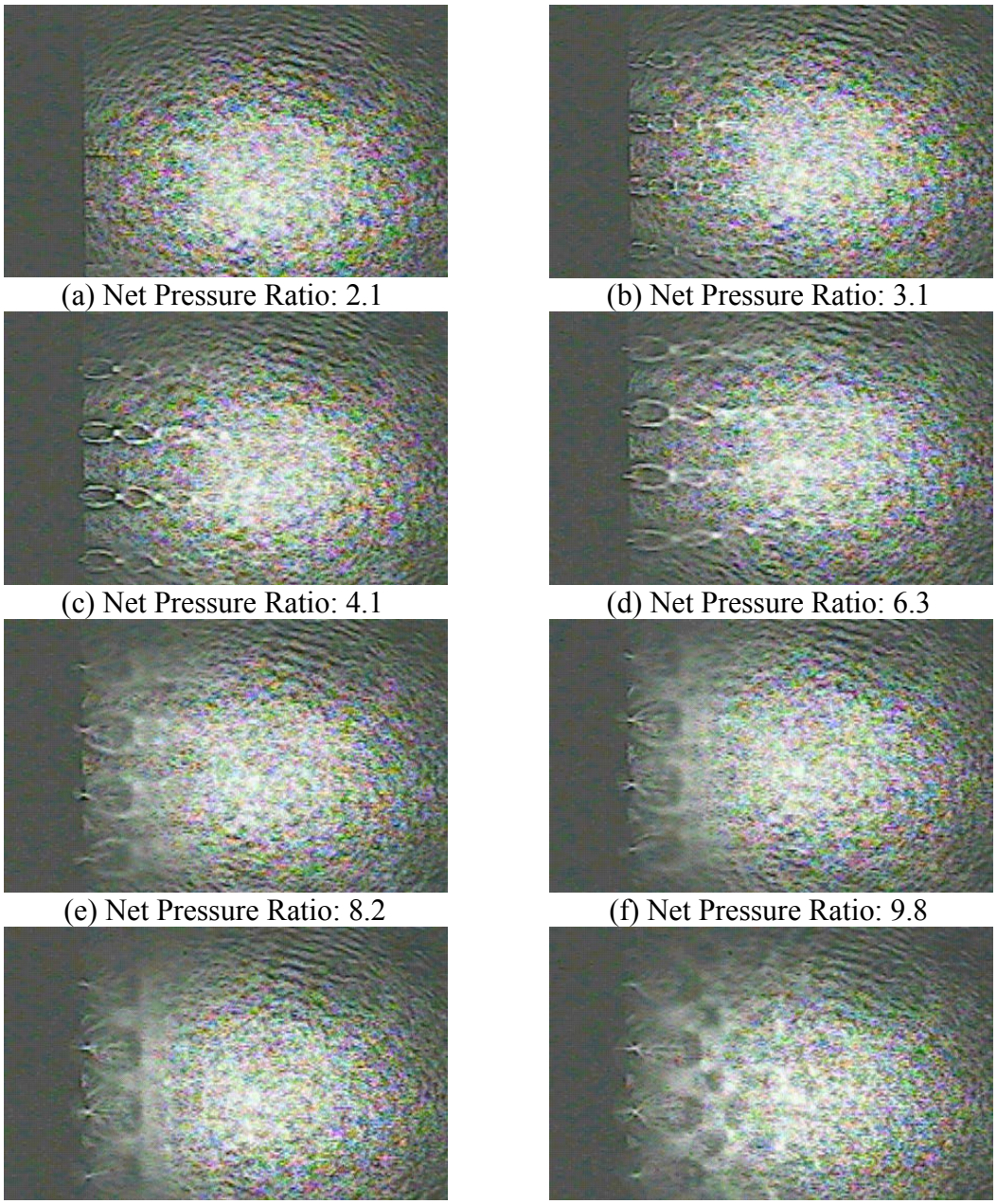

(a) Net Pressure Ratio: 2.1 (b) Net Pressure Ratio: 3.1

(c) Net Pressure Ratio: 4.1 (d) Net Pressure Ratio: 6.3

(e) Net Pressure Ratio: 8.2 (f) Net Pressure Ratio: 9.8

(g) Net Pressure Ratio: 11.5 (h) Net Pressure Ratio: 14.5

Figure C.10: Shadowgraph Images for a 1/4 inch Diameter Jet Array with S/d Ratio of 2.5 and at NPR Values Ranging From 2.1 to 14.5.

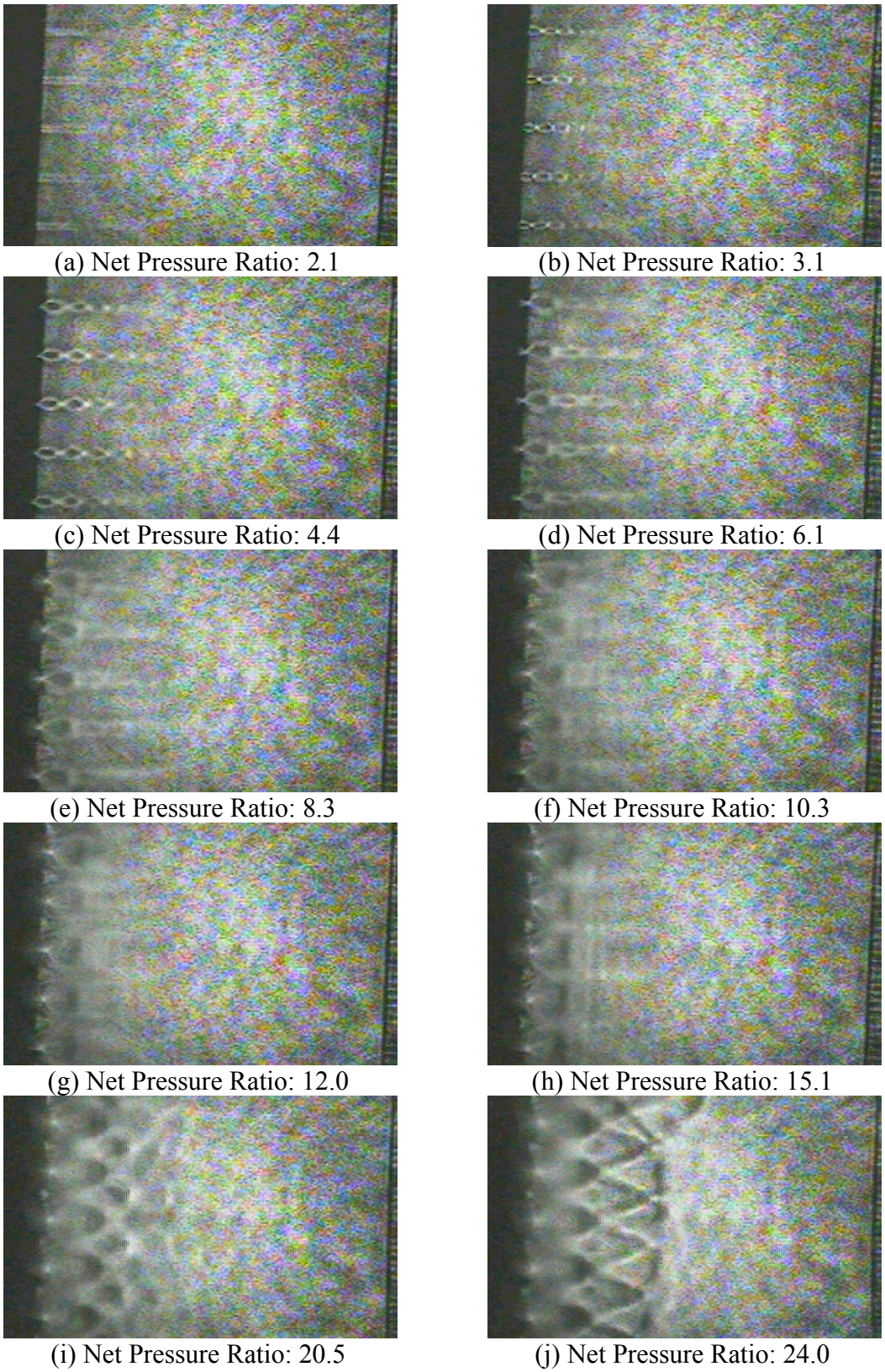

(a) Net Pressure Ratio: 2.1
(b) Net Pressure Ratio: 3.1
(c) Net Pressure Ratio: 4.4
(d) Net Pressure Ratio: 6.1
(e) Net Pressure Ratio: 8.3
(f) Net Pressure Ratio: 10.3
(g) Net Pressure Ratio: 12.0
(h) Net Pressure Ratio: 15.1
(i) Net Pressure Ratio: 20.5
(j) Net Pressure Ratio: 24.0

Figure C.11: Shadowgraph Images for a 1/8 inch Diameter Jet Array with S/d Ratio of 3 and at NPR Values Ranging From 2.1 to 24.0.

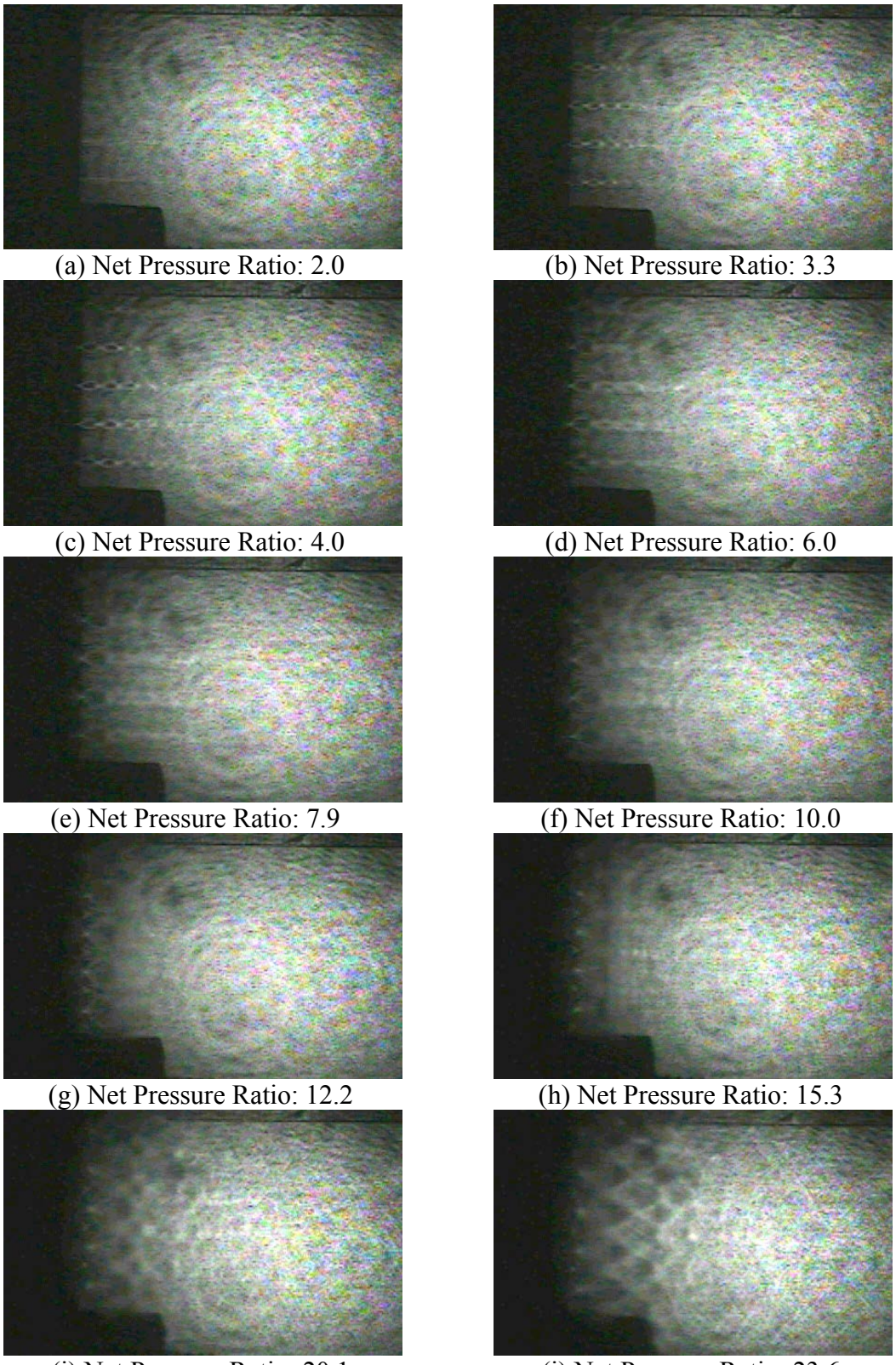

(a) Net Pressure Ratio: 2.0
(b) Net Pressure Ratio: 3.3
(c) Net Pressure Ratio: 4.0
(d) Net Pressure Ratio: 6.0
(e) Net Pressure Ratio: 7.9
(f) Net Pressure Ratio: 10.0
(g) Net Pressure Ratio: 12.2
(h) Net Pressure Ratio: 15.3
(i) Net Pressure Ratio: 20.1
(j) Net Pressure Ratio: 23.6

Figure C.12: Shadowgraph Images for a 18/125 inch Diameter Jet Array with S/d Ratio of 3 and at NPR Values Ranging From 2.0 to 13.6.

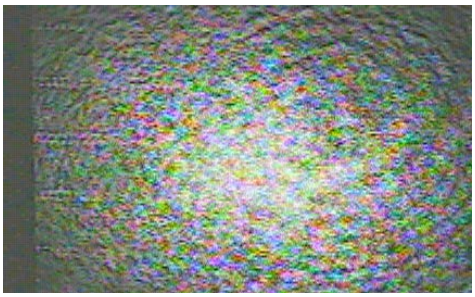

(a) Net Pressure Ratio: 2.3

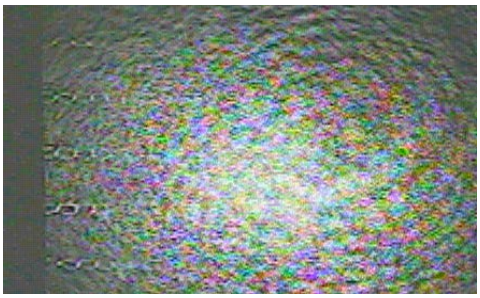

(b) Net Pressure Ratio: 3.2

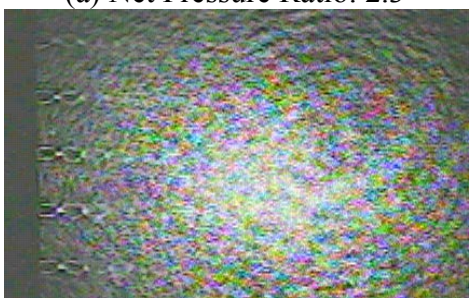

(c) Net Pressure Ratio: 3.9

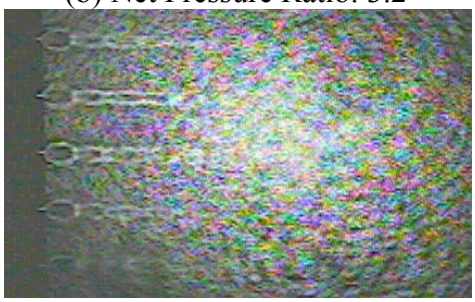

(d) Net Pressure Ratio: 6.3

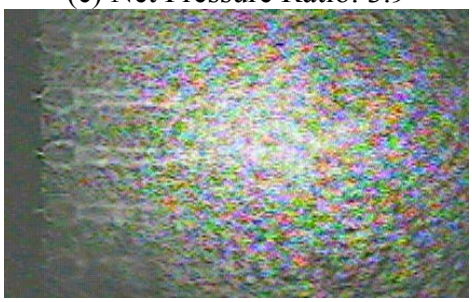

(e) Net Pressure Ratio: 8.0

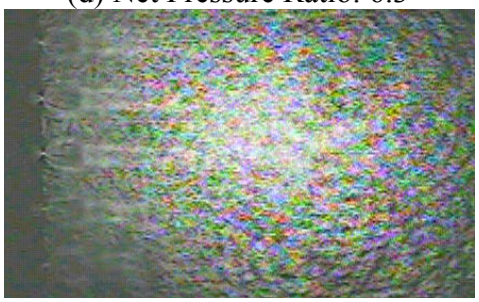

(f) Net Pressure Ratio: 9.9

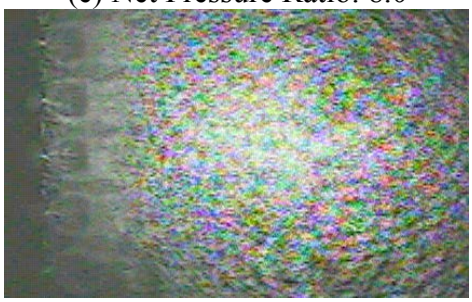

(g) Net Pressure Ratio: 13.2

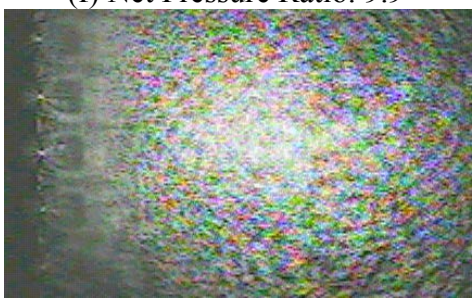

(h) Net Pressure Ratio: 14.5

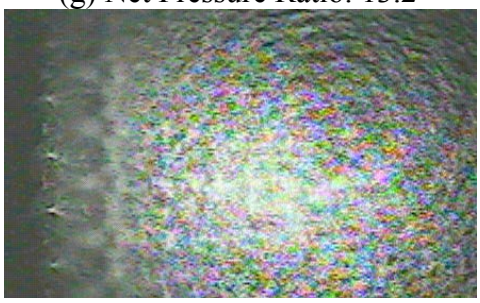

(i) Net Pressure Ratio: 19.7

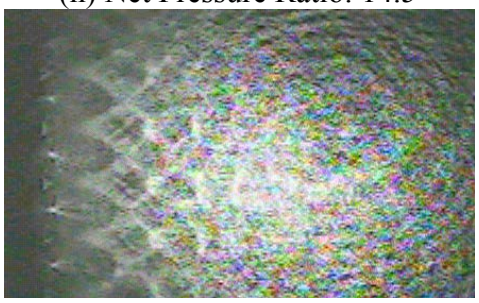

(j) Net Pressure Ratio: 23.2

Figure C.13: Shadowgraph Images for a 5/32 inch Diameter Jet Array with S/d Ratio of 3 and at NPR Values Ranging From 2.3 to 23.2.

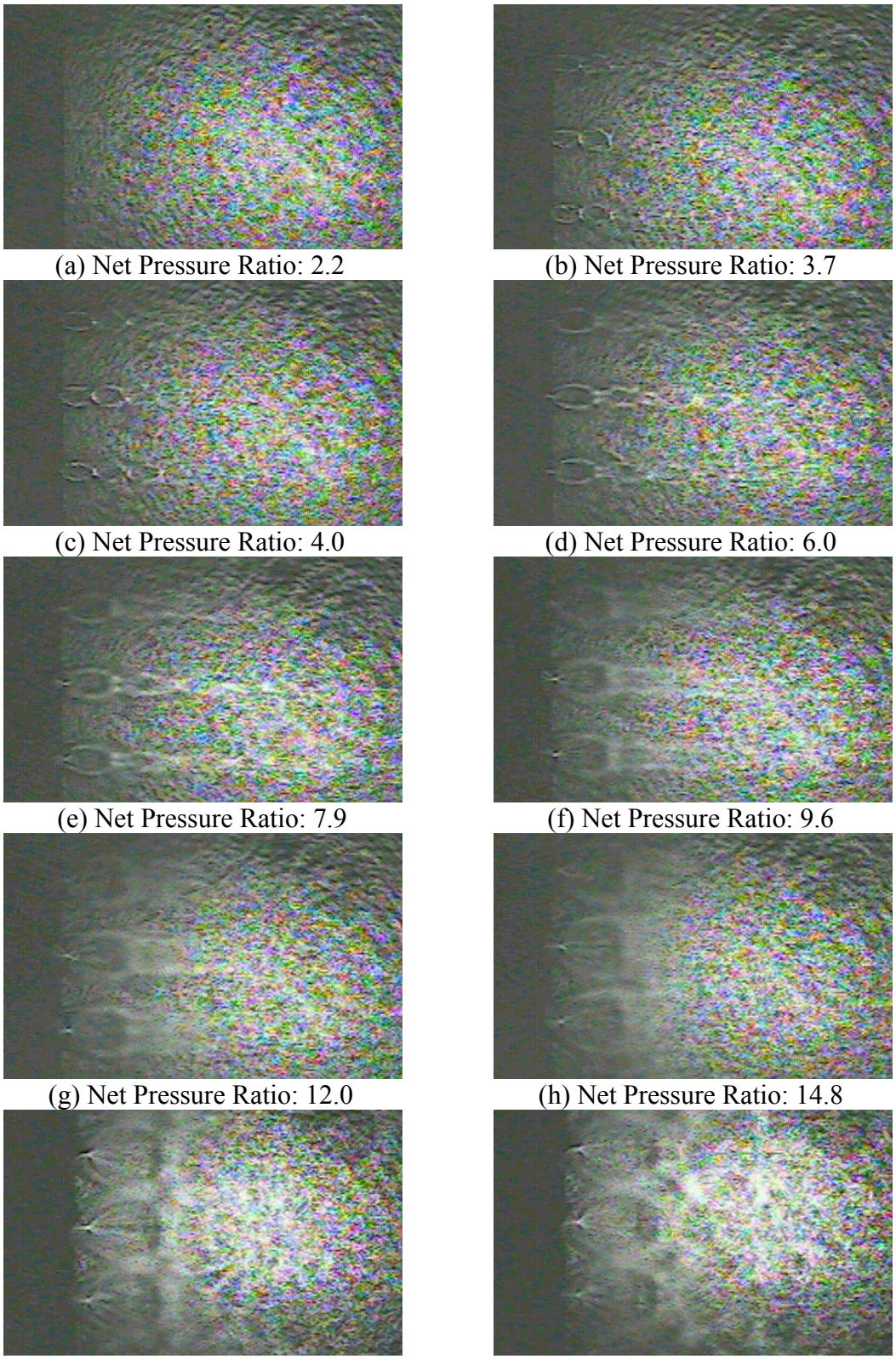

(a) Net Pressure Ratio: 2.2
(b) Net Pressure Ratio: 3.7
(c) Net Pressure Ratio: 4.0
(d) Net Pressure Ratio: 6.0
(e) Net Pressure Ratio: 7.9
(f) Net Pressure Ratio: 9.6
(g) Net Pressure Ratio: 12.0
(h) Net Pressure Ratio: 14.8
(i) Net Pressure Ratio: 19.6
(j) Net Pressure Ratio: 21.6

Figure C.14: Shadowgraph Images for a 1/4 inch Diameter Jet Array with S/d Ratio of 3 and at NPR Values Ranging From 2.2 to 21.6.

Appendix D: Frequency Domain Spectra

Appendix D presents the acoustic pressure in the frequency domain for single jets and 8x8 jet arrays. Data was acquired at 30° offset of the centerline axis of the flow and at a 1 m radius. At this position is the highest sound pressure output from a single supersonic axisymmetric jet. The acoustic emissions from the noise mechanisms being acquired are turbulent mixing noise and narrowband shock associated noise, or screech. The Figures begin with spectra for the single nozzles than presents spectra for the jet arrays beginning with S/d = 1.44 jet arrays and concluding with S/d = 3.

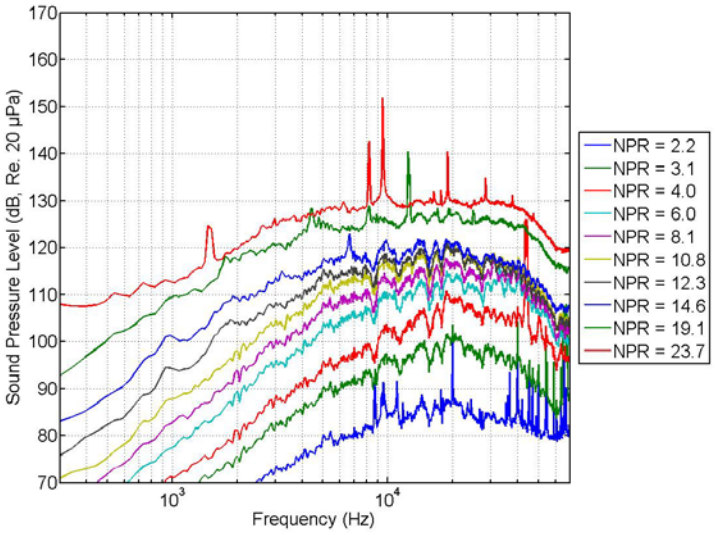

Figure D.1: Frequency Spectra for a Single 1/8 inch Nozzle Diameter Jet and at NPR Values Ranging From 2.2 to 23.7.

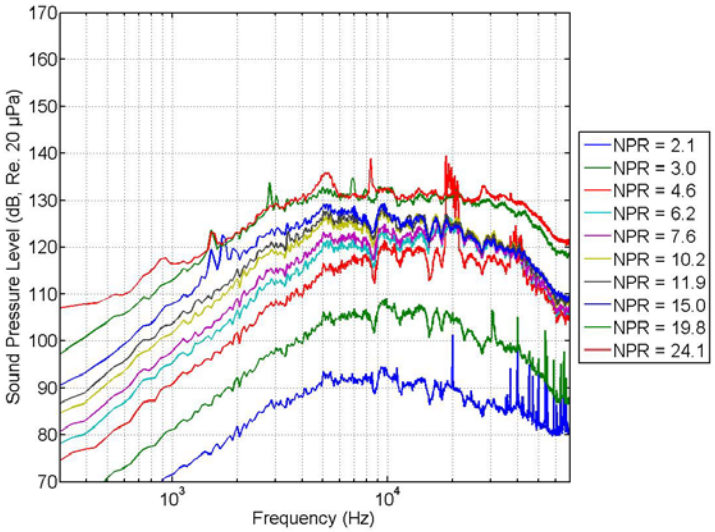

Figure D.2: Frequency Spectra for a Single 1/4 inch Nozzle Diameter Jet and at NPR Values Ranging From 2.1 to 24.1

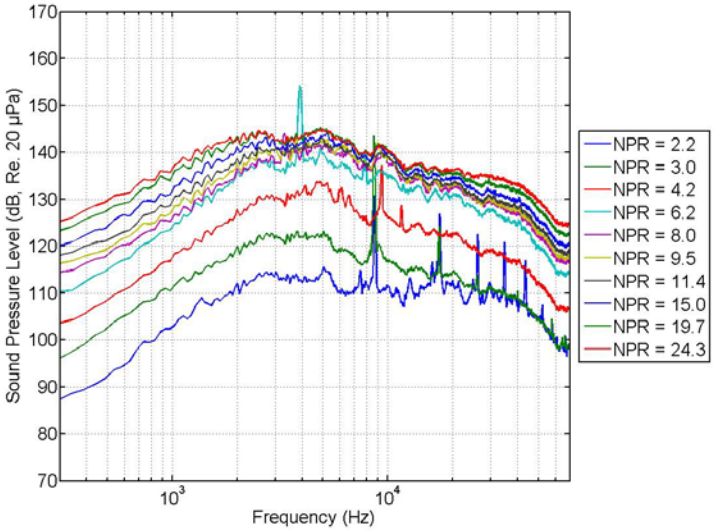

Figure D.3: Frequency Spectra for a Single 1 inch Nozzle Diameter Jet and at NPR Values Ranging From 2.2 to 24.3.

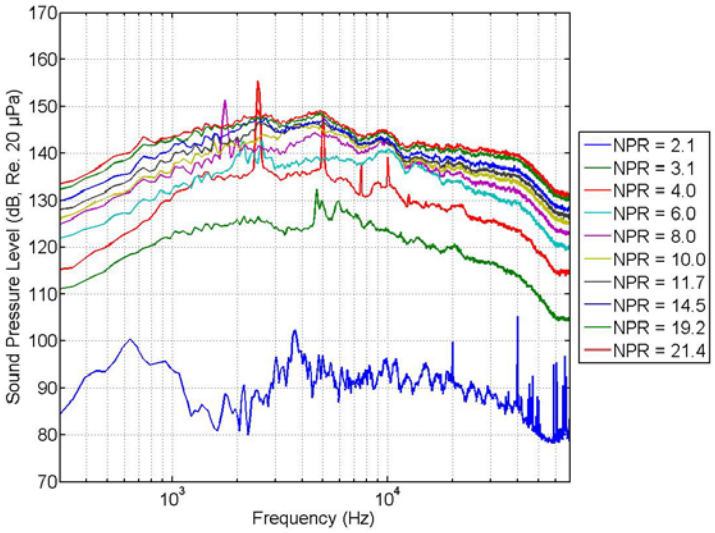

Figure D.4: Frequency Spectra for a Single 2 inch Nozzle Diameter Jet and at NPR Values Ranging From 2.1 to 21.4.

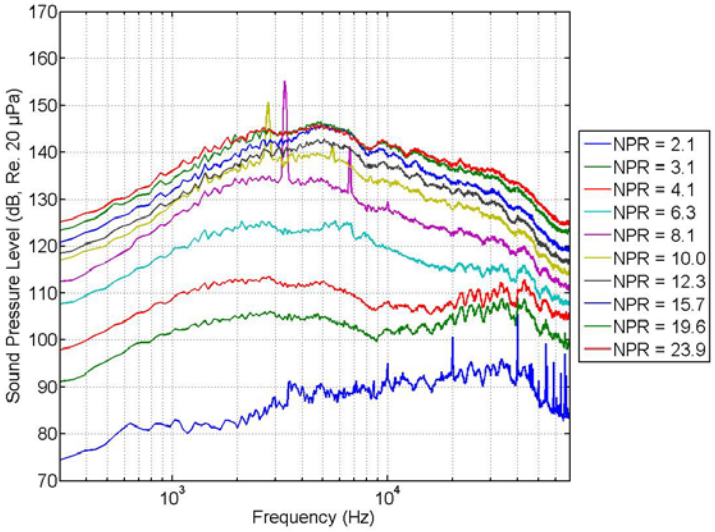

Figure D.5: Frequency Spectra for a 1/8 inch Diameter Jet Array with S/d Ratio of 1.44 and at NPR Values Ranging From 2.1 to 23.9.

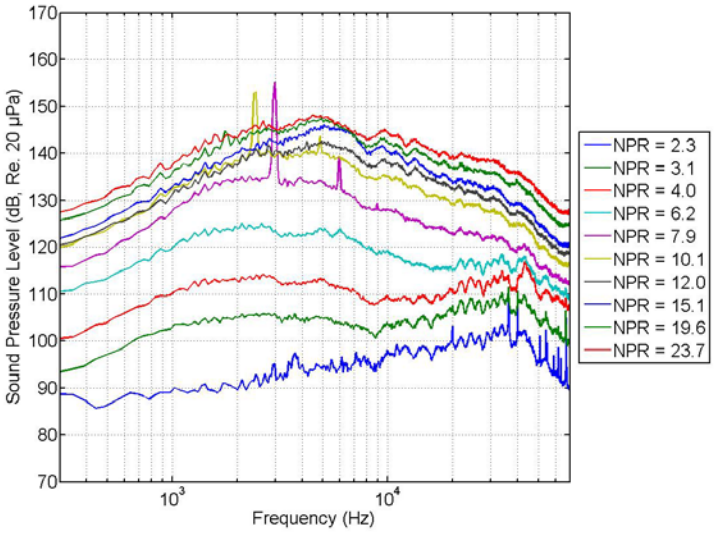

Figure D.6: Frequency Spectra for a 18/125 inch Diameter Jet Array with S/d Ratio of 1.44 and at NPR Values Ranging From 2.3 to 23.7.

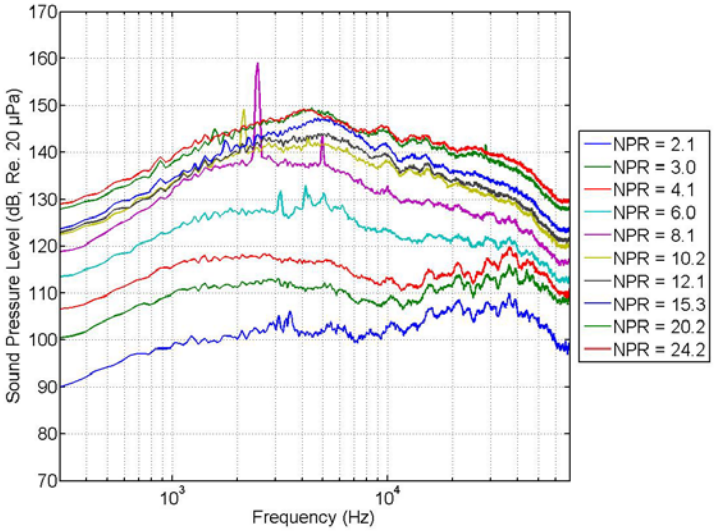

Figure D.7: Frequency Spectra for a 5/32 inch Diameter Jet Array with S/d Ratio of 1.44 and at NPR Values Ranging From 2.1 to 24.2.

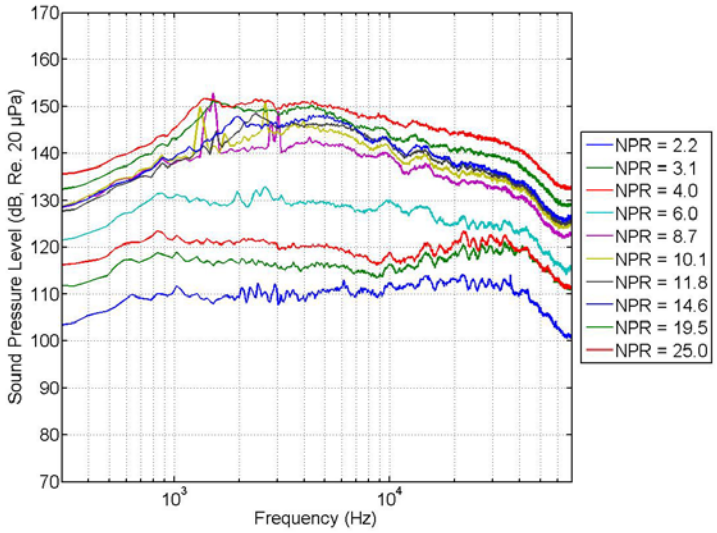

Figure D.8: Frequency Spectra for a 1/4 inch Diameter Jet Array with S/d Ratio of 1.44 and at NPR Values Ranging From 2.2 to 25.0.

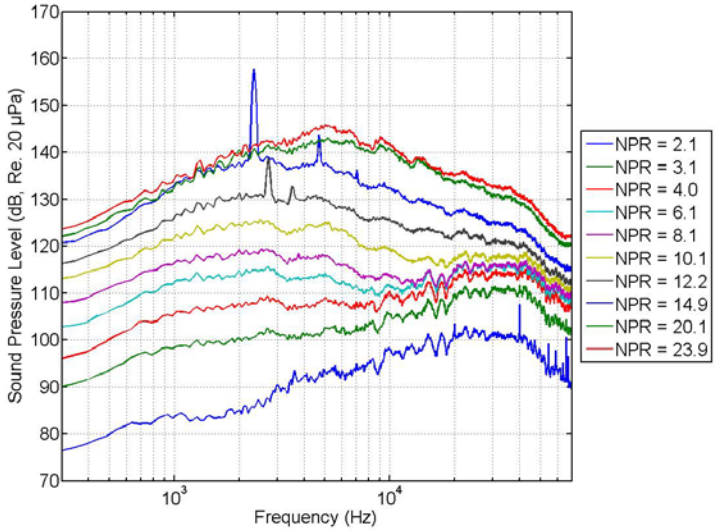

Figure D.9: Frequency Spectra for a 1/8 inch Diameter Jet Array with S/d Ratio of 2 and at NPR Values Ranging From 2.1 to 23.9.

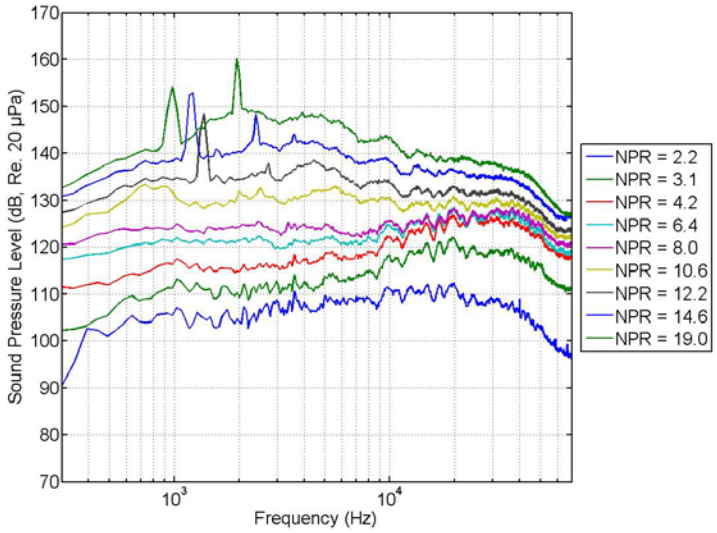

Figure D.10: Frequency Spectra for a 1/4 inch Diameter Jet Array with S/d Ratio of 2 and at NPR Values Ranging From 2.2 to 19.0.

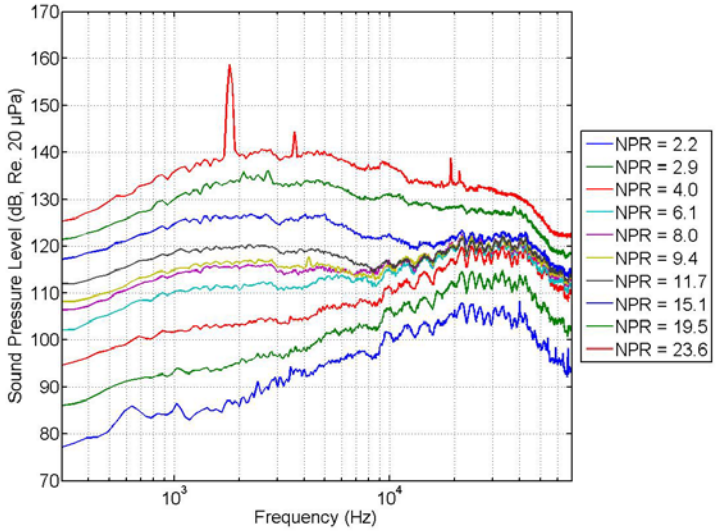

Figure D.11: Frequency Spectra for a 1/8 inch Diameter Jet Array with S/d Ratio of 2.5 and at NPR Values Ranging From 2.2 to 23.6.

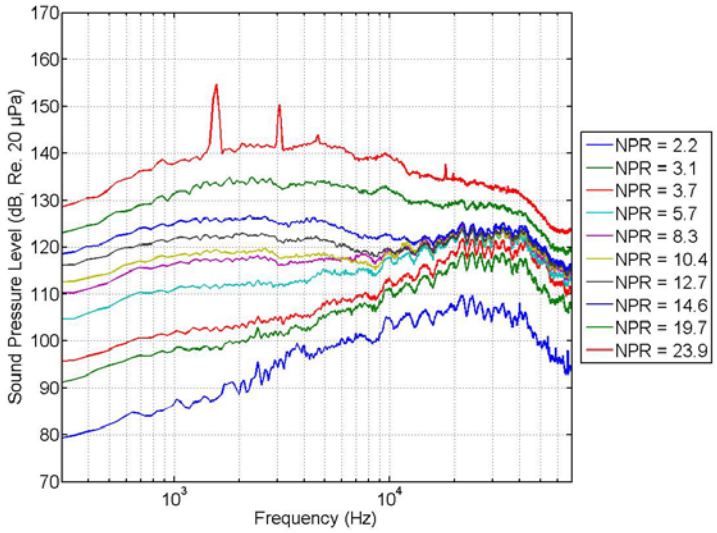

Figure D.12: Frequency Spectra for a 18/125 inch Diameter Jet Array with S/d Ratio of 2.5 and at NPR Values Ranging From 2.2 to 23.9.

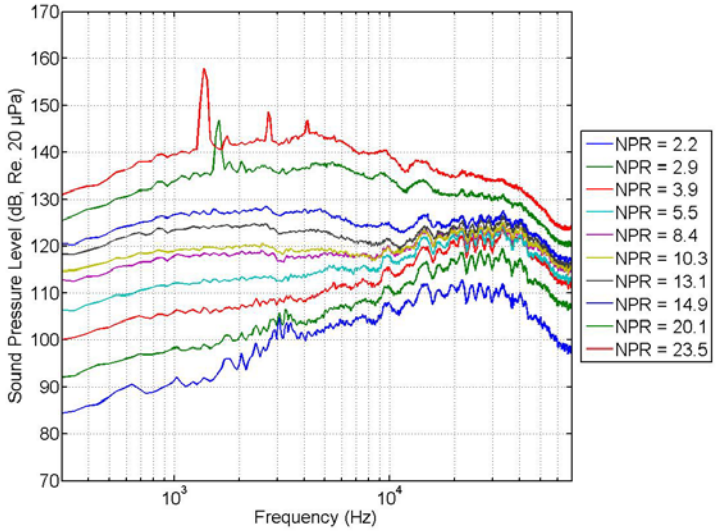

Figure D.13: Frequency Spectra for a 5/32 inch Diameter Jet Array with S/d Ratio of 2.5 and at NPR Values Ranging From 2.2 to 23.5.

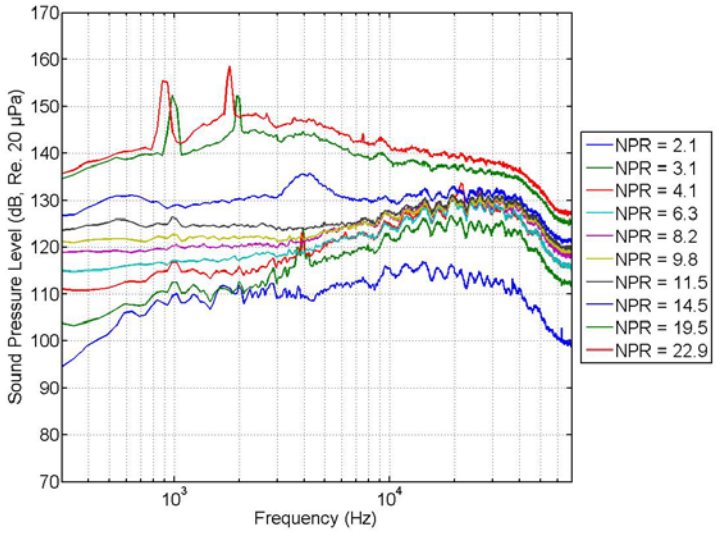

Figure D.14: Frequency Spectra for a 1/4 inch Diameter Jet Array with S/d Ratio of 2.5 and at NPR Values Ranging From 2.1 to 22.9.

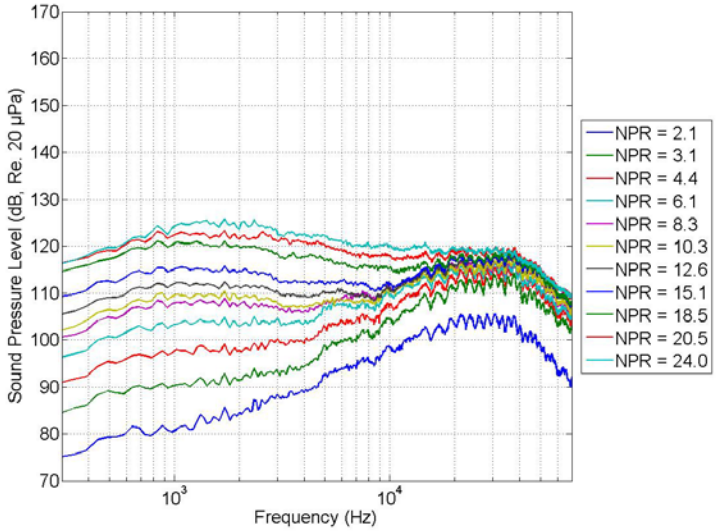

Figure D.15: Frequency Spectra for a 1/8 inch Diameter Jet Array with S/d Ratio of 3 and at NPR Values Ranging From 2.1 to 24.0.

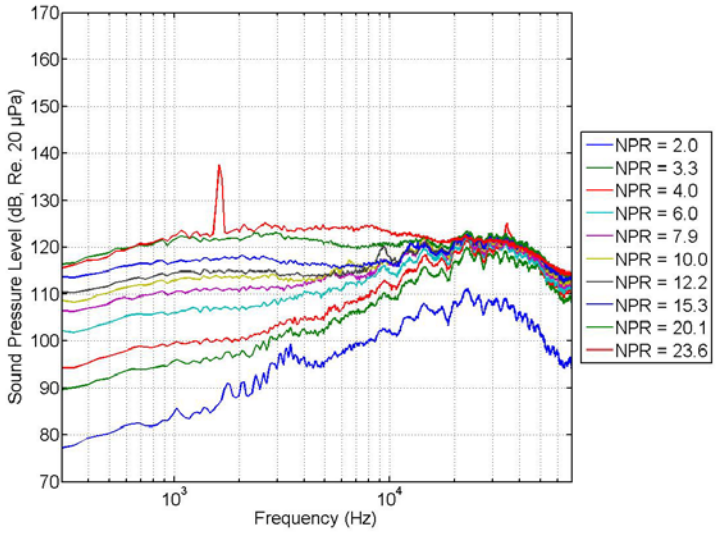

Figure D.16: Frequency Spectra for a 18/125 inch Diameter Jet Array with S/d Ratio of 3 and at NPR Values Ranging From 2.0 to 23.6.

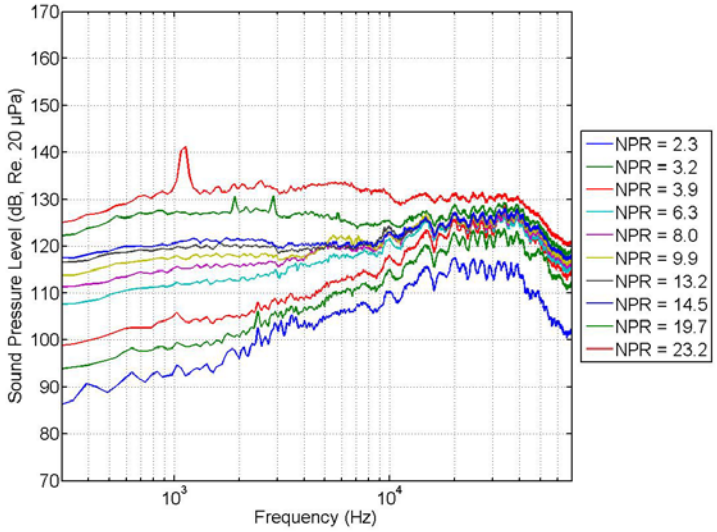

Figure D.17: Frequency Spectra for a 5/32 inch Diameter Jet Array with S/d Ratio of 3 and at NPR Values Ranging From 2.3 to 23.2.

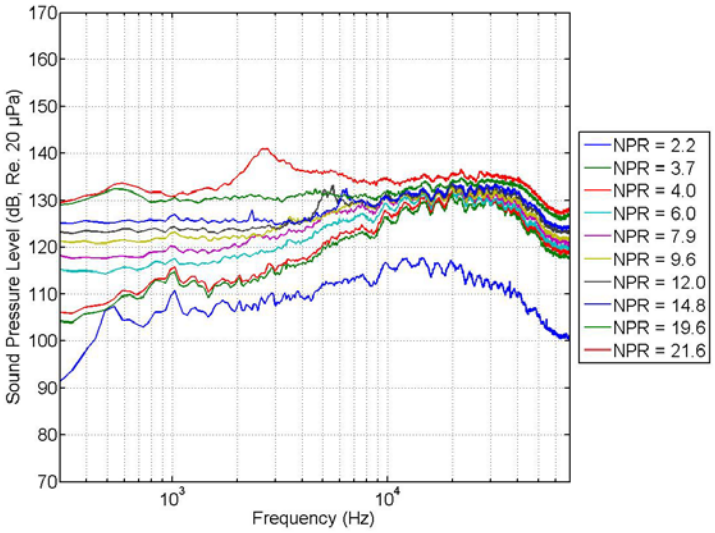

Figure D.18: Frequency Spectra for a 1/4 inch Diameter Jet Array with S/d Ratio of 3 and at NPR Values Ranging From 2.2 to 19.6.

Appendix E: Strouhal Domain Spectra

Appendix E presents the AP/DP in the Strouhal number domain. These spectra are non-dimensional forms of the spectra observed in Appendix D. The spectra for the single jets are presented initially followed by spectra for the 8x8 jet arrays, beginning with jet arrays with S/d = 1.44 and concluding with jet arrays with S/d = 3.

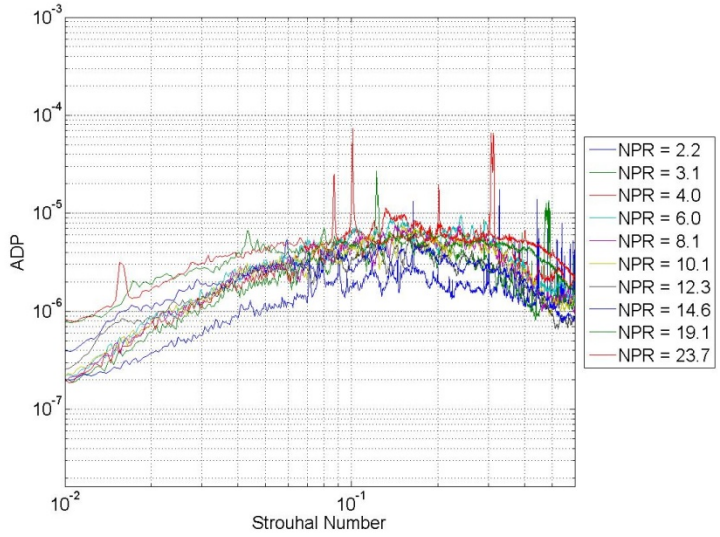

Figure E.1: Non-Dimensional Spectra for a Single 1/8 inch Nozzle Diameter Jet and at NPR Values Ranging From 2.2 to 23.7.

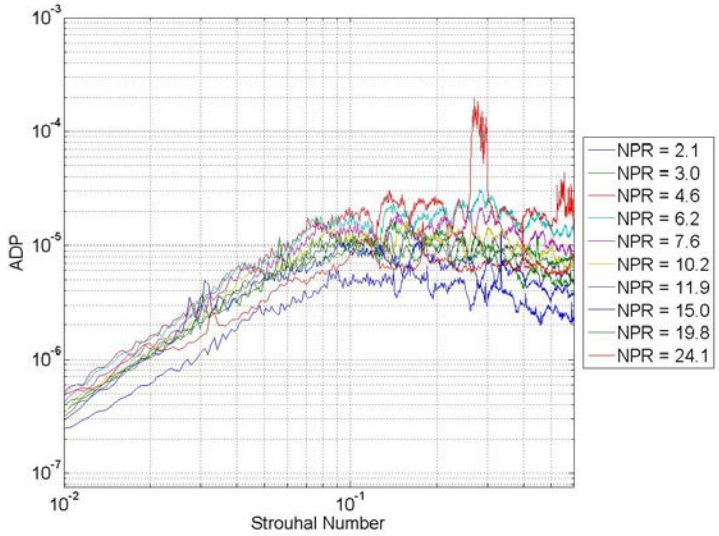

Figure E.2: Non-Dimensional Spectra for a Single 1/4 inch Nozzle Diameter Jet and at NPR Values Ranging From 2.1 to 24.1

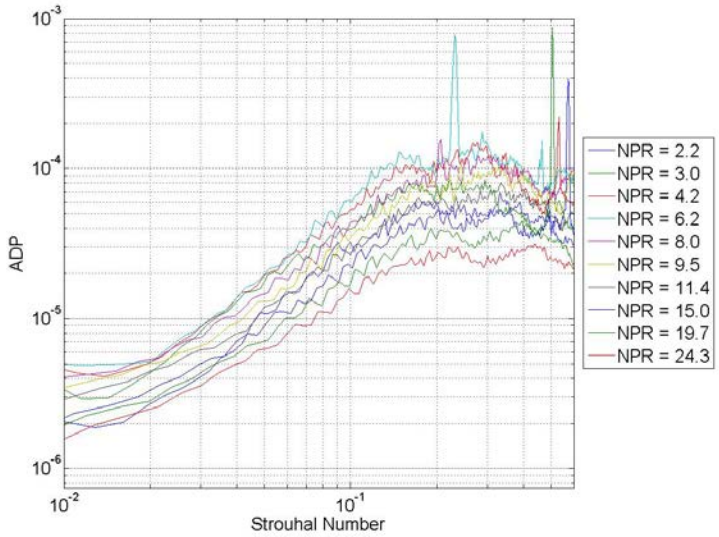

Figure E.3: Non-Dimensional Spectra for a S ingle 1 inch Nozzle Diameter Jet and at NPR Values Ranging From 2.2 to 24.3.

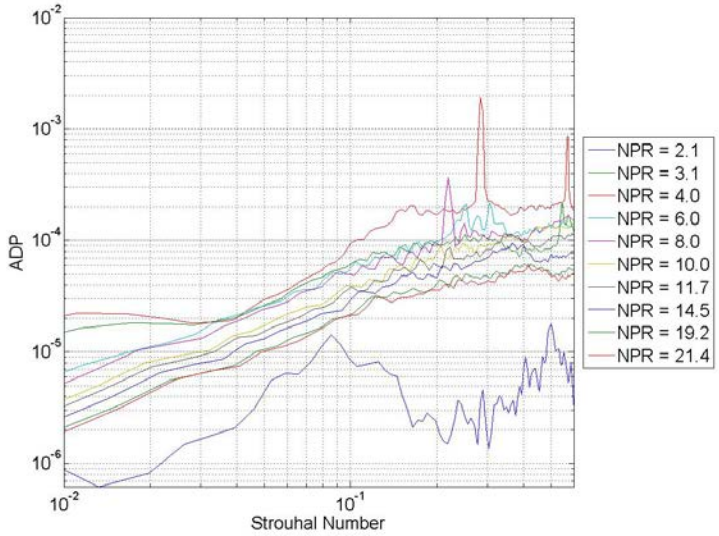

Figure E.4: Non-Dimensional Spectra for a S ingle 2 inch Nozzle Diameter Jet and at NPR Values Ranging From 2.1 to 21.4.

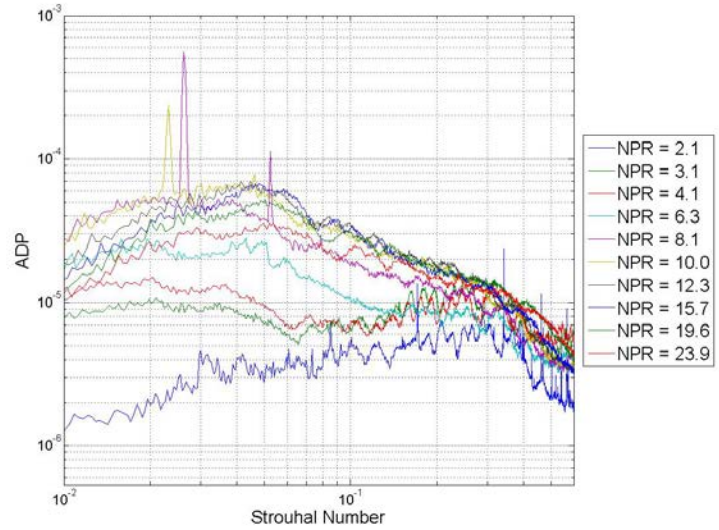

Figure E.5: Non-Dimensional Spectra for a 1/8 inch Diameter Jet Array with S/d Ratio of 1.44 and at NPR Values Ranging From 2.1 to 23.9.

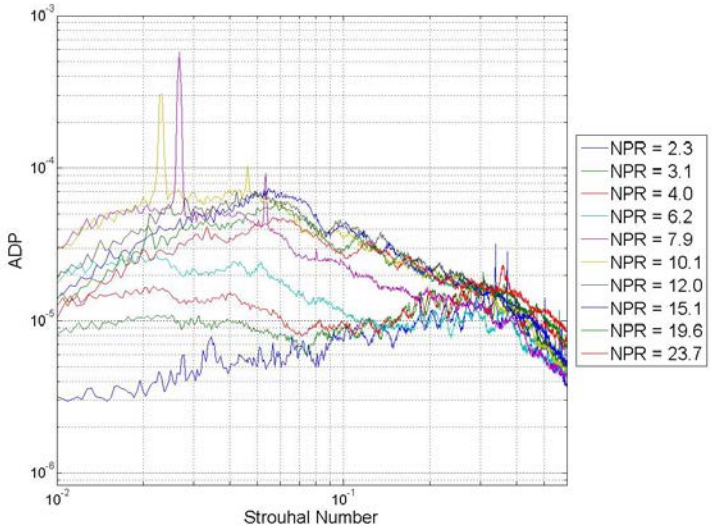

Figure E.6: Non-Dimensional Spectra for a 18/125 inch Diameter Jet Array with S/d Ratio of 1.44 and at NPR Values Ranging From 2.3 to 23.7.

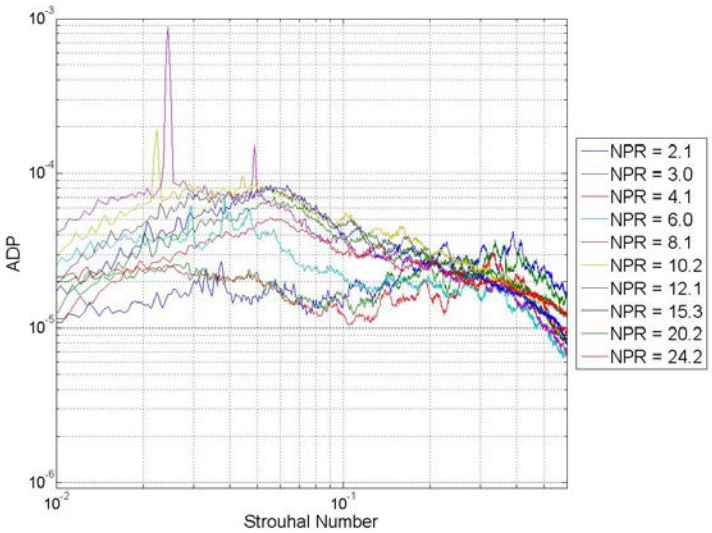

Figure E.7: Non-Dimensional Spectra for a 5/32 inch Diameter Jet Array with S/d Ratio of 1.44 and at NPR Values Ranging From 2.1 to 24.2.

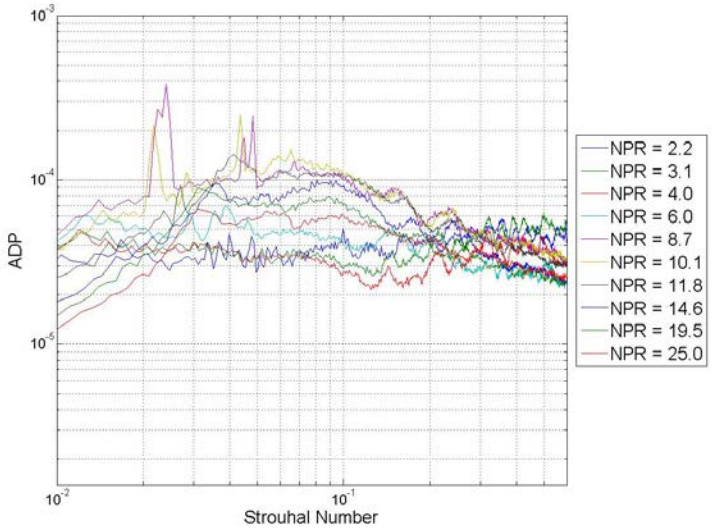

Figure E.8: Non-Dimensional Spectra for a 1/4 inch Diameter Jet Array with S/d Ratio of 1.44 and at NPR Values Ranging From 2.2 to 25.0.

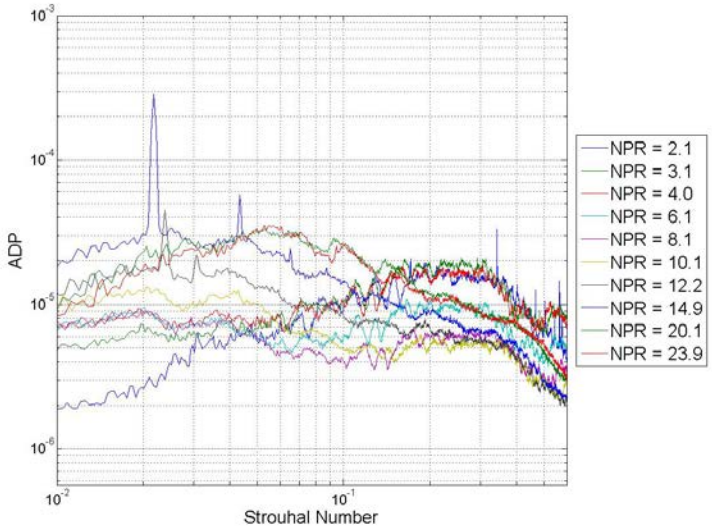

Figure E.9: Non-Dimensional Spectra for a 1/8 inch Diameter Jet Array with S/d Ratio of 2 and at NPR Values Ranging From 2.1 to 23.9.

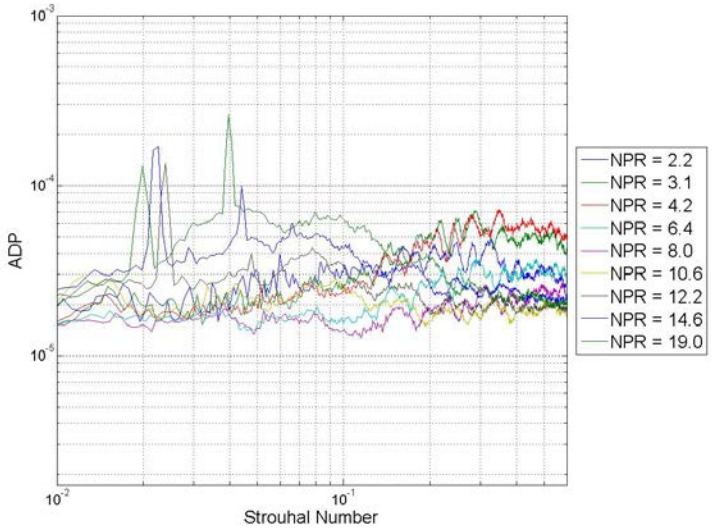

Figure E.10: Non-Dimensional Spectra for a 1/4 inch Diameter Jet Array with S/d Ratio of 2 and at NPR Values Ranging From 2.2 to 19.0.

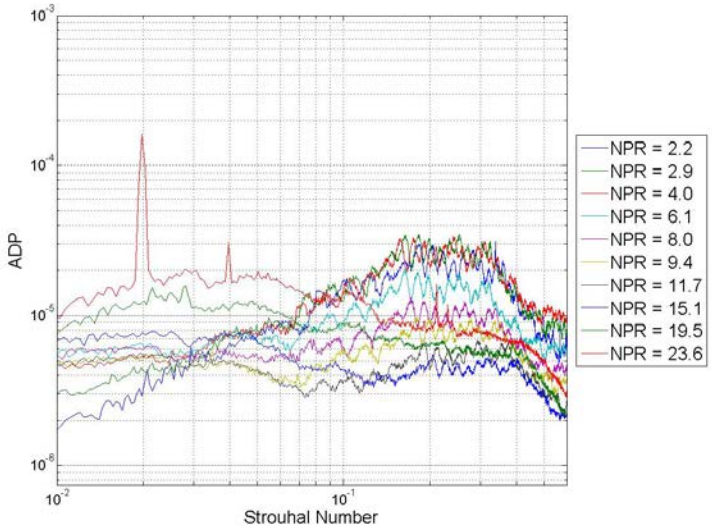

Figure E.11: Non-Dimensional Spectra for a 1/8 inch Diameter Jet Array with S/d Ratio of 2.5 and at NPR Values Ranging From 2.2 to 23.6.

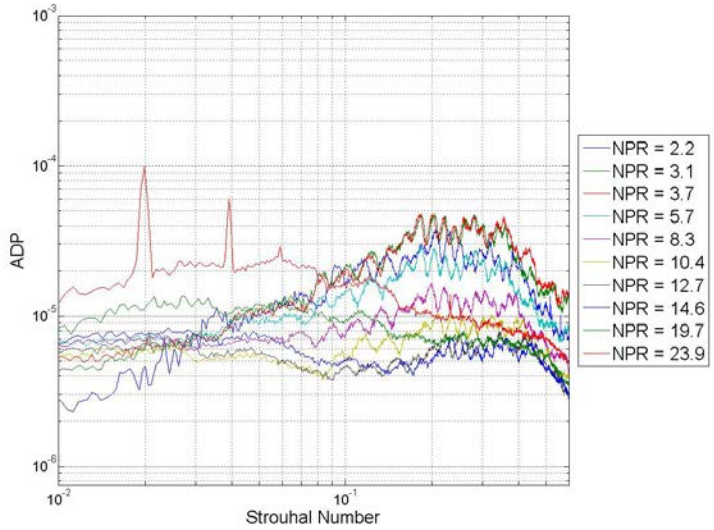

Figure E.12: Non-Dimensional Spectra for a 18/125 inch Diameter Jet Array with S/d Ratio of 2.5 and at NPR Values Ranging From 2.2 to 23.9.

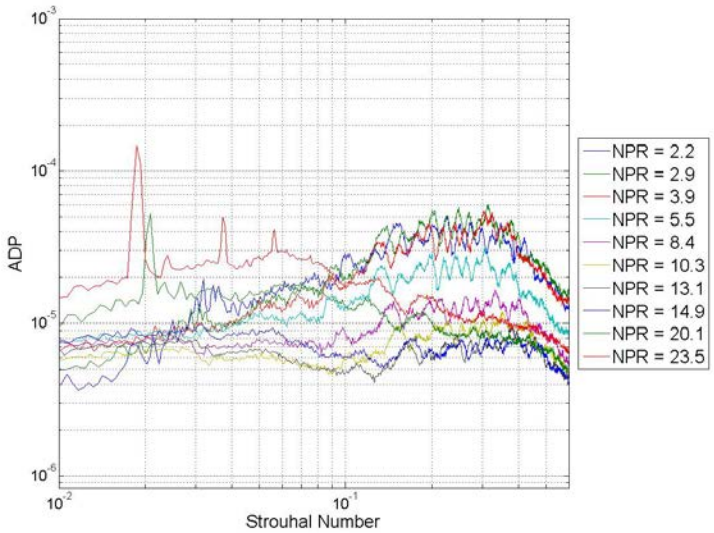

Figure E.13: Non-Dimensional Spectra for a 5/32 inch Diameter Jet Array with S/d Ratio of 2.5 and at NPR Values Ranging From 2.2 to 23.5.

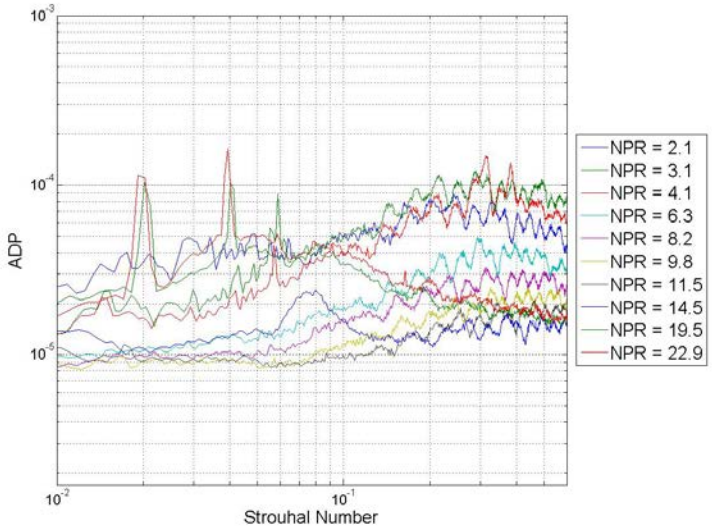

Figure E.14: Non-Dimensional Spectra for a 1/4 inch Diameter Jet Array with S/d Ratio of 2.5 and at NPR Values Ranging From 2.1 to 22.9.

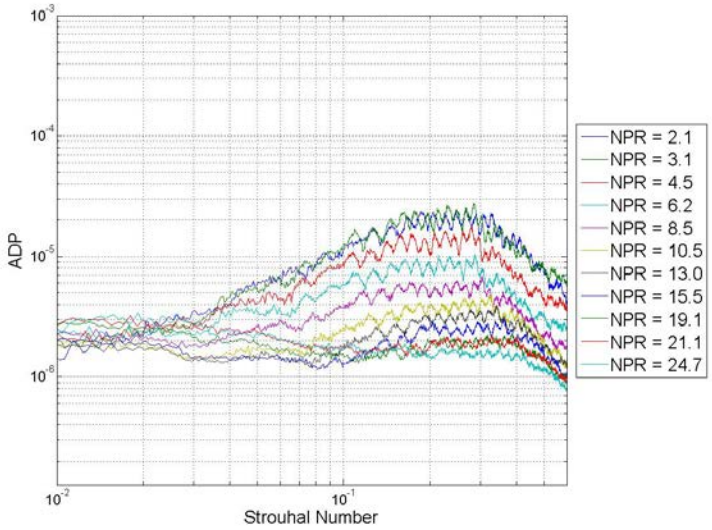

Figure E.15: Non-Dimensional Spectra for a 1/8 inch Diameter Jet Array with S/d Ratio of 3 and at NPR Values Ranging From 2.1 to 24.0.

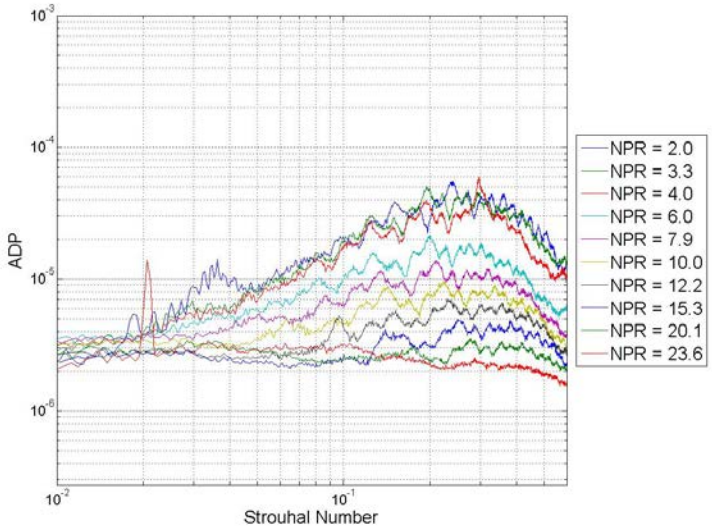

Figure E.16: Non-Dimensional Spectra for a 18/125 inch Diameter Jet Array with S/d Ratio of 3 and at NPR Values Ranging From 2.0 to 23.6.

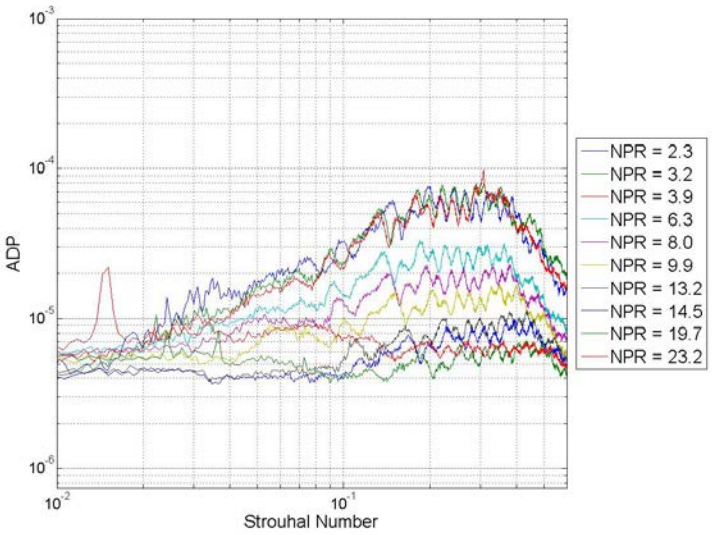

Figure E.17: Non-Dimensional Spectra for a 5/32 inch Diameter Jet Array with S/d Ratio of 3 and at NPR Values Ranging From 2.3 to 23.2.

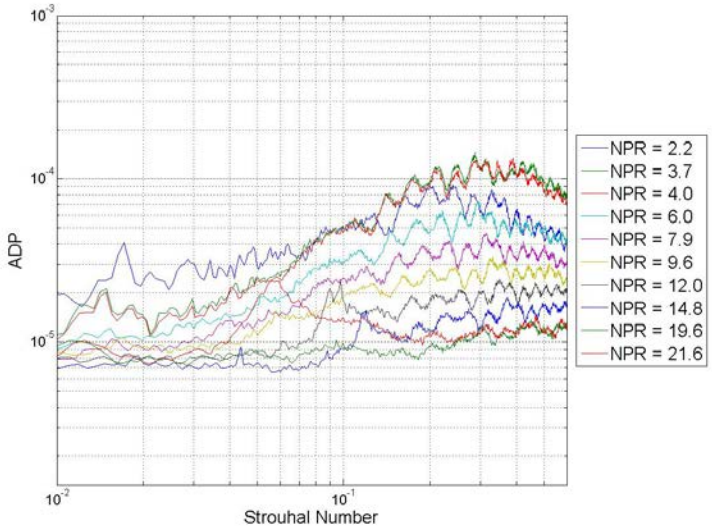

Figure E.18: Non-Dimensional Spectra for a 1/4 inch Diameter Jet Array with S/d Ratio of 3 and at NPR Values Ranging From 2.2 to 21.6.

Appendix F: Matlab Code for the Method of Characteristics

Appendix F presents the Matlab code which applies the Method of Characteristics to determine the size of a shock cell in order to determine the fully expanded diameter in Chapter 4. The inputs for this code include NPR, temperature, and nozzle exit diameter.

```
clear all;
clc;

%   Input Parameters
NPR = ;
Temp = ;
h_th = ;    % Throat  height (meters)

for n = 1:length(NPR)

%   Problem parameters
T_c = Temp(n)+273.15;     % Temperature in the combustion chamber (K)
P_c = NPR(n)*101e3;    % Pressure in the combustion chamber (Pa)
P_amb = 101e3;  % Ambient pressure (Pa)
T_amb = 290;    % Ambient temperature (K)
gamma = 1.4;   % Ratio of Specific Heats Cp/Cv (Gamma)
W = 30;       % Molecular weight of gas (kg/kmol)
width = .1;     % Nozzle width (meters)

%   Method of Characteristics
num = 30;       % Number of Characteristic lines
theta_i = .03;  % Initial step in theta
plotter = 0;    % Set to '1' to plot nozzle

dh = h_th/100;
max_iter = 10000;
R = 8314/W;

%   Part A

%find where P becomes u
h(1) = h_th;
A_star = h_th*width;
M =1;
dM1 = .1;
```

```
for i=1: max_iter
    h(i) = h(1) + (i-1)*dh;
    Ae(i) = h(i)*width;
    A_Asq = (Ae(i)/A_star)^2;
    A_ratio(i)=sqrt(A_Asq);

    %Newton Rhapson on Eq. 5.20 - Anderson text
    res = 1;
    if i > 1
        M = Ma(i-1);
    end

     while res > .001
        M2 = M + dM1;
        funa1 = -A_Asq + (1/M^2)*((2/(gamma+1))*(1+(gamma-
1)*M^2/2))^((gamma+1)/(gamma-1));
        funa2 = -A_Asq + (1/M2^2)*((2/(gamma+1))*(1+(gamma-
1)*M2^2/2))^((gamma+1)/(gamma-1));
        dv_dm = (funa2-funa1)/dM1;

        M = M - funa1/dv_dm;
        res = abs(funa1);

    end
    Ma(i) = M;

    % Find Pressure
    P(i) = P_c*(1+(gamma-1)*Ma(i)^2/2)^(-gamma/(gamma-1));

    % Find thrust for each point
    Te(i) = T_c/(1+(gamma-1)*Ma(i)^2/2);
    Tt(i) = T_c/(1+(gamma-1)/2);
    Ve(i) = Ma(i)*sqrt(Te(i)*gamma*R);
    Vt(i) = sqrt(Tt(i)*gamma*R);
    rhot(i) = P(i)/(R*Te(i));
    mdot(i) = rhot(i)*Ve(i)*Ae(i);
    TT(i) = mdot(i)*Ve(i) + (P(i) - P_amb)*Ae(i);

    if P(i) < P_amb
        %break
        %Calculate the pressure if shock wave exists at the exit plane
        P_exit = P(i)*(1+(gamma*2/(gamma+1))*(Ma(i)^2-1));

         if P_exit <= P_amb
             P(i) = P_exit;
             break
         else
         end

    else
    end

end

% figure(2)
```

```
% plot(Ae,TT)
% title('Thrust curve')
% xlabel('Exit Area (m^2)')
% ylabel('Thrust (N)')

%   Part B
%   Determine the nominal exit area of the nozzle
%   to maximize thrust

[a,b]=max(TT);
%   Over or Underexpand the nozzle
b = b;
A_max = Ae(b);
Max_thrust = TT(b);
hold on;
% plot(A_max,Max_thrust,'r*')
% legend('Thrust Curve','Max Thrust')

%   Part C
%   Method of Characteristics

M_e = Ma(b);       %Mach number at ideal exit


%Find theta_max by using equation 11.33
theta_max = (180/pi)*(sqrt((gamma+1)/(gamma-1))*atan((sqrt((gamma-1)*(M_e^2-
1)/(gamma+1))))-atan(sqrt(M_e^2-1)))/2;

%  D_theta for each char line
del_theta = (theta_max - theta_i)/(num-1);

% Find

for i=1:num
    %   Initialize mach numeber

    for j=1:num
        if i==1
            %Theta for each line (first lines)
            theta(i,j) = theta_i + del_theta*(j-1);
            nu(i,j) = theta(i,j);
            K_m(i,j) = theta(i,j) + nu(i,j);
            K_p(i,j) = theta(i,j) - nu(i,j);

        elseif i > 1

            K_p(i,j) = -K_m(1,i);

            % Find Thetas
            if j >= i
                theta(i,j) = del_theta*(j-i);
            else
                %theta(i,j) = theta(j,i-1);
                theta(i,j) = theta(j,i);
```

```
            end
            nu(i,j) = theta(i,j) - K_p(i,j);
            K_m(i,j) = theta(i,j) + nu(i,j);
        end

    % Prandtl-Meyer function (using Newton Rhapson)
    dM = .1; % Leave at about .1
    if j == 1
        M_ex(i,j) = 1.00;
    else
        M_ex(i,j) = M_ex(i,j-1);
    end
    M = M_ex(i,j);

    res = 1;
    while res > .01
        M2 = M + dM;
        funv1 = (-nu(i,j)*(pi/180)+(sqrt((gamma+1)/(gamma-
1))*atan((sqrt((gamma-1)*(M^2-1)/(gamma+1))))-atan(sqrt(M^2-1))));
        funv2 = (-nu(i,j)*(pi/180)+(sqrt((gamma+1)/(gamma-
1))*atan((sqrt((gamma-1)*(M2^2-1)/(gamma+1))))-atan(sqrt(M2^2-1))));
        dv_dm = (funv2-funv1)/dM;

        M = M - funv1/dv_dm;
        res = abs(funv1);

    end
    M_ex(i,j) = M;

    % Find the angle mu
    mu(i,j) = (180/pi)*asin(1/M_ex(i,j));

    end

    % Add last point to char line
    theta(i,num+1) = theta(i,num);
    nu(i,num+1) = nu(i,num);
    K_m(i,num+1) = K_m(i,num);
    K_p(i,num+1) = K_p(i,num);
end

char = zeros(num,num+1,2);
for i=1:num

    for j=1:num+1

% Draw points of intersection
        %   Point 1 of all char lines
        if j == 1
            char(i,j,1) = 0;
            char(i,j,2) = h_th/2;
        end
```

```
        %   Where first line hits the symmetry line
        if i == 1 & j==2
            char(i,j,1) = (-h_th/2)/tan((pi/180)*(theta(1,j-1)-mu(1,j-1)));
            char(i,j,2) = 0;
        end

        %   Where all other lines hit the symmetry line
        if j == i+1 & j>2
              char(i,j,1) = -char(i-1,j,2)/tan((pi/180)*(.5*theta(i,j-2)-
.5*(mu(i,j-2)+mu(i,j-1)))) + char(i-1,j,1);
              char(i,j,2) = 0;
              test(i,j) = (theta(i,j-2)-.5*(mu(i,j-2)+mu(i,j-1)));
              testpty(i,j) = char(i-1,j,2);
              testptx(i,j) = char(i-1,j,1);
        end

        %   All other data points for char 1 calculated
        if i ==1 & j>2 & j ~= i+1
            C_p = tan((pi/180)*(.5*(theta(i,j-2)+theta(i,j-1))+.5*(mu(i,j-
2)+mu(i,j-1))));
            C_m = tan((pi/180)*(.5*(theta(j-1,1)+theta(i,j-1))-.5*(mu(j-
1,1)+mu(i,j-1))));
            A = [1,-C_m;1,-C_p];
            B = [char(1,1,2) - char(1,1,1)*C_m;
                char(1,j-1,2) - char(1,j-1,1)*C_p];
                iterm(1,:)=inv(A)*B;
                char(i,j,1) = iterm(1,2);
                char(i,j,2) = iterm(1,1);
        end

        %   All other points for all char lines calculated
        if i > 1 & j~=i+1 & j>2
            C_p = tan((pi/180)*(.5*(theta(i,j-2)+theta(i,j-1))+.5*(mu(i,j-
2)+mu(i,j-1))));
            C_m = tan((pi/180)*(.5*(theta(i-1,j-1)+theta(i,j-1))-.5*(mu(i-
1,j-1)+mu(i,j-1))));
            A = [1,-C_m;1,-C_p];
            B = [char(i-1,j,2) - char(i-1,j,1)*C_m; char(i,j-1,2) - char(i,j-
1,1)*C_p];

            iterm(1,:) = inv(A)*B;
            char(i,j,1) = iterm(1,2);
            char(i,j,2) = iterm(1,1);
        end
    end
end


%  Fill in similar points (where char lines share points)
for i = 2:num
    for j=2:num
        char(j,i,1) = char(i-1,j+1,1);
        char(j,i,2) = char(i-1,j+1,2);
    end
end
```

```
% ******Make the nozzle shape and extend the char lines to wall******

%   Initial start point of the nozzle (at throat)
noz(1,1) = 0;
noz(1,2) = h_th/2;

%   Find all the points of the nozzle
for i = 2 : num
    %   Find different slopes and points to intersect
    m1 = tan((pi/180)*(theta(i-1,num)+mu(i-1,num)));
    if i ==2
        m2 = (pi/180)*theta_max;
    else
        m2 = ((pi/180)*(theta(i-1,num+1)));
    end
    m3 = ((pi/180)*(theta(i-1,num)));
    m4 = tan((m2+m3)/2);

    A = [1,-m4; 1,-m1];
    B = [noz(i-1,2) - noz(i-1,1)*m4; char(i-1,num+1,2) - char(i-
1,num+1,1)*m1];

    iterm(1,:) = inv(A)*B;
    noz(i,1) = iterm(1,2);
    noz(i,2) = iterm(1,1);

    %   Extend char lines to wall
    char(i-1,num+2,1)= noz(i,1);
    char(i-1,num+2,2)= noz(i,2);
end

%Last line
m1 = tan((pi/180)*(theta(num,num)+ mu(num,num)));
m2 = ((pi/180)*(theta(num-1,num)));
m3 = ((pi/180)*(theta(num,num+1)));
m4 = tan((m2+m3)/2);

A = [1,-m4; 1,-m1];
B = [noz(num,2) - noz(num,1)*m4; char(num,num+1,2) - char(num,num+1,1)*m1];

iterm(1,:) = inv(A)*B;
noz(num+1,1) = iterm(1,2);
noz(num+1,2) = iterm(1,1);


%   Extend char lines to wall
char(num,num+2,1)= noz(num+1,1);
char(num,num+2,2)= noz(num+1,2);

if plotter ==1

%   Plot the nozzle shape
% figure(1);clf;
```

```
% subplot(2,1,1);
% plot(noz(:,1),noz(:,2),'k','LineWidth',3)
% hold on;
% [a,b] = max(noz);
% plot(a(1),A_max/width/2,'g*')
% grid on

%   Plot for loop for char lines
% for i = 1 : num
%     figure(1)
%     hold on;
%     plot(char(i,:,1),char(i,:,2))
%     hold on;
%     plot(char(i,:,1),-char(i,:,2))
% end

%   Plot the nozzle shape (bottom side)
% figure(1)
% subplot(2,1,1)
% hold on;
% plot(noz(:,1),-noz(:,2),'k','LineWidth',3)
% hold on;
% plot(a(1),-A_max/width/2,'g*')
% title('Max Thrust (minimum length) Nozzle Design')
% xlabel('Nozzle length (m)')
% ylabel('Nozzle height (m)')
% legend('Nozzle shape','Area_e_x_i_t(predicted)','Char. Lines')
else
end

%   Find  % errors in A/A* and Mexit
error_Area = 100*(width*2*noz(num,2) - A_max)/(A_max);
error_Mach = 100*(M_e - M_ex(num,num))/M_e;


%   Plot Mach Number and pressure through nozzle using the quasi-1D
%   area relations.  (Isentropic expansion through nozzle)
Mnoz(1) = 1.0;  %   Choked Flow
M = Mnoz(1);
for i=1: size(noz,1)
    Ae(i) = 2*noz(i,2)*width;
    A_Asq = (Ae(i)/A_star)^2;
    A_ratio(i)=sqrt(A_Asq);

    %Newton Rhapson on Eq. 5.20 - Anderson text
    res = 1;
    if i > 1
        M = Mnoz(i-1);


     while res > .001
        M2 = M + dM1;
        funa1 = -A_Asq + (1/M^2)*((2/(gamma+1))*(1+(gamma-
1)*M^2/2))^((gamma+1)/(gamma-1));
```

```
        funa2 = -A_Asq + (1/M2^2)*((2/(gamma+1))*(1+(gamma-
1)*M2^2/2))^((gamma+1)/(gamma-1));
        dv_dm = (funa2-funa1)/dM1;

        M = M - funa1/dv_dm;
        res = abs(funa1);

    end
    Mnoz(i) = M;
    end
    % Find Pressure
    Pnoz(i) = P_c*(1+(gamma-1)*Mnoz(i)^2/2)^(-gamma/(gamma-1));
end

% figure(1);
% subplot(2,1,2)
% plot(noz(:,1),Mnoz,'r*')
% hold on;
% plot(noz(:,1),Pnoz/P_amb,'b*')
% hold on;
% plot(noz(size(noz,1),1),M_e,'go')
% hold on;
% plot(noz(size(noz,1),1),1,'go')
% xlabel('Nozzle length (m)')
% ylabel('Mach number and P/P_c')
% legend('Mach Number','P/P_a_m_b','M_e_x_i_t(predicted)','P_a_m_b/P_a_m_b')
% grid on

celld(n,1) = 2*noz(length(noz),2)/0.0254;
end

celld
```